Nonlinear Propagation in Periodic Microstructures

Patricia Millar

ACKNOWLEDGEMENTS.

I would first of all like to say a big thank you to my supervisor Stewart Aitchison for his invaluable guidance, support, encouragement, patience and friendship.

I would also like to express my appreciation to all the technical staff in the Engineering department for their help and advice, especially those staff that I pestered on a weekly basis including: Dave Clifton, Gillian, Jim Gray, Jimmy Young, Joan Carson and last but not least Robert Harkins.

I am also greatly indebted to the following people without whose help there wouldn't have been much of a thesis to write: Gordon Kennedy and Wilson Sibbett from St Andrews University, Jin Kang and George Stegeman from the University of Central Florida and Alain Villeneuve from the Universitè Laval.

I am also very grateful to all the research staff and students at Glasgow University that I've came to know over the past few years and would like to thank them all for their friendship and help and for the fond hazy memories I have of nights out at the "Doublet". In particular, I would like to thank my old pal Jude for being a great friend and for accompanying me to the "Beer Bar" in times of despair and boredom.

Finally I would like to say a huge big thank you to my family and my boyfriend Richie for their love and support and for helping me through many a PhD panic attack,

Thanks.

Mum and Dad.

ABSTRACT.

The main objectives of this research project related to the observation of ultrafast, all-optical switching within AlGaAs structures operated in the half-band gap spectral region. The switching configurations investigated were based on nonlinear periodic structures and included nonlinear waveguide arrays and Bragg gratings.

Theoretical simulations of the switching characteristics of various nonlinear coupled arrays were carried out using both a fourth order Runge-Kutta algorithm and a split step Fast Fourier Transform code. The effects of linear absorption, dispersion and multi-photon absorption on the efficiency of the switch were taken into consideration. All-optical switching was demonstrated for the first time in uniformly and non-uniformly spaced three, four and eight core couplers. The experimental transmission characteristics compared well to the theoretical simulations.

First and second order grating filters were fabricated using both a two step holographic process and a single-step electron beam writing process. Gratings with a 70% reflection efficiency and stopband width of 0.9 nm were fabricated. The linear losses of the filters were measured using a Fabry-Perot technique. The electron beam defined gratings were found to have no significant scattering losses associated with them. In contrast the holographically fabricated gratings were found to increase the losses of the waveguides considerably. Finally the nonlinear response of the grating filters were investigated.

PUBLICATIONS.

Conference Publications.

P.Millar, C.J.Hamilton, J.S.Aitchison, G.T.Kennedy and W.Sibbett, "Nonlinear three core couplers in AlGaAs", QE-12 Technical Digest, p1-22 (1995).

P.Millar, J.S.Aitchison, J.U.Kang, G.I.Stegeman, A.Villeneuve, "Nonlinear multi-core directional couplers in AlGaAs", Nonlinear Guided Waves and their Applications, Opt.Soc.Am. Technical Digest Series, **15**, pp 125-127 (1996).

Journal Publications.

P.Millar, R.Harkins and J.S.Aitchison, "Fabrication of low loss, waveguide grating filters using electron beam lithography" Electron. Lett., **33**, pp 1031-1032 (1997).

P.Millar, J.S.Aitchison, J. U. Kang ,G. I. Stegeman, G.T.Kennedy, W.Sibbett and A.Villeneuve, "Nonlinear waveguide arrays in AlGaAs" J. Opt. Soc. Am. B (still to be published Nov 1997).

CONTENTS.

Chapter One: Introduction.

Chapter Two: The Nonlinear Optical Properties of AlGaAs.

Chapter Three: Semiconductor Waveguide Design, Fabrication and Charactersiation.

Chapter Four: Nonlinear Coupled Waveguide Arrays.

Chapter Five: Grating Structures.

Chapter Six: Summary of Thesis.

CHAPTER 1

Introduction.

1.1. Introduction.

In this thesis the switching characteristics of several different all-optical switching devices were investigated. This introductory chapter will outline the aims and objectives of the thesis and will present an introduction to nonlinear optics and all-optical switching.

The chapter begins with a brief outline of the advances made within the field of telecommunications systems over the past few decades and explains the need for all-optical switches within future optical computing and communication networks. In section 1.2 the objectives of the thesis are outlined and in section 1.3 the basics of nonlinear optics are reviewed. The phenomena that arise due to the nonlinear properties of a material including the optical Kerr effect are dealt with in section 1.4. In section 1.5 the desirable characteristics of a nonlinear switching device are outlined. Finally in section 1.6 a summary of each chapter of the thesis is given.

1.1.1. The Evolution of Communications Systems.

Telecommunication systems have come a long way since the production of the first optical fibres in the mid-sixties. The increasing demands made by the market place, in combination with new technological advances, have produced a communications revolution. The internet (including electronic mail), video-phones, faxes, long-haul fibre telecommunication networks, satellite systems for TV and scientific applications are some of the recent advances in communications. These new applications have been brought about by improved low loss optical fibres networks, efficient laser diodes, optical fibre amplifiers, advances in integrated circuit technology (VLSI and ULSI) and the use of nonlinear optical devices. However, the communication revolution is by no means over and further research is needed to refine, exploit and improve the technology and systems in use today.

In the future, demands placed on optical communication and computing systems will increase so much so that new improved networks will be needed. Vital to the development of these new networks is the production of ultrafast switching components for information processing.

Switches enable a signal, or signals, to control another signal and are used in the networks to perform such functions as memory, logic and signal routing operations. Current optical fibre systems operating in the low loss telecommunications windows at 1.3 μm and 1.55 μm have a huge potential bandwidth of approximately 40 Terahertz (4 x 10^{13} Hz)[1] in a single optical fibre. The bandwidth of a system ultimately determines the density of information flow in that network. Consequently fibre telecommunication systems have a massive potential information carrying capacity. At the moment the switching in these networks is achieved using electronic gates, such as bipolar transistors and field effect transistors. The switching speeds of these electronic gates, which are limited by stray capacitance to tens of picoseconds, severely restrict the bandwidth of the fibre systems.

1.1.2. All-Optical Switching.

To make better use of the information capacity of optical networks, by expanding the usable bandwidth of these systems, it is envisaged that, in the future, information processing will be conducted using all-optical switches/logic gates based on nonlinear optical effects. All-optical switches have great potential for future communications and computing applications for several reasons. One major advantage over electronic gates is that the speed of an all-optical switch depends solely on the speed of the nonlinearity which for a nonresonant nonlinearity can be effectively instantaneous. In addition, all-optical switches are not affected by magnetic, or electric disturbances as is the case for electrical components. Furthermore, processing all-optically has the added advantage that bottlenecks caused by the conversion between optics and electronics are eliminated. Therefore, by processing all-optically not only would both time and energy be saved but the information carrying capacity of optical fibre networks would increase.

1.2. Objectives of Research.

It was the aim of this thesis to develop all-optical switching elements which could be potentially used for future information processing applications. To achieve this goal the nonlinear properties of periodic microstructures formed in AlGaAs and operated below half the band gap, were examined. In particular, the research involved the design, modelling, fabrication and experimental demonstration of two different all-optical switching elements. The first optical device examined involved the coupling of light between cores of several different nonlinear multi-guide coupler arrays. The second all-optical switch that was investigated considered the coupling of light between the forward and backward propagating field modes of a nonlinear grating filter.

1.3. Nonlinear Optics.

Nonlinear optics is the term used to described the changes in the optical properties of a material caused by the interaction of intense light with the material. To observe nonlinear effects a high intensity optical field, i.e.~ 2.5 kW/cm^2 is required. Therefore research into nonlinear optic behaviour did not begin until the demonstration of the first operational, pulsed ruby, laser by Mainman in 1960. Before that the available light sources were not intense enough to produce nonlinear effects. The first nonlinear effect to be observed was the discovery of second harmonic generation by Franken et al[2]. Since then, a wide variety of optically nonlinear phenomenon have been explored in many different material systems including semiconductors, glasses and in nonlinear organic materials in various macroscopic forms i.e., crystals, liquid crystals, polymers and films. In the following section some of these nonlinear effects are described.

1.4. Nonlinear Effects.

The nonlinear response of matter to an incident light field may be written[3]:

$$P_i = \varepsilon_0\left(\sum_j \chi_{ij}{}^{(1)}E_j + \sum_{jk}\chi_{ijk}{}^{(2)}E_jE_k + \sum_{jkl}\chi_{ijkl}{}^{(3)}E_jE_kE_l + \ldots\right) \quad (1.1)$$

In equation (1.1), $\chi^{(n)}$ is an (n+1) th rank tensor which relates the input fields, (polarisation, amplitude and intensity), E, to the induced polarisation P. Here $\chi^{(1)}$ is the linear susceptibility, the real part of which is related to the linear refractive index and the imaginary part is related to a linear absorption term. The coefficients $\chi^{(2)}$ and $\chi^{(3)}$ are the second and third order susceptibilities respectively. In equation 1.1 above the frequency dependency of the polarisation has been neglected.

1.4.1. Second Order Nonlinearities.

Assuming the third and subsequent higher order susceptibilities are zero, equation 1.1 can be written as:

$$P_i = \varepsilon_0 [\sum_j \chi_{ij}{}^{(1)} E_j + \sum_{jk} \chi_{ijk}{}^{(2)} E_j E_k] \qquad (1.2)$$

Where $\chi^{(2)}$ is the second order nonlinear susceptibility which gives rise to nonlinear effects such as second harmonic generation, sum and difference frequency mixing and optical parametric oscillation. Second order nonlinear effects can only occur in crystals that are noncentrosymmetric, i.e. do not display inversion symmetry, such as GaAs and Lithium niobate. Figure 1.1 is a schematic of the second harmonic effect. The radiation from the YAG laser produces intense laser light at 1.06 μm. Supposing the time dependent part of the incident light field can be expressed as:

$$\mathbf{E}(t) = (\mathbf{E}_0 e^{-i\omega t} + \mathbf{E}_0^* e^{i\omega_0 t}) / 2 \qquad (1.3)$$

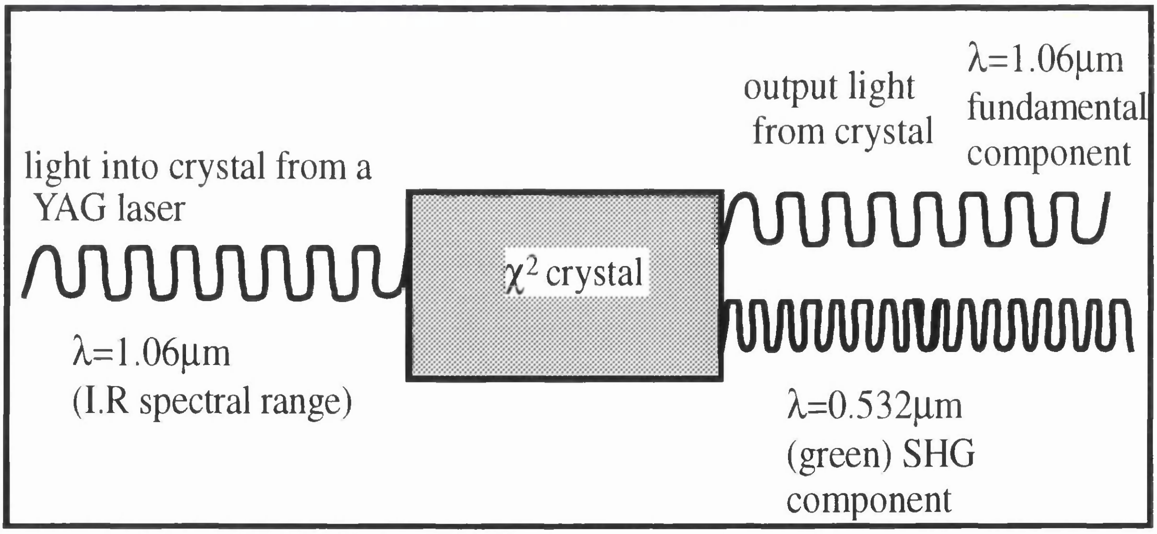

Figure 1.1. Schematic of second harmonic generation.

When the laser light interacts with the nonlinear crystal the induced polarisation can be written as:[4]

$$P_i^{(2)}(\omega)=\frac{\varepsilon_0}{4}\left\{\left[\chi_{ijk}^{(2)}(\omega_0,-\omega_0)E_{oj}E_{ok}^{*}+\chi_{ijk}^{(2)}(-\omega_0,\omega_0)E_{oj}^{*}E_{ok}\right]\delta(\omega-0)\right.$$
$$+\chi_{ijk}^{(2)}(\omega_0,\omega_0)E_{oj}E_{ok}\delta(\omega-2\omega_0) \qquad (1.4)$$
$$\left.+\chi_{ijk}^{(2)}(-\omega_0,-\omega_0)E_{oj}^{*}E_{ok}^{*}\delta(\omega+2\omega_0)\right\}$$

The delta functions ensure that the output polarisations oscillate at summations of the frequencies. In equation 1.4, assuming a monochromatic input field of frequency ω_0, the first term on the left hand side of the equation, describes optical rectification, i.e the production of a second order polarisation at a frequency of 0 and the remaining terms on the left hand side of the equation describe the production of a polarisation at $\pm 2\omega_0$, i.e. second harmonic generation. Second harmonic generation can be used in the production of coherent optical sources at different wavelengths. A major drawback to producing optical devices based on the second order effect is that the output wavelength differs from the input wavelength and phase matching is required. Therefore, cascading of light between second order devices is difficult.

1.4.2. Third Order Nonlinearities.

In centro-symmetric nonlinear optical materials the induced polarisation can be expressed as:

$$P_i = \varepsilon_0 [\sum_j \chi_{ij}{}^{(1)} E_j + \sum_{jkl} \chi_{ijkl}{}^{(3)} E_j E_k E_l] \quad (1.5)$$

The third order nonlinear susceptibility, $\chi^{(3)}$ is a 4th rank tensor, which produces effects such as the optical Kerr effect, optical bistability, saturable absorption, frequency tripling, four-wave mixing, stimulated Raman scattering, self-focusing, self-phase modulation, cross-phase modulation and the production of solitons. Some of these nonlinear effects, which are relevant to this research, are discussed below.

1.4.2.1. The Optical Kerr Effect.

The real part of the third order nonlinearity is related to an intensity dependent refractive index. This relation can be derived as follows:

Substituting equation 1.8 into the following equation for the electric displacement D of a medium:

$$\mathbf{D} = \varepsilon_0 \mathbf{E} + \mathbf{P} \quad (1.6)$$

gives the following expression for the dielectric displacement due to the induced polarisation of the nonlinear material:

$$\mathbf{D} = \varepsilon_0 \mathbf{E}(1 + \chi^{(1)} + \chi^{(3)} \mathbf{E}^2) \quad (1.7)$$

In terms of the linear relationship:

$$\mathbf{D} = \varepsilon_0 \varepsilon \mathbf{E} = \mathrm{n_0}^2 \varepsilon_0 \mathbf{E} \quad (1.8)$$

where n_0 is the linear refractive index.The third order susceptibility therefore gives rise to an amplitude dielectric constant given by:

$$\varepsilon = \varepsilon_1 + \chi^{(3)} \mathbf{E}^2 = \varepsilon_1 + (n^2 - 1)\mathbf{E}^2 \qquad (1.9)$$

where ε_1 is the linear dielectric constant. Consequently an intensity dependent refractive index, n_2 can be defined by:

$$n = n_0 + n_2 I \quad (1.10)$$

where n_0 is the linear refractive index, I is the intensity of the incident field and n_2 is the nonlinear refractive index. In the nonresonant case, where the changes in the optical properties of the material are caused soley by the optical field, this expression is commonly know as the optical Kerr effect. n_2 is related to the third order susceptibility by the following equation:[5]

$$n_2(\mathrm{S.I}) = \frac{\chi^{(3)}}{2cn_0^2\varepsilon_0} \quad (1.11)$$

χ^3 and n_2 characterise what can be regarded as an instantaneous nonlinear response to the applied field. The time constant is the dielectric relaxation time which is typically of the order of $\hbar/\Delta E$, where ΔE is the difference in energy between the photon and the nearest allowed transition state. It should be noted that lifetimes of thermally and optically generated carriers also contribute to the time constant. It is the optical Kerr effect which is used in this research to achieve all-optical switching.

The imaginary part of the third order nonlinearity gives rise to a nonlinear absorption term α which is defined as follows:

$$\alpha = \alpha_0 + \alpha_2 I \quad (1.12)$$

where α_0 is the linear absorption, α_2 is the nonlinear absorption coefficient and again I is the local light intensity.

1.4.2.2. Self Phase Modulation.

Self phase modulation (SPM) is the term used to describe the power dependent spectral broadening of an optical pulse propagating in a nonlinear material. Self-phase modulation arises due to a combination of the time varying amplitude of the optical pulse and nonlinear , intensity dependent, index profile of the material. The nonlinear refractive index of a material can be calculated by observing the self phase modulation induced spectral broadening of a pulse.

The frequency spectrum of a pulse after SPM is given by the Fourier transform of the pulse amplitude[6].

$$F(\omega) = \frac{1}{2\pi}\int_{-\infty}^{\infty} P(t)^{1/2} e^{i\Delta\phi(t)} e^{-i(\omega-\omega_0)t} dt \qquad (1.13)$$

where P(t) is the pump power and $\Delta\phi$ is the nonlinear phase change related to n_2 by the following equation:

$$\Delta\phi = \frac{2\pi}{\lambda} L n_2 I \qquad (1.14)$$

Where L is the effective interaction length, I is the intensity of the light pulse and λ is the wavelength of the light in vacuum. It can be seen from equation 1.17, that the nonlinear refraction coefficient can be estimated by measuring the phase modulation experienced by a high peak powered pulse after propagation through the nonlinear medium.

Figure 1.2 displays the calculated frequency spectra of a Gaussian pulse after propagating through a nonlinear medium as a function of light intensity . Each spectra is labelled with the maximum phase shift at the peak of the pulse. It has been shown that when the pulse is non Gaussian it will broaden slightly differently to that of the Gaussian pulse but the number of peaks in the output pulse spectrum is still dependent on the phase shift rather than the pulse shape itself. Also any asymmetry in the input pulse will result in an asymmetric spectrally broadened output pulse.

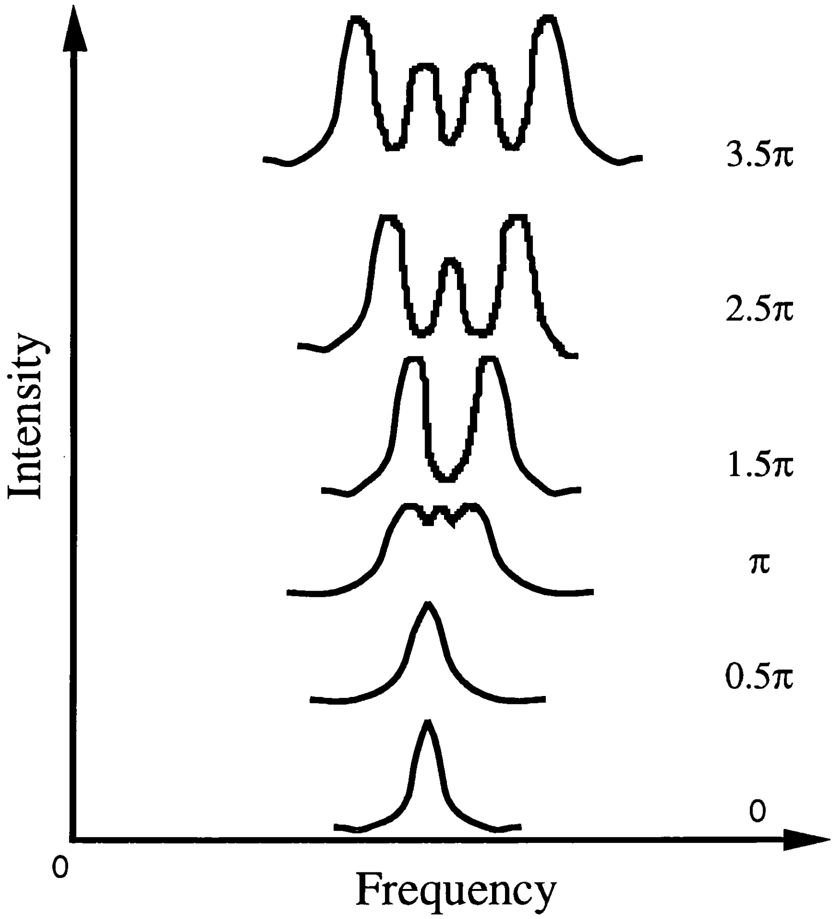

Figure 1.2. The calculated spectra for a Gaussian pulse as a function of light intensity. Each spectra is labelled with the maximum phase shift at the peak of the pulse.

The 1/e full width of the broadened spectrum Δf, is related to the pulse width and the maximum phase shift by the following equation[6].

$$\Delta\tau_p(\mathrm{fw1/e}) = 1.72\Delta\phi_{\mathrm{max}} / \pi\Delta f \quad (1.15)$$

where $\Delta\tau_p$ is the pulse width and $\Delta\phi_{max}$ is the maximum phase shift which corresponds to the number of interference peaks on the output pulse spectrum.

1.4.2.3. Self-Focusing.

Let us consider the propagation of a high intensity light pulse through a third order nonlinear material with a positive n_2. In the case of a Gaussian shaped pulse the intensity of light falls gradually away from being a maximum at the centre to a minimum at the edges. Hence, the local refractive index of the material will be greater at the centre of the light beam than at the edges. Therefore, the nonlinear medium acts as a positive lens and a light pulse will tend to focus as it propagates through the nonlinear material. Damage to the nonlinear medium can occur providing the intensity of the light pulse is high enough and if the nonlinear medium is long enough for the light to reach a focal point within the material.

1.4.2.4. Solitons.

Soliton is the term used to describe an intensity distribution, in time or space, which remains constant as it propagates. In the following section the main types of optical soliton, relevant to this thesis, will be described.

1.4.2.4.1. Spatial Solitons.

Spatial Solitons are self guiding or self-trapped beams that propagate without changing their spatial shape. Spatial solitons are stable when diffraction is limited to one spatial dimension and have been observed in CS_2 liquid waveguides[7], AlGaAs semiconductor waveguides[8] and in ion exchange glass waveguides[9].

The propagation of a spatial soliton can be described using the nonlinear Schrödinger equation of the form:

$$\frac{\partial \mathbf{E}}{\partial z}=\left[\frac{i}{2k}\frac{\partial^2 \mathbf{E}}{\partial x^2}\right]+\left[ik_0 n_2|\mathbf{E}|^2\mathbf{E}\right] \quad (1.16)$$

where E is the electric field strength, z is the propagation distance, k_0 and k are the wave numbers in free space and in the material respectively. The first term on the right hand side of the equation describes the diffraction of the light in the x-direction and the second term is related to the self-focusing effects of the nonlinear material when the nonlinear refractive coefficient is positive and describes a self-defocusing effect when the nonlinear material has a negative nonlinear refractive index coefficient.

In a positive nonlinear material spatial solitons are formed when the effects of diffraction are balance by self-focusing which tends to concentrate the energy of the light beam. The fundamental soliton can be described by the following equation:[10]

$$\mathbf{E}(x,z) = A_0 \operatorname{sech}\left(\frac{x}{a_o}\right)\exp\left(\frac{iz}{2ka_0^2}\right) \quad (1.17)$$

where a_0 is a measure of beam width:

$$A_0 = \frac{1}{ka_0}\sqrt{\frac{n_0}{n_2}} \quad (1.18)$$

The total soliton power in the beam is given by[9]:

$$P_t = \frac{n_0 2w}{n_2 a_o k^2} \quad (1.19)$$

where w is the transverse mode size .For effficient two dimensional propagation $w \ll a_0$ since under these conditions the self-focusing effects are limited to one spatial direction. Higher order solutions exist at intensity levels of N^2P_t, where N is an integer.

1.4.2.4.2. Temporal Solitons.

Temporal solitons are self-guiding beams of light which do not disperse temporally as they propagate. Temporal solitons occur in optical fibres as a result of the balancing effect between the anomalous group velocity dispersion, where the group velocity increases with increasing frequency, present in the fibre and nonlinear phase modulation. They too can be described in the same way as a spatial soliton by the nonlinear Schrödinger equation. The mathematical treatment of these solitons can be found in many text books/papers (see Ref. 3 and 11).

1.4.2.4.3. Bragg Solitons.

Bragg solitons are temporal-like solitons which occur at the upper band edge of the stop-band of a grating where the anomoulous group velocity dispersion is high and the grating is still transmissive. The soliton is produced by the counter balancing effect between the large anomalous dispersion associated with the periodic variation in the refractive index and the self phase modulation produced by the nonlinear medium. Bragg grating solitons have been succesfully demonstrated in optical fibres by Eggleton[11] et al. In that experiment, the Bragg solitons produced were seen to travel at a slower speed than that of light in the medium without a grating. The typical interaction lengths for soliton formation in the fibre grating were substantially shorter than that required for soliton formation in a uniform fibre due to the large dispersion close to the stop-band.

1.4.2.4.4. Gap solitons.

Gap solitons were first theoretically predicted by Chen and Mills[13]. They showed that light with a frequency within the stop band of a grating structure for certain values of intensity can be perfectly transmitting. The shape of the envelope of this transmitted wave is a hyperbolic sech function hence it is commonly known as a soliton. The soliton effectively burns itself slowly through the stop gap by locally changing the refractive index of the material, through the nonlinearity of the material. Numerical simulations indicate that zero velocity gap solitons may be generated in a grating of finite length by illuminating both ends of the grating with two counter-propagating equally intense light beams[14]. Theoretical analysis using coupled mode theory has shown that gap solitons may also propagate inside the grating with a group velocity controlled by selecting the waveguide parameters, which can in principle lie between c/n and 0, where n is the average effective index of the guide.

In chapter 5 the transmission of light through a nonlinear grating structure is studied and the application of gap and Bragg soliton devices is discussed further.

1.5. Desirable Attributes of a Nonlinear Optical Switch.

The desirable attributes for an efficient nonlinear switch include a high switching speed and low switching power requirements together in a compact form. The switching speed of a nonlinear switch is in general dependent on the origin of the nonlinearity. Nonresonant nonlinear processes are a great deal faster than those of resonantly enhanced processes, which are produced as a result of material excitation caused by light absorption, and are therefore more suited to ultrafast switching applications. The power requirements of a nonlinear switch depend on the magnitude of the nonlinear coefficient, the device structure and the value of the linear and nonlinear optical losses of the material. The subject of multi-photon absorption together with a discussion of the nonlinear properties of AlGaAs, which make it the ideal material to observe all-optical switching, are discussed in detail in chapter 2.

1.6. Layout of Thesis.

In this chapter, the potential of all-optical switches within future computing and telecommunication systems and the objective of the thesis were outlined. An introduction to nonlinear optics was given and the properties of nonlinear materials were discussed.

In chapter 2 the opto-electronic properties of AlGaAs are described, including a review of its crystal structure, band structure, and its nonlinear properties.

Chapter 3 describes the design, fabrication and linear and nonlinear characterisation of semiconductor optical waveguides. The chapter begins with a look at the basic modes of a slab waveguide before going on to describe the various waveguide structures and the methods used to calculate the light fields propagating within the guides. The fabrication of the waveguides using a combination of photolithography and reactive ion etching and the Fabry-Perot technique used to measure the linear loss of the guides are also described. In addition the experimental set up used to observe nonlinear effects within the guides is described and measurements of the nonlinear refraction coefficient and two photon absorption coefficient are presented.

Chapter 4 describes the design, fabrication and experimental characterisation of several different nonlinear coupled waveguide arrays. The chapter begins with a brief outline of the past and future applications of nonlinear couplers followed by linear and nonlinear coupler theory. The modelling of the switching characteristics of uniformly spaced and non-uniformly spaced couplers is described using two different numerical techniques before the fabrication process used to produce the couplers is described. Finally, the experimentally obtained switching characteristics of the couplers investigated are presented and compared to the theoretically simulated switching results.

Chapter 5 describes the design, fabrication and characterisation of an all-optical switch based on the nonlinear properties of a grating waveguide filter. The chapter begins with a summary of the past, present and future applications of both linear and nonlinear grating structures followed by some basic linear and nonlinear grating theory. The nonlinear grating filter design and simulations of the switching characteristics of the grating structure using a Runge-Kutta algorithm are also given. The fabrication of the grating filter using both a holographic technique and a E-beam writing method are described and the linear characterisation of the grating filter is presented. Finally, a preliminary nonlinear result observed in a grating filter is discussed.

Chapter 6 summarises the conclusions formed in this research and discusses further work which could be carried out both in the field of nonlinear coupled arrays and in nonlinear gratings filters.

References.

1. C.N. Ironside, "Ultra-fast all-optical switching", Contemporary Physics, **34**, pp 1-18 (1993).
2. P.A. Franken, A.E. Hill, C.W. Peters and G. Weinreich, " Generation of optical harmonics", Phys. Rev. Lett. , **7**, pp 118-119 (1961).
3. R.W. Boyd, "Nonlinear optics", Academic Press, (1992).
4. D.C.Hutchings, "Applied nonlinear optics", University of Glasgow course notes, 1997.
5. A.C. Walker, "A comparison of optically nonlinear phenomena in the context of optical information processing", Optical Computing and processing ,**1**, pp 91-106 (1991).
6. R. Stolen and C. Lin,"Self-phase-modulation in silica optical fibers", Phys. Rev. A, **17**, pp 1448-1453 (1978).
7. J.S. Aitchison, A.M. Weiner, Y. Silberberg, D.E. Leaird, M.K. Oliver, J.L. Jackel and P.W.E. Smith, "Experimental observation of spatial soliton interactions", Opt. Lett. , **16**, pp 16-17 (1990).
8. J.S. Aitchison, K. Al-Hemyari, C.N. Ironside, R.S. Grant and W. Sibbett, " Observation of spatial solitons in AlGaAs waveguides", Electron. Lett. , **28**, pp 1879-1880 (1992).
9. J.S. Aitchison, A.M. Weiner, Y. Silberberg, M.K. Oliver, J.L. Jackel, D.E. Leaird, E.M. Vogel and P.W.E. Smith, "Observation of spatial optical solitons in a nonlinear glass waveguide", Opt. Lett. , **15**, pp 471-473 (1990).
10. Y.Silberberg,"Self-induced waveguides:spatial optical solitons", Anisotropic and nonlinear optical waveguides, Elsevier Science Publications, pp 143-157 (1992).
11. H.A. Haus and W.S. Wong, "Solitons in optical communications", Rev. of mod. phys. , **68**, pp 423-444 (1996).
12. B.J. Eggleton, R.E. Slusher, C. Martijn de Sterke, P.A. Krug, J.E. Sipe, "Bragg grating solitons", Phys. Rev. Lett. , **58**, pp 1627-1630 (1996).
13. W. Chen and D.L. Mills," Gap solitons and the nonlinear optical response of superlattice", Phys. Rev. Lett. , **58**, pp 160-163 (1992).
14. A.B. Aceves, C.De Angelis, S. Wabnitz," Self-induced transparency solitons in nonlinear refractive periodic media", Opt. Lett. , **17**, pp 1566-1570 (1992).

Chapter 2

The Nonlinear Optical Properties of AlGaAs.

Introduction.

AlGaAs has become a popular material for the construction of nonlinear devices for several reasons. First of all, the value of n_2 in AlGaAs is approximately three orders of magnitude greater than that of silica. This means that AlGaAs devices are typically a few centimetres in length and are therefore more compact than comparable fibre devices, which can be tens of meters long. In addition, they can potentially be used for monolithic integration with other opto-electronic/electronic components. High purity, low defect materials can be manufactured, which can be selectively doped with great accuracy. The mature fabrication technology allows a range of relatively complex devices to be constructed. Another advantage of using AlGaAs is that the index of refraction and bandgap of the compound semiconductor can be easily changed by varying the Al content to suit the operational characteristics of the particular device. Thus AlGaAs provides an ideal test system for investigating nonlinear optical effects.

In this chapter the nonlinear optical properties of AlGaAs are considered. To begin with the crystal structure and methods used to produce AlGaAs are explained in section 2.1. The band structure of AlGaAs and other zinc-blende semiconductors are described in section 2.2. In section 2.3 the different types of nonlinearities in semiconductor materials are discussed and in particular the advantages of operating in the half band gap spectral region are outlined. In section 2.4 the theoretical methods used to determine the dispersion and scaling of the nonlinear coefficient of AlGaAs are described. Multi-photon absorption in semiconductors is considered in section 2.5. Finally in section 2.6 the conclusions drawn from this chapter are summarised.

2.1.1. The Crystal Structure of AlGaAs.

The crystal structure of GaAs is shown in fig. 2.1. GaAs has a "zinc blende" structure consisting of 2 inter-penetrating, face-centred cubic lattices, one composed of Ga atoms and the other of As atoms. The cubic unit cell contains 4 atoms each of gallium and arsenic. Each atom is tetrahedraly surrounded by four atoms of the opposite species. The length of each side, the lattice constant, a, is 0.565 nm at 300 K. The crystal does not have a centre of symmetry and can therefore be used to produced second order as well as third order nonlinear effects. The semiconductor AlGaAs is produced by replacing some of the Ga atoms with Al atoms in the crystal structure. The lattice constants of GaAs and AlGaAs differ by less than 0.15%. Therefore it is possible to grow layers of $Al_xGa_{1-x}As$, where x denotes the percentages of aluminium in the layer, on top of one another without introducing significant stress.

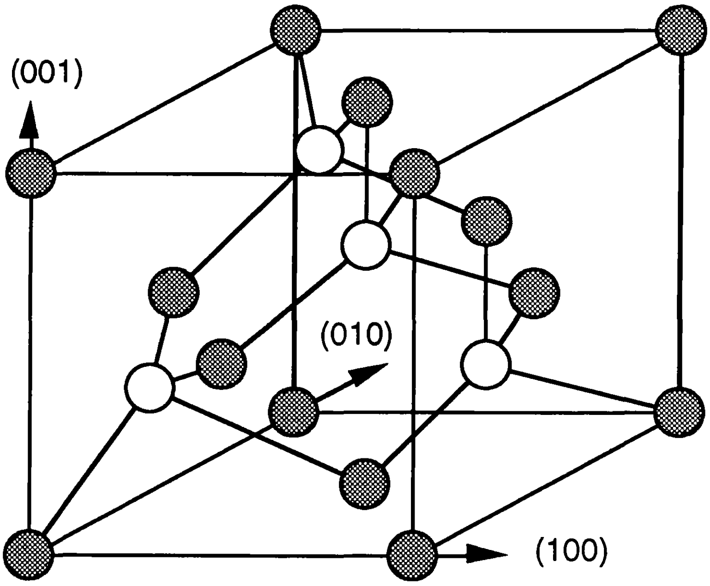

Figure 2.1. The crystal structure of GaAs.

By altering the fraction x in the compound $Al_xGa_{1-x}As$, the refractive index of the material can vary from 2.92 for pure AlAs up to 3.43 for GaAs at a wavelength of 1.5 μm. The band gap of the alloy varies from 1.42 eV (870 nm) for GaAs up to 2.17 eV (570 nm) for AlAs[1].

2.1.2. Fabrication of AlGaAs.

Molecular-beam epitaxy and vapour-phase epitaxy are two of the common methods which are used in the production of high quality epitaxial semiconductors[2]. Epitaxial growth involves the crystalline growth of thin layers of the semiconductor material on a crystalline substrate base. The thickness, doping and composition of the layers are all well controlled in these processes. In this study, the AlGaAs wafers had been fabricated using molecular beam epitaxy (MBE). In this section the basics of the MBE technique are described.

Figure 2.2[3] is a greatly simplified schematic diagram of the MBE machine. The substrate, in this case GaAs, is placed on a heated rotating holder, at 600°C, which is rotated through the growth process to ensure that crystal growth is uniform over the substrate surface. The elements Ga, As and Al are contained within furnaces called Knudsen cells (K-cells) which have openings in the direction of the substrate and have shutters placed in front of these openings so that the escape of molecules from each of the cells can be controlled. The growth process is conducted in a chamber which is evacuated to a very low pressure of $\sim 5\times10^{-11}$ mbar. At this low pressure molecules emerging from the cells form beams which travel in straight lines and do not interact with each other. When these beams reach the substrate surface they cause crystal growth. The position of the shutters and the temperature of the K-cells determine the composition of the crystal growth.

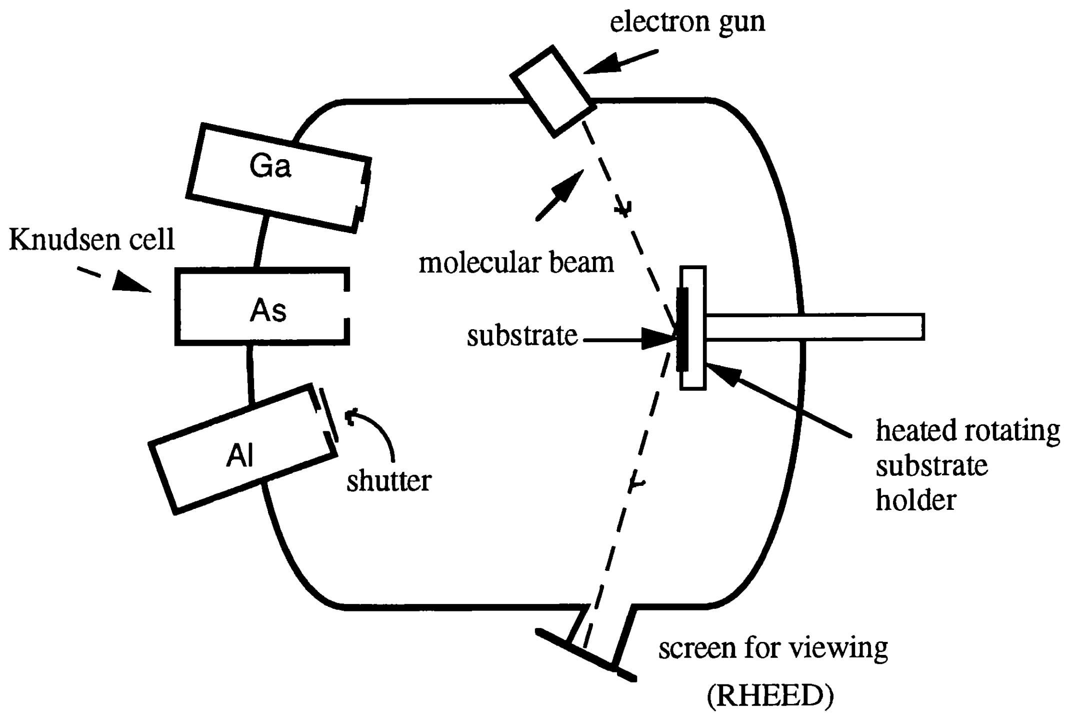

Figure 2.2. Simplified schematic of the MBE process. (Ref. 10).

2.2. Band structure of III-V Compound Semiconductors.

Figure 2.3 shows the four band Kane model[4] which is commonly used to describe the band structure of III-V compound semiconductors. The model consists of one doubly-degenerate conduction band and three doubly-degenerate valence bands (light hole, heavy hole, split off). GaAs has eight outer electrons and of these eight, two electrons fill S-like states, referred to as the light hole band, where each electron has a total angular momentum of 1/2 .The other six electrons fill the P-like states and have a total angular momentum of 3/2 and are referred to as the heavy hole band. Fundamental optical absorption occurs between the heavy/light hole valence bands and the first electron level in the conduction band. At higher photon energies transitions involving the lower split off valence band, which is seperated from the light and heavy hole bands by 0.34 eV due to spin-orbit splitting, take place.

GaAs is a direct band gap semiconductor where the position of the minimum energy of the conduction band occurs at the same value of k, the wave vector of the electron, as the maximum of the energy of the valence band. An electron moving from the top of the valence band to the bottom of the conduction band changes its energy but not its momentum. This leads to a sharp band-edge. In contrast, for indirect band gap materials such as silicon and germanium the transition of an electron from the valence to the conduction band involves a change in both the energy and momentum. The additional momentum is provided by a lattice vibrational phonon.

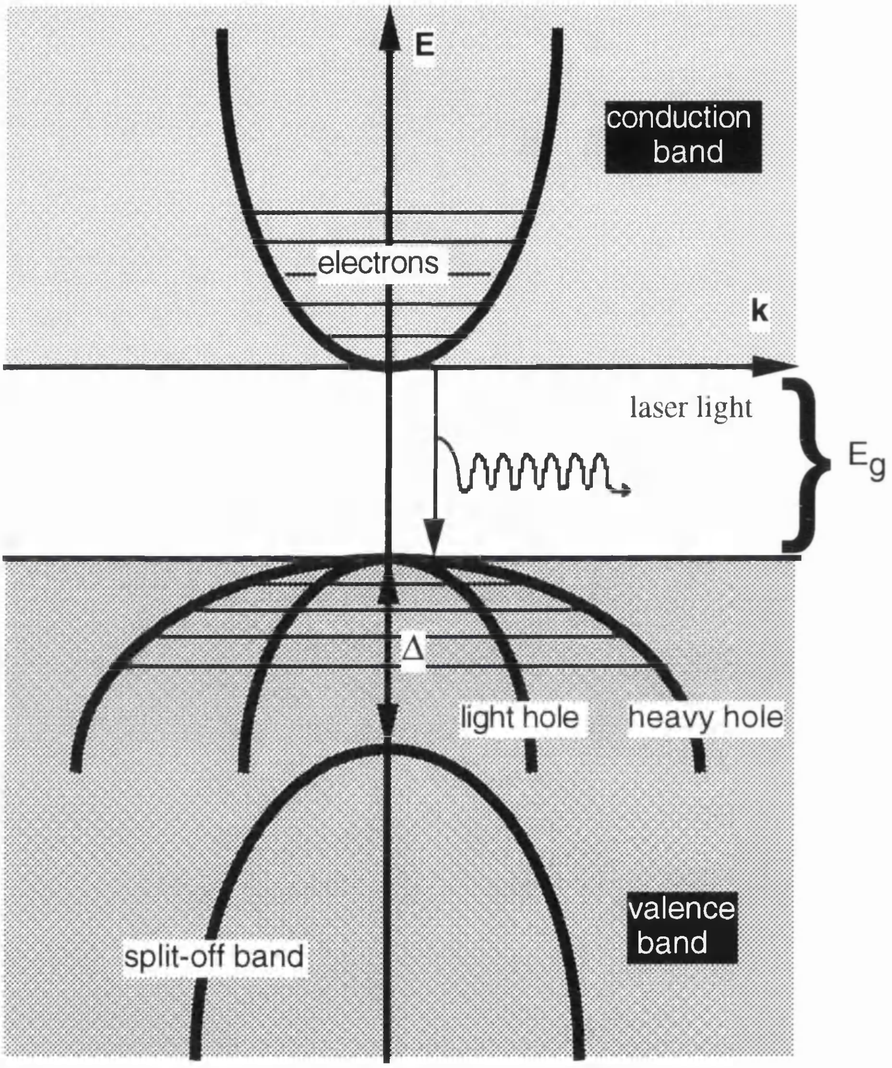

Figure 2.3. Band structure of III-V compound semiconductors as given by the Kane model.

2.3. Types of Nonlinearities in Direct Gap Semiconductors.

The magnitude and origin of n_2 in compound semiconductors depends on the wavelength of the incident light beam in relation to the position of the band-gap of the semiconductor. In general the optical nonlinearities fall into two categories, i.e. they are either resonant or nonresonant.

2.3.1. Resonant Nonlinearities.

The resonant nonlinearities occur at optical wavelengths close to the linear bandgap absorption edge. There are several different mechanisms which are responsible for the nonlinear response including band filling[5], excitonic effects[6], plasma[7] and opto-thermal effects[8].
In general these processes involve the absorption of light, resulting in the establishment of real excited populations which through the Kramers-Krönig relation, as discussed in section 2.4, leads to a change in the refractive index of the material. Such effects produce large optical nonlinearities. However, the response times of these effects, which are governed by the relaxation time of the electrons from the excited states, are slow (about a few nanoseconds). The speed can be improved by applying an electric field to remove the carriers. However, the absorption of light results in a low throughput (10%) and undesirable thermal effects. Devices based on resonantly enhanced nonlinearities are also very wavelength sensitive and can suffer from saturation effects. On the whole this type of nonlinearity is not suitable for ultrafast switching applications.

2.3.2. Non-Resonant Nonlinearities.

Nonresonant nonlinearities occur at photon energies far from the bandgap absorption edge where the change in the optical properties of the material is caused directly by the optical field. In AlGaAs operated below half the band gap the nonlinear refractive index is approximately 1.5×10^{-13} cm^2/w. Nonresonant processes are almost instantaneous and wavelength insensitive and are therefore, suited for ultrafast switching applications. However, they do require larger intensities than the resonant nonlinearities but in contrast to resonant nonlinearities the performance of a nonresonant device is not limited by linear absorption effects.

2.4. Measurement of the Nonlinear Coefficient.

2.4.1. Kramers-Krönig Relation.

The Kramers-Krönig (K-K) formalism is a common dispersion relation equation in linear optics which relates the refractive index, n, of a material to the absorption coefficient, α, over all frequencies, Ω and can be expressed by[9]:

$$n(\omega) - 1 = \frac{c}{\pi}\int_0^\infty \frac{\alpha(\Omega)d\Omega}{\Omega^2 - \omega^2} \qquad (2.1)$$

The K-K formalism can be modified to calculate a change in refractive index, Δn, from a change in absorption, Δα, due to some external perturbation, ξ. For example in a resonant nonlinear process the material excitation can be regarded as the perturbation. The change in refractive index is derived by applying the relation (2.1) to a system, before and after the perturbation and then taking the difference between the two cases. The change in refractive index can be expressed as:[9]

$$\Delta n(\omega;\xi) = \frac{c}{\pi}\int_0^\infty \frac{\Delta\alpha(\omega',\xi)}{\omega'^2 - \omega^2}\partial\omega' \qquad (2.2)$$

This expression has been used in the past to calculate the dispersion of the nonlinear refraction coefficient, n_2, since the index change induced by the local intensity, I, is related to n_2 by the following equation:

$$\Delta n = n_2 I \qquad (2.3)$$

The scaling and dispersion of n_2 in a semiconductor crystal over the entire spectral range for photon energies below the fundamental absorption edge has been carried out using the K-K formalism. The calculations showed that in the half-band gap spectral region there is an enhancement in the size of n_2, and that the magnitude of n_2 depends on E_g^{-4}. In that analysis a two-parabolic band model was used and two-photon absorption and the ac stark shift were assumed to be the dominant nonlinear absorption processes[10].

2.4.2. Higher Band Models.

Studies have shown that the magnitude of n_2 depends on the polarisation of the light and also on the orientation of the crystal. In order to study the effects of the polarisation on the nonlinear refraction coefficient as well as its anisotropy, the K-K method for calculating the dispersion of n_2 has recently been superseded by methods based on calculating n_2 directly from the real part of the nonlinear susceptibility using higher band structure models.

The 4 band Kane model, shown in fig. 2.3 has been used to obtain the dispersion of the nonlinear refractive index of direct-gap semiconductors. The standard expression for n_2 obtained using perturbation theory is given by [10]:

$$n_2(\omega) = \frac{3}{4\varepsilon_0 c n_0^2} \mathrm{Re}\,\chi^{(3)}_{xxxx}(-\omega,\omega,\omega,) \quad (2.4)$$

It was found using this model that $\chi^{(3)}_{xxxx}$ can be expressed as:

$$\chi^{(3)}_{xxxx} \propto \frac{\sqrt{E_p}}{E_g^4} f(\hbar\omega/E_g, \Delta/E_g) \quad (2.5)$$

where $f\left(\hbar\omega/E_g, \Delta/E_g\right)$ is a dimensionless spectral function and Δ is the energy difference between the upper valence band and the split off energy band as illustrated in fig. 2.2. E_p is the Kane momentum energy given by:

$$E_p = \frac{2m\,P^2}{\hbar^2} \approx 20\ \mathrm{eV} \quad (2.6)$$

where P is the Kane momentum parameter and m is electron mass.

A seven band model[11,12] has also been used to study the effects of dichroism on the value of n_2 in zinc-blende semiconductor compounds and in additon the effects of the crystallographic orientation on the magnitude of n_2 have been studied using this higher band model. Dichroism produces different values of n_2 for linear and circular polarised light. It was seen from this analysis that:

$$n_2(TE) > n_2(TM)$$

Figure 2.4 shows the recent experimentally measured dispersion of the nonlinear refraction coefficient for $Al_{0.18}Ga_{0.82}As$ for TE and TM polarisation, obtained by measuring the self-phase modulation of a light pulse propagating through the material[11].The samples used in this experiment consisted of 5 μm wide strip loaded AlGaAs waveguides etched 1.35-1.45 μm deep into the top cladding layer of an AlGaAs wafer with the following structure: The guiding region was composed of a 1.5μm thick $Al_{0.18}Ga_{0.82}As$ layer.The upper cladding was a 1.5μm thick $Al_{0.24}Ga_{0.76}As$ layer and the lower cladding was a 4μm thick $Al_{0.24}Ga_{0.76}As$ layer.

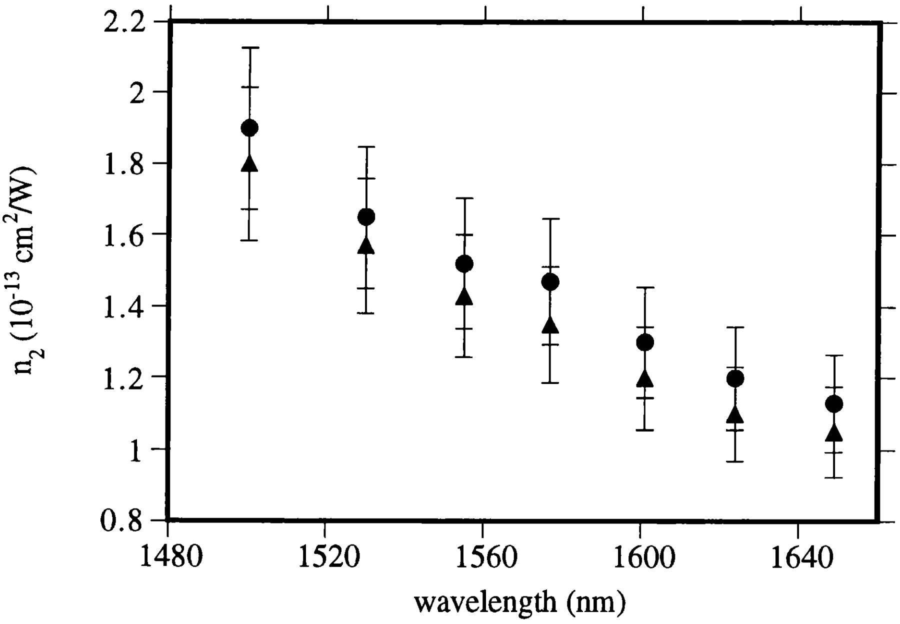

Figure 2.4. The measured dispersion of n_2 for TE (solid dots) and TM (solid triangles) light.

2.5. Multi-Photon Absorption in AlGaAs Guides.

In this study switching configurations composed of AlGaAs waveguides are investigated. The loss experienced by a light field propagating through the AlGaAs guide can be expressed as[13]:

$$\frac{dI(z)}{dz} = -\alpha I - \alpha_2 I^2 - \alpha_3 I^3 \ldots\ldots \quad (2.7)$$

where I is the light intensity, α, is the linear absorption coefficient and α_2 and α_3 are the two-photon and three-photon absorption coefficients respectively. At low light intensities linear loss is the dominant loss mechanism. The linear loss is dependent on the energy of the photons, scattering and thermal effects. If L is the length of the guide then the intensity of the light propagated through guide is related to the incident light intensity, I_0 into the guide by the following equation:

$$I = I_0 e^{-\alpha L} \quad (2.8)$$

When the energy of a light photon E_{ph} given by:

$$E_{ph} = \hbar\omega \quad (2.9)$$

is larger than the bang-gap energy, E_g, of the semiconductor, a direct inter-band transition can occur. This means that a single photon is absorbed and results in the transition of an electron from the valence band to the conduction band. At photon energies well below the band-gap energies i.e. at half-the band gap direct inter-band transitions are not possible and so the linear loss is mainly due to scattering losses and thermal effects. Linear loss in AlGaAs operating in the half-band gap spectral region is discussed further in chapter 3.

As the light intensity increases the effect of two- and three-photon absorption increase and can drastically affect the performance of a nonlinear switching device.

2.5.1. Two-Photon Absorption.

When the energy of the photon is below the band-gap energy in the range expressed by:

$$\frac{1}{2}E_g < \hbar\omega < E_g$$

then the transition of an electron from the valence band to the conduction band requires the absorption of two-photons. Two-photon absorption is related to the imaginary part of the third order nonlinear susceptibility as discussed in section 1.4 and is dependent on the intensity of the light as expressed in (1.15).

The dispersion of the two-photon absorption coefficient for AlGaAs operating below the fundamental band gap has been analysed using the Kane band model. It was found that the two-photon absorption coefficient can be expressed as:[5]

$$\alpha_2 = K\frac{\sqrt{E_p}}{n^2E_g^3}f\left(\frac{\hbar\omega}{E_g}\right) \qquad (2.10)$$

where E_p is the Kane momentum energy and K is a material independent constant given by:

$$K = \frac{2^9\pi}{5}\frac{e^4}{\sqrt{m_0}c^2} \approx 3100\ \mathrm{cmGW^{-1}eV^{5/2}} \qquad (2.11)$$

where e,m_0 and c are the charge,free electron mass and the speed of light respectivley.

The function $f\left(\hbar w/E_g\right)$ is related to the band structure of the semiconductor. For semiconductors with parabolic energy bands $f\left(\hbar w/E_g\right)$ is given by:

$$f\left(\frac{\hbar\omega}{E_g}\right)=\frac{\left(2\frac{\hbar\omega}{E_g}-1\right)^{\frac{3}{2}}}{\left(2\frac{\hbar\omega}{E_g}\right)^{5}} \quad (2.12)$$

To observe efficient switching within a nonlinear device, such as a nonlinear directional coupler in the presence of two photon absorption, the following condition must be met[14]:

$$\alpha_2 a_2 I_c L_c < 0.5 \quad (2.13)$$

where I_C is the critical switching intensity, a_2 represents the overlap integral over the mode profiles in the waveguide for the third order nonlinearity and L_C is the half beat coupling length.

Figure 2.5 shows the recent experimental measurement of the dispersion of the two-photon absorption coefficient for both TE and TM polarised light[11]. The AlGaAs waveguides used in this experiment were the same as those described in section 2.4.2.

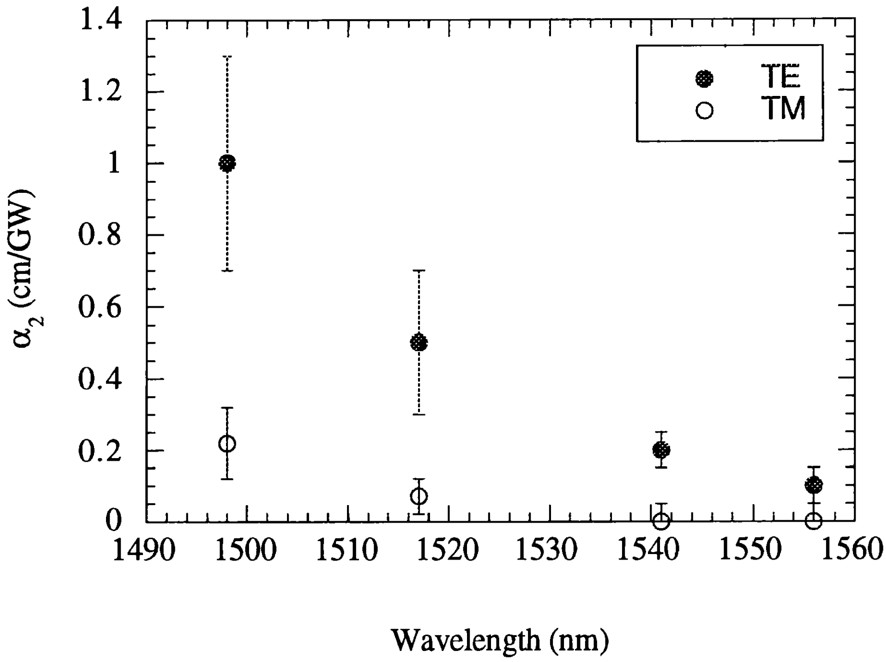

Figure 2.5. The experimentally measured values of α_2 as a function of wavelength for TE (solid circles) and TM (open circles) light for 5μm wide strip loaded AlGaAs waveguides.

The two photon absorption coefficient exhibits optical polarisation dependence due to the fact that the third order susceptibility tensor contains off-diagonal elements.

2.5.2. Three Photon Absorption.

Three photon absorption (3PA) is a fifth order absorption process involving the simultaneous absorption of three photons. Three photon absorption occurs when the energy of the photons are below the half-band gap spectral region. The value of the three photon absorption coefficient, α_3, for AlGaAs operating below the band-gap has been defined as[15]:

$$\alpha_3 = \frac{3^{10}\sqrt{2}}{8}\pi^2\left(\frac{e^2}{\hbar c}\right)^3 \frac{\hbar^2 E_p^{\;3}}{n_0^3 E_g^7} \frac{\left(3\frac{\hbar\omega}{E_g}-1\right)^{\frac{1}{2}}}{\left(3\frac{\hbar\omega}{E_g}\right)^9} \qquad (2.14)$$

The criterion for nonlinear switching in the presence of three photon absorption requires that [14]:

$$I_c^2\alpha_3 a_3 L_c < 1 \qquad (2.15)$$

where a_3 is the overlap integral over the mode profiles in the waveguides for the fifth-order nonlinearity.

Figure 2.6 shows the theoretically calculated dispersion of the three photon absorption coefficient for different concentrations of Al[11].

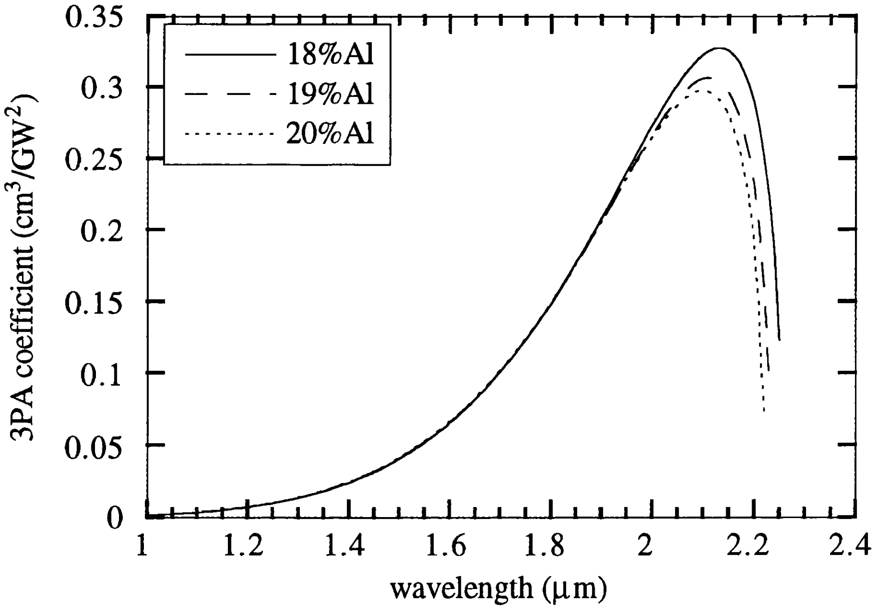

Figure 2.6. The calculated dispersion of α_3 for different concentrations of Al.

This graph shows that the three photon absorption coefficient is at a maximum at a wavelength of ~ 2.1 μm. However, in the half band gap region the 3PA coefficient is still large enough to affect the switching efficiency of an all-optical switch. Figure 2.7 shows the recent experimentally measured dispersion of α_3 calculated using the AlGaAs waveguides as described in section 2.4.2. These experimental results agree well with the theoretically predicted dispersion of α_3.

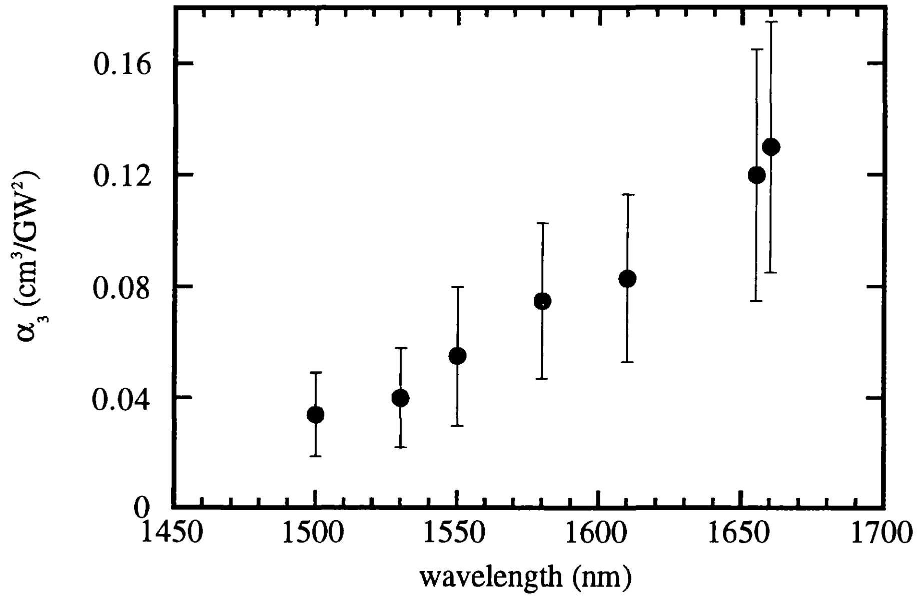

Figure 2.7 Experimental values of α_3 as a function of wavelength.

2.6. Conclusions of Chapter.

In this chapter the nonlinear properties of AlGaAs were outlined. In particular the crystal and band structure of AlGaAs were discussed. In addition, the techniques used to estimate the dispersion of the nonlinear refraction coefficient and nonlinear absorption coefficients of AlGaAs were described. AlGaAs was found to have various attributes which make it an ideal material for the observation of nonlinear switching effects including the fact that when operating below half-the band gap spectral region there is an enhancement in the nonlinear coefficient and the effects of two-photon absorption are minimised.

References.

1. A. Villeneuve, "Optical nonlinearities and applications of semiconductors near half the band gap", Ph. D. Thesis , University of Arizona (1992).
2. E.F. Scubert, "Dopings in III-V semiconductors", Cambridge University Press, chp.4, pp 137-164 (1993).
3. J.H. Davies, "Heterostructures", University of Glasgow lecture notes, pp 68-96 (1994).
4. E.O. Kane, " Band structure of Indium Antimonide", J. Phys. Chem. Solids, **1**, pp 249-261 (1957).
5. A. Villeneuve, "Optical nonlinearities and applications of semiconductors near half the band gap", Ph. D Thesis , University of Arizona, Chp. 2 (1992).
6. F.R. Laughton, "Nonresonant optical nonlinearities in GaAs/AlGaAs multiple quantum well waveguides", Ph. D Thesis, University of Glasgow, chp.2 (1991).
7. D.A.B. Miller, S.D. Smith and B.S. Wherrett, "The microscopic mechanism of third order nonlinearity in InSb", Opt. Commun. , **35**, pp 221-224 (1985).
8. M.C. Gabriel, H.A. Haus and E.P. Ippen, "Thermal index changes by optical absorption in group III-V semiconductor waveguides", J. Lightwave Tech. , **4**, pp 1482-1493 (1986).
9. D.C. Hutchings, M. Shiek-Bahae, D.J. Hagan and E.W. Van Stryland, "Kramers-Krönig relations in nonlinear optics", Opt. and Quant. Elec. , **24**, pp 1-30 (1992).
10. D.C. Hutchings and B.S. Wherret, "Theory of the dipersion of ultrafast nonlinear refraction in zinc-blende semiconductors below the band-edge", Phys. Rev. ,**50**, pp 4622-4630 (1994).
11. J.S. Aitchison, D.C. Hutchings, J.U. Kang, G.I. Stegeman and A. Villeneuve, "The nonlinear optical properties of AlGaAs at the half band gap", IEEE J. of Quant. Elec. , **33**, pp 341-347 (1997).
12. D.C. Hutchings, B.S. Wherret, "Theory of the anisotropy of ultrafast nonlinear refraction in zinc-blende semiconductors", Phys. Rev. B, **52**, pp 8150-8159 (1995).
13. J.U. Kang, A. Villeneuve, M. Sheik-Bahae, G.I. Stegeman, K. Al-Hemyari, J.S. Aitchison and C.N. Ironside, "Limitation due to three-photon absorption on the useful spectral range for nonlinear optics in AlGaAs below halfband gap.", Appl. Phy. Lett. , **65** , pp147-149 (1994).
14. C.C. Yang, A. Villeneuve and G.I. Stegeman, "Effects of three-photon absorption on nonlinear directional coupling", Opt. Lett. **17**, pp 710-712 (1992).
15. B.S. Wherrett," Scaling rules for multiphoton interband absorption in semiconductors", Opt. Soc. Am. B, **1**, pp 67-72 (1984).

CHAPTER 3

Semiconductor Waveguide Design, Fabrication and Characterisation.

Introduction.

Semiconductor waveguides are attractive elements for the implementation of a range of all-optical switching devices since high optical power densities can be maintained over long interaction lengths. To date ultrafast switching has successfully been demonstrated in nonlinear directional couplers[1], Mach-Zender interferometers[2] and X-junction devices[3]. In this chapter the design, fabrication and characterisation of semiconductor waveguides for ultrafast switching effects will be discussed.

The chapter begins with an outline of the main properties of semiconductor waveguides. In section 3.2 basic waveguide theory is reviewed and in particular the equations which describe the propagation of electromagnetic waves within a slab waveguide are summarised. Section 3.3 describes the different waveguide configurations and the parameters used in the design of the guides. This includes a discussion of the sources of linear loss. The fabrication process used to produce waveguides is covered in section 3.4 and the methods used for linear characterisation are outlined in section 3.5. In section 3.6 the experimental set up used to observe nonlinear effects within the guides is described and measurements of the nonlinear characteristics of the waveguides are presented. Finally, in section 3.7 the conclusion drawn from the chapter are summarised.

3.1. Properties of Semiconductor Optical Waveguides.

Semiconductor waveguides are ideal elements for the construction of nonlinear, all-optical devices. The main attributes of such waveguides will be outlined below.

3.1.1.1. Optimum Geometry.

Nonresonant nonlinearities are small compared to their resonant counterparts, i.e. n_2 for AlGaAs operating in the half band gap region is approximately 1×10^{-13} W/cm^2. Therefore, to observe ultrafast all-optical switching effects the nonlinear phase shift required must be accumulated over a large propagation distance. Optical waveguides provide the optimum interaction geometry, since they allow high optical intensities to be maintained over long propagation lengths. The waveguides enable diffractionless propagation in one, or two, transverse directions. By contrast in a non-waveguide geometry, diffraction limits the length over which the high optical intensity can be maintained. In addition, the index of refraction of compound semiconductors such as AlGaAs can be easily altered, as discussed in chapter 2. The waveguides can then be constructed from an AlGaAs wafer composed of different layers of AlGaAs grown one on top of another.

3.1.2.1 Compactness and Potential for Monolithic Integration.

Future communication and computing networks require compact integrated optical devices for coupling, modulating and switching applications. Semiconductor waveguide devices are typically a few centimetres in length and are therefore, much more compact than equivalent fibre devices which can be tens of meters long. Semiconductor waveguides can also be integrated with other opto-electronic/ electronic components. For example, a GaInAsP/InP directional coupler switch has been successfully monolithically integrated with a tunable MQW-DBR laser[4].

3.1.1.3. Mature Fabrication Technology.

Semiconductors have a mature, advanced fabrication technology which allows a wide range of complex integrated devices to be fabricated. Another advantage of semiconductor waveguides is that the scribe and cleave technique used for end facet preparation in these guides is simple as opposed to the cut and polish method used in other nonlinear materials such as $LiNbO_3$ and glass. The resulting waveguides can also have very low propagation losses.

3.2. Basic Optical Waveguide Theory.

3.2.1. Snell's Law and Total Internal Reflection.

The propagation of light in a dielectric waveguide can be described in terms of geometric optics. This approach allows the major waveguide properties to be defined. However, it should be noted that this approach is approximate and a full description requires the application of Maxwell's equations with the appropriate boundary conditions. When a light ray strikes the boundary between two transparent media at an angle θ, a fraction of the light will be reflected while the rest of the light is transmitted through the interface at an angle known as the refracted angle. Figure 3.1 shows an incident light ray i, incident on an interface between two media and the resulting reflected, r, and transmitted fraction, t, of the ray. The relationship between the incident and transmitted ray is given by the law of refraction commonly known as Snell's laws, as stated below[5]:

$$n_1 \sin\theta_i = n_2 \sin\theta_t \qquad (3.1)$$

where θ_i and θ_t are the angles the light makes with the normal to the interface in the mediums with refractive index n_1 and n_2 respectively.

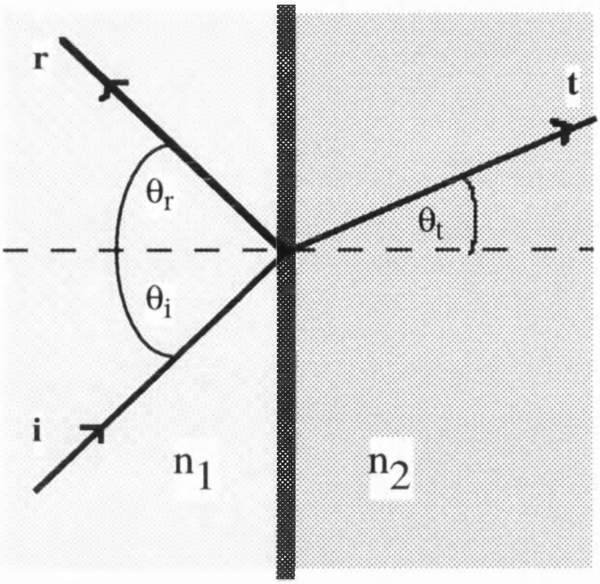

Figure 3.1. Shows the incident, reflected and transmitted rays at an interface boundary between two different media with refractive indices n_1 and n_2 .

When light travels from a medium of index n_1, to a lower index region n_2 there is a specific angle of incidence, θ_c, for which the refracted ray will propagate parallel to this surface. This is called the critical angle. If the incident angle is greater than θ_c the light is totally reflected by the interface.

From Snell's law θ_c is given by;

$$\theta_c = \sin^{-1}\left(\frac{n_2}{n_1}\right) \qquad (3.2)$$

An important feature of the total internal reflection process is that when a light ray is reflected by an interface the ray will penetrate slightly into the low index medium producing an evanescent field. In addition there is a phase shift upon reflection.

3.2.2 Propagation of Light in a Dielectric Slab Waveguide.

In this section ray optics will be used to describe the propagation of an EM wave in a slab waveguide. The slab waveguide consists of a transparent dielectric material of high refractive index sandwiched between two layers of dielectric material with lower refractive index. Figure 3.2 illustrates the path of a ray as it propagates through such a dielectric slab. Propagation of light in a slab dielectric medium is similar to that of light travelling through an optical fibre.

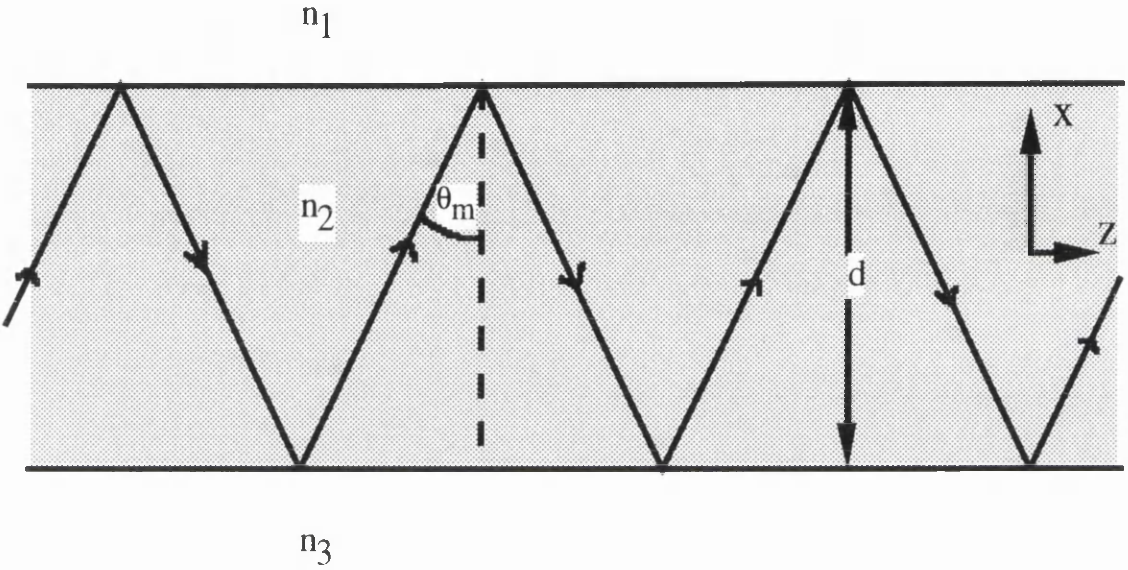

Figure 3.2. illustrates the path of a ray of light travelling within the guiding region of a dielectric slab .

The conditions which must be satisfied to achieve guiding within a dielectric slab can be summarised as follows :

1 . The refractive index of the guiding medium must be greater than those of the adjacent layers, i .e . $n_2 > n_1, n_3$.

2 . The angle θ_m must be greater than the critical angle θ_c.

3. For a guided wave the transverse field must form a standing wave. If not then it will be a travelling wave and the field will dissipate power. This means that the total phase change experienced by a light ray in one round trip across the waveguide must be an

integral number of 2π. This rule can be expressed by the following equation:

$$\frac{2d}{\lambda_x}2\pi - 2\phi = 2m\pi \qquad (3.3)$$

where ϕ is the polarisation sensitive, phase change experienced by the ray when reflected from the index boundaries and λ_x is the wavelength of the transverse E_x field.

Mode cut off occurs at low incident frequencies, when the angle of incidence is low enough to inhibit total internal reflection, causing the light to escape from the guiding region into the surrounding medium.

It can be shown that the mode angle θ_m , of each mode propagating in the guide is given by:

$$\cos\theta_m = \frac{(m\pi + \phi)\lambda_0}{2\pi d n_2} \qquad (3.4)$$

where λ_0 is the wavelength of the light in vacuum.

3.2.3. Maxwell's Equations.

Since light is an electromagnetic field, the wave characteristics of modes propagating within the simple slab guide can also be determined using Maxwell's equations. These equations are mathematical formulae which describe the propagation of electromagnetic fields in materials, were the wavelength is much bigger than the atomic, or molecular dimensions. In this section the basics mode equations are discussed. For complete derivation of the mode solutions for the slab guide see ref. 6.

Assuming the waveguide medium is nonconductive, has no charges and is isotropic the equations which described the electric and magnetic fields within the slab guide are as follows:

$$\nabla \bullet \varepsilon E = 0 \qquad (3.5a)$$

$$\nabla \bullet \mu \mathbf{H} = 0 \quad (3.5b)$$

$$\nabla x \mathbf{E} = -\mu\mu_0 \frac{\partial \mathbf{H}}{\partial t} \quad (3.5c)$$

$$\nabla x \mathbf{H} = \varepsilon\varepsilon_0 \frac{\partial \mathbf{E}}{\partial t} \quad (3.5d)$$

where E and H are the electric and magnetic field strengths, μ_0 and μ are the permeability of free space and of the material respectively, while ε_0 and ε are the permittivity of free space and the permittivity of the material respectively. By taking the curl of equation 3.5c the following equation is obtained.

$$\nabla x \nabla x \mathbf{E} = \nabla(\nabla . \mathbf{E}) - \nabla^2 \mathbf{E} = -\mu\mu_0 \frac{\partial(\nabla x \mathbf{H})}{\partial t} \quad (3.6)$$

Substituting equation 3.5d into equation 3.6 gives:

$$\nabla^2 \mathbf{E} = \mu\mu_0\varepsilon\varepsilon_0 \frac{\partial^2 \mathbf{E}}{\partial t^2} = \left(\frac{n}{c}\right)^2 \frac{\partial^2 \mathbf{E}}{\partial t^2} \quad (3.7)$$

Assuming the wave is monochromatic, travelling in the z direction and is confined only in the x direction, the electric field E and magnetic field H can be expressed by the following :

$$\begin{aligned} \mathbf{E} &= \mathbf{E}(x,y)e^{i(\omega t - \beta z)} \\ \mathbf{H} &= \mathbf{H}(x,y)e^{i(\omega t - \beta z)} \end{aligned} \quad (3.8)$$

Combining equation (3.8) and (3.7) gives:

$$\nabla^2 \mathbf{E}(x,y) + k_0^2 n^2 \mathbf{E}(x,y) \quad (3.9)$$

where $k_0=2\pi/\lambda_0$.

In a one dimensional slab waveguide where δ/δy=0, two types of solution exist for the equation 3.9 depending on the polarisation of the light. The first is known as the transverse electric, or (TE) modes, these are composed of Ey, Hx, Hz components only. The second is known as the transverse magnetic fields or (TM) which are composed of the Hy, Ex and Ez components. Using equation 3.9 the TE fields propagating within the three separate regions of the slab guide can be described by the following equation.

$$\frac{\partial^2 E_y}{\partial x^2}+(k_o^2 n_i^2-\beta^2)E_y=0 \quad (3.10)$$

where i=1, 2, 3. Similarly the TM modes are described by:

$$n_i^2\frac{\partial}{\partial x}\left[\frac{1}{n_i^2}\frac{\partial H_y}{\partial x}\right]+\left(n_i^2 k_0^2-\beta^2\right)H_y=0 \qquad (3.11)$$

The TE and TM guided mode solutions can be obtained by solving equations 3.10 and 3.11 with suitable the boundary conditions. At the interface for TE modes, Ey and δEy/δx must be continuous. Likewise for TM modes, Hy and δHy/δx must be continuous. It should be noted that as x tends to plus or minus infinity then Ey or Hy will tend to zero.

Figure 3.3 illustrates the different type of fields which propagate within the 3 regions which make up the slab guide. As shown in figure 3.3 the guided waves of the slab obey the following condition $k_0n_3 < \beta < k_0n_2$ and correspond to a field which varies in a sinusoidal manner within the guiding layer and exponentially decays in the lower index regions.

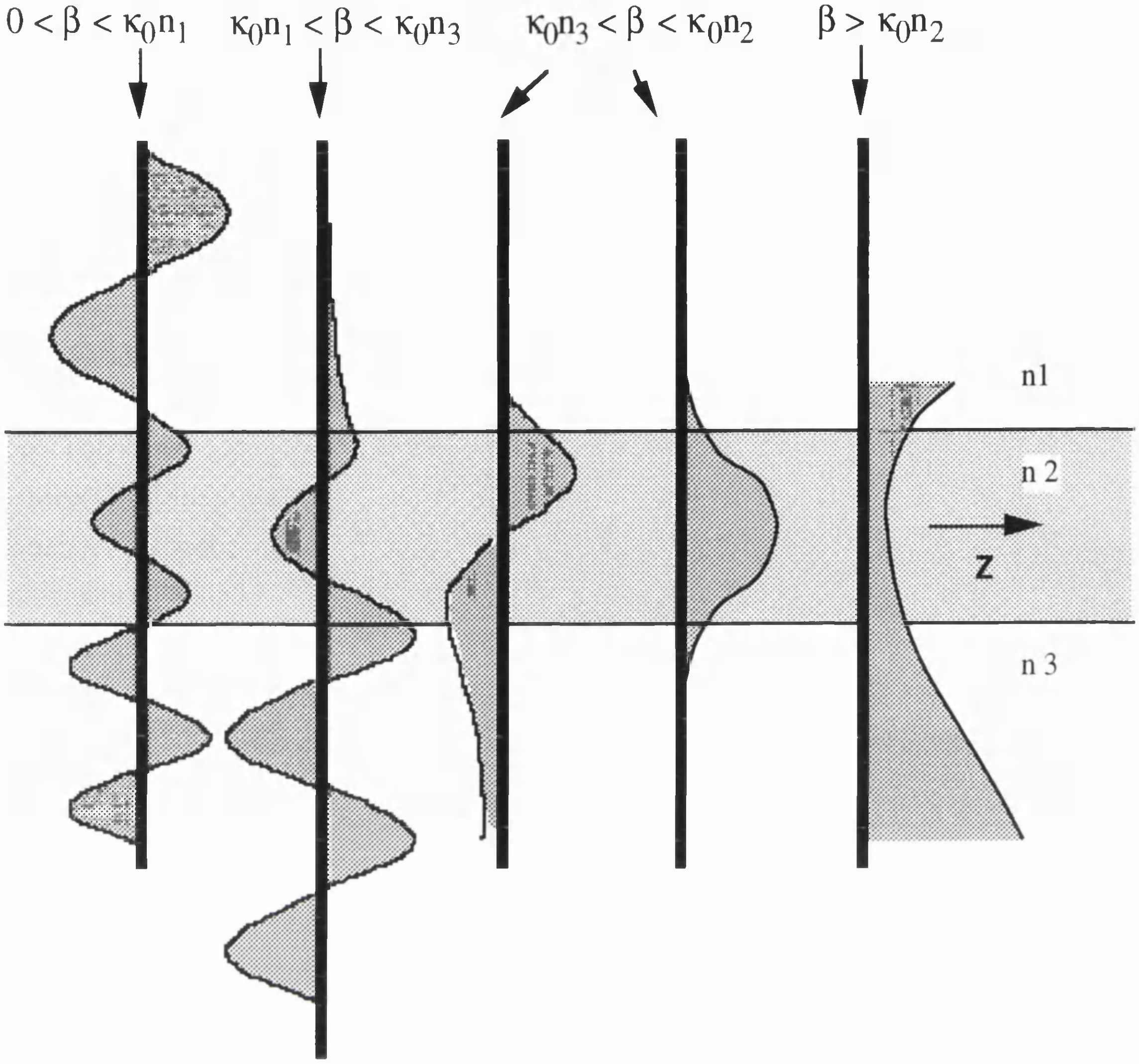

Figure 3.3. Illustrates the field characteristics in each layer of the slab guide for various values of propagation constant.

3.3 Optical Waveguide Design.

In the waveguide design process, the important factors which must be taken into account include, the operating wavelength, geometry of the waveguide structure, losses within the structure and wafer composition.

In this research single mode AlGaAs waveguides operating below the half-band gap and within the low loss communications window at 1.55 μm were fabricated. In this spectral region the detrimental effects due to two photon and three photon absorption can be minimised .

3.3.1. Waveguide Geometries.

In section 3.2 we looked at the simple slab guide were the light is confined in one transverse dimension. In practical waveguide structures light must be confined is two dimensions. Vertical confinement is usually achieved by refractive index differences between the layers which make up the wafer. In the lateral direction, optical confinement can be introduced in several ways including carrier indiffusion and superlattice disordering. However, the most frequently used method is by etching a rib into the material layers. The confinement is then due to effective index differences between the etched and unetched regions. Figure 3.4 below illustrates four types of rib waveguide structures that are commonly used.

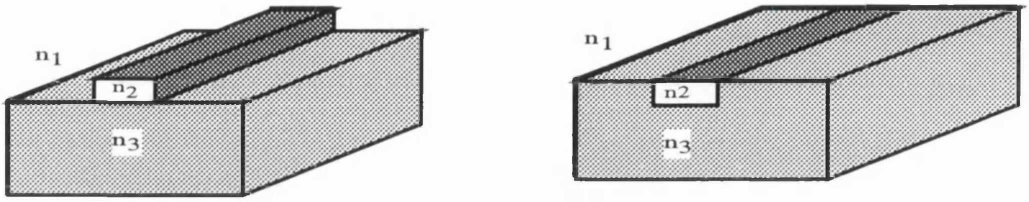

a] strip guide

b] embedded strip guide

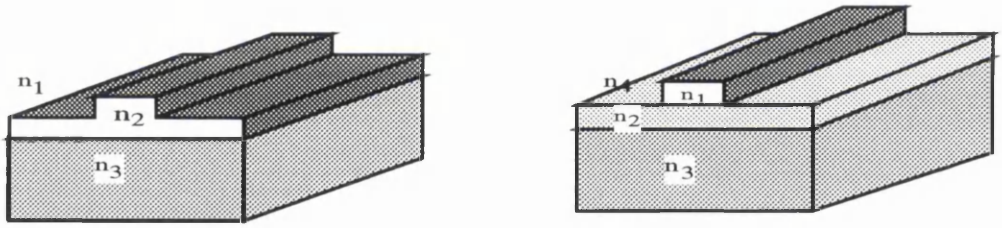

c] ridge waveguide

d] strip loaded guide

Figure 3.4. Illustration of the various method of lateral confinement by using various types of rib waveguide geometries used.

In this research strip loaded guides were fabricated. This structure was chosen as both coupled waveguides, grating structures on ridge guides and curved waveguides can be fabricated. The guiding characteristics of the guide can be controlled by varying the height, or width, of the rib structure. In general deeply etched ridges produce strongly confined modes suitable for the production of curved structures. Shallower ribs form weaker guides which are suitable in coupled waveguide and grating systems.

3.3.2. Sources of Linear Loss within Semiconductor Waveguides.

Low loss waveguides are essential for optical guided wave applications. Therefore, potential sources of loss within optical waveguides and the ways in which these loss mechanisms can be reduced are important factors which need to be considered when designing waveguides.

Linear propagation losses within AlGaAs waveguides operating below half the band gap are caused by a combination of absorption, scattering and leakage[7]. In this section we look at each source of loss in turn and discuss the methods employed in this research to reduce these loss mechanisms.

3.3.2.1. Scattering losses are caused by epilayer and rib sidewall roughness and also scattering from imperfections. In this research the AlGaAs wafer used to fabricate the waveguides was grown by MBE, which results in high quality layers with minimum scattering. Losses due to sidewall roughness have been shown to depend on the rib width and also on $(\Delta n_{eff})^2$, where Δn_{eff} is the effective index differences between the etched and unetched regions of the waveguide. The smaller the rib width and deeper the rib is etched, the greater the scattering loss in the optical waveguides. With this in mind the width of the guides in this research were chosen to be 4 μm wide. In addition, the guides were fabricated using an up to date photolithographic and dry etch process which has been shown to produce guides with excellent surface/sidewall definition[8].

3.3.2.2. Leakage of light from the guiding region into the substrate layer occurs when the substrate material has a similar, or higher refractive index to the guiding layer. This loss decreases exponentially with the cladding thickness. Therefore, loss due to leakage can be reduced by growing a thick lower cladding layer.

3.3.2.3. Absorption is also a major source of loss in AlGaAs guides. Operating at a wavelength below half band gap avoids linear absorption. However, defect and impurity absorption can also occur in AlGaAs waveguides. Defect absorption can occur through lattice mis-matching. In this research the wafers used to fabricate the guides were composed of various AlGaAs layers which were almost lattice matched and were fabricated as mentioned earlier using a well controlled MBE process which minimised the introduction of impurities and defects into the AlGaAs material grown.

3.3.3. Wafer Composition.

The composition of the AlGaAs wafer grown was as follows. The substrate used was GaAs which has a high refractive index of 3.43 at 1.5 μm. To ensure light confinement in the guiding layer and to prevent leakage of the light into the substrate layer, a lower AlGaAs cladding layer, 4 μm thick and containing 24% Al, with a refractive index of 3.305 at 1.5 μm, was grown on top of the substrate before the growth of the waveguide layer. The AlGaAs guiding layer was 1.5 μm thick, contained 18% Al and had a index of refraction of 3.336 at 1.5 μm. Finally the upper AlGaAs cladding was 1 μm thick with 24% Al. The refractive index of the AlGaAs layers were calculated using the Adachi method.[9]

3.3.4 Estimation of the Propagation Constant.

To calculate the propagation constant of an optical waveguide many numerical techniques have been used including the beam propagation method (BPM), the effective index method (EIM) and finite element, finite difference and variational techniques. These techniques provide an estimation of the effective index, or propagation constant, of the mode and the mode field profile. They can therefore, be used to determine how many modes propagate in a particular waveguide structure and how well the modes are confined. The two methods used in this research are outlined in the following section.

3.3.4.1. The Effective Index Method (EIM).

This is an approximate method whereby the effective indices of the guided modes are estimated by considering the slab regions which make up the guide structure. The EIM produces accurate results providing the modes are far from the cut off[10] and the height of the slab regions do not differ greatly from one another.

Figure 3.5 below illustrates the steps used in the analysis of a rib waveguide structure by the EIM. The process is conducted in two stages. In the first stage the effective indices of the slab regions at each side of the rib structure labelled 1 and the effective index of the slab region under the rib, labelled 2 in fig.3.5(a) were calculated using electromagnetic analysis[10]. The effective indexes calculated for each slab region labelled $n_{eff(1)}$ and $n_{eff(2)}$ and shown in fig. 3.5(b) were then used to form another slab guide the effective index of which gives an estimation of the guided mode of the rib structure. In this research a program called "slabsolve" based on the effective index method was used to roughly estimate the modes propagating within the waveguide structures designed using the wafer discussed in section 3.3.3.

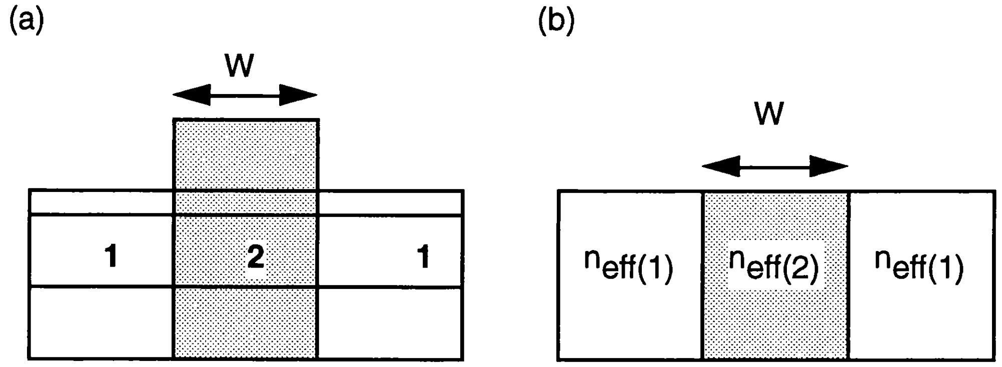

Figure 3.5. illustrations of the two stage EIM.

3.3.4.2. The Scalar Finite Difference Method.

A more accurate and comprehensive analysis of the field within the ridge guides was carried out using a program called "F-wave" based on a finite difference technique[11] and written by MichaelTaylor of this department .In this method the cross section of the waveguide is covered by a rectangular mesh, the points on the grid representing the electric/magnetic field component of the optical fields. The second order derivatives of the wave equation, (equations 3.9 and 3.10), are replaced by a finite difference approximation and the equation is rearranged to be solved at each grid point. In this way the propagation constant and profile of the modes of the structure can be calculated. Figure 3.6 shows the TE_{00} field profile obtained for a 4 μm wide guide etched 0.8 μm into the upper cladding layer of the AlGaAs wafer. The wavelength of the light was chosen to be 1.55 μm. The contour lines in the figure indicate the field profile and show that the light is well confined both vertically and laterally. This designed guide was shown to be single moded. Single mode operation is desired to avoid inter-modal dispersion caused by the group velocity difference between the different modes of a waveguide .

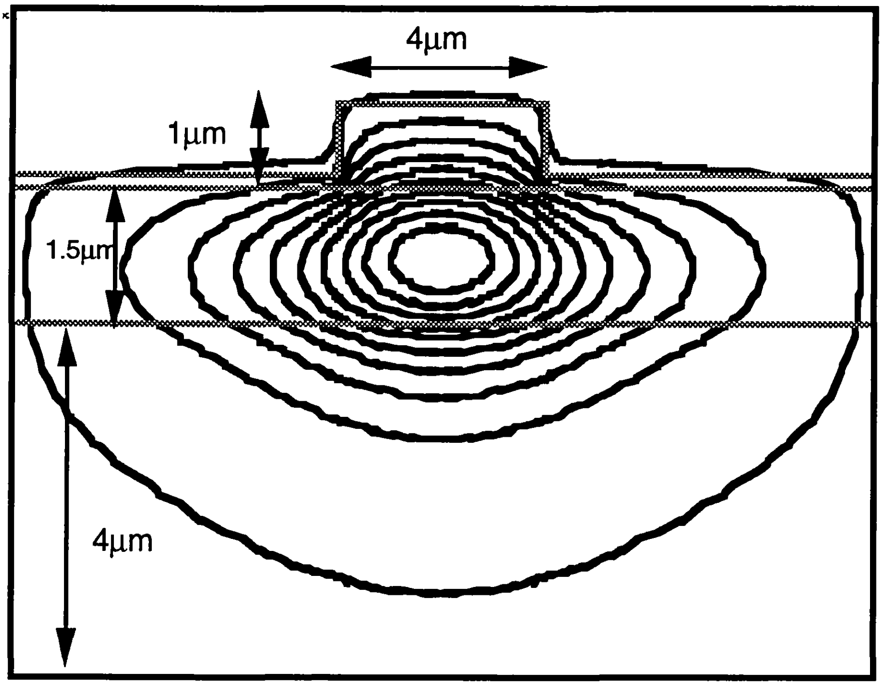

Figure 3.6. Illustration of the fundamental TE_{00} mode of a 4 μm guide modelled using a finite difference technique.

3.4. Fabrication of the Optical Waveguides.

Waveguides were fabricated using a combination of standard photolithography and reactive ion etching. The steps involved are outlined below.

3.4.1. Photolithography.

This is a patterning process whereby the desired waveguide design is transferred to the AlGaAs sample, via a light sensitive polymer mixture called photoresist. The pattern can then be etched to form the waveguide device.

The photolithographic process was carried out in a class 10000 clean room using a class 100 cabinet to ensure that contamination of the sample surface during the fabrication process was kept to a minimum. The steps involved in this process are as follows:

Step 1: Sample Preparation.

The AlGaAs wafer was cut using a scribe and cleave technique into the desired sample sizes.

The samples were initially precleaned before patterning. This is a very important stage as dirt and grease particles present on the surface of the samples can cause poor resist adhesion and coating non-uniformity and so can drastically affect the quality of the pattern produced. The cleaning procedure used involved the use of an ultrasonic bath to agitate the sample for five minutes while it was immersed in the following sequence of solvents.

1. **Opticlear**
2. **Acetone**
3. **Methanol**
4. **R.O. Water**

Finally, the samples were blown dry using filtered N_2 and placed on a hot plate at ~45°C to remove any remaining moisture which can cause adhesion problems at the resist coating stage.

Step 2: Resist Coating and Baking.

A Shipley positive photoresist resist, S1400-31 was used. When the humidity level in the clean room was high (>50%) the extra moisture in the air caused problems with the adhesion of the resist to the sample surface. To combat this problem a primer which is a substance which promotes resist adhesion was first applied to the surface of the AlGaAs sample before the coating of resist. The resist was then dispensed through a syringe filter, to remove contamination before application to the sample and spun at a spin speed of 4000 rpm for 30 s to give a uniform resist coating thickness of 1.8 μm.

The samples were then softbaked at 90°C for 30 minutes to remove most of the solvent in the resist coating and in doing so making the resist photosensitive.

Step 3: UV Exposure.

Exposure of positive resist to UV light renders the resist more soluble to developer solution than unexposed resist. UV light was used to transfer the waveguide pattern via a standard chrome mask onto the AlGaAs samples. The chrome mask, produced using E-beam writing, was carefully positioned above and in contact with the coated AlGaAs sample using a mask aligner. The sample was then exposed through the mask to UV light for 12 seconds.

Step 4: Development Stage.

The pattern was developed by immersing the sample in a 1:1 solution of AZ developer and R.O water and gently agitating the sample in the solution for about 75 s. Finally the sample was rinsed again in R.O water and dried on a hot plate.

3.4.2. Reactive Ion Etching.

The patterned sample was then etched using a reactive ion etching process with $SiCl_4$. An interferometer was used in the dry etch process to monitor the etch depth of the guides.

3.5 Waveguide Loss Measurements.

In this research the Fabry-Perot technique[11] was used to estimate the linear losses of the waveguides. This technique is based on the fact that the two end facets of the waveguide can effectively act as a Fabry-Perot resonator. The optical length of the resonator is temperature dependent and therefore the guide refractive index/phase can be varied by either heating or cooling the guide. As a result, periodic Fabry-Perot transmission fringes can be obtained. The fringe contrast , as explained further on in this section, can be used to calculate the linear waveguide losses. This method is a reliable and accurate means of obtaining the on chip losses of the waveguides as it is insensitive to coupling misalignment inaccuracies and is highly reproducible. In addition this technique is non-invasive. The experimental set up used to measure the linear losses of the optical waveguides is shown in figure 3.7.

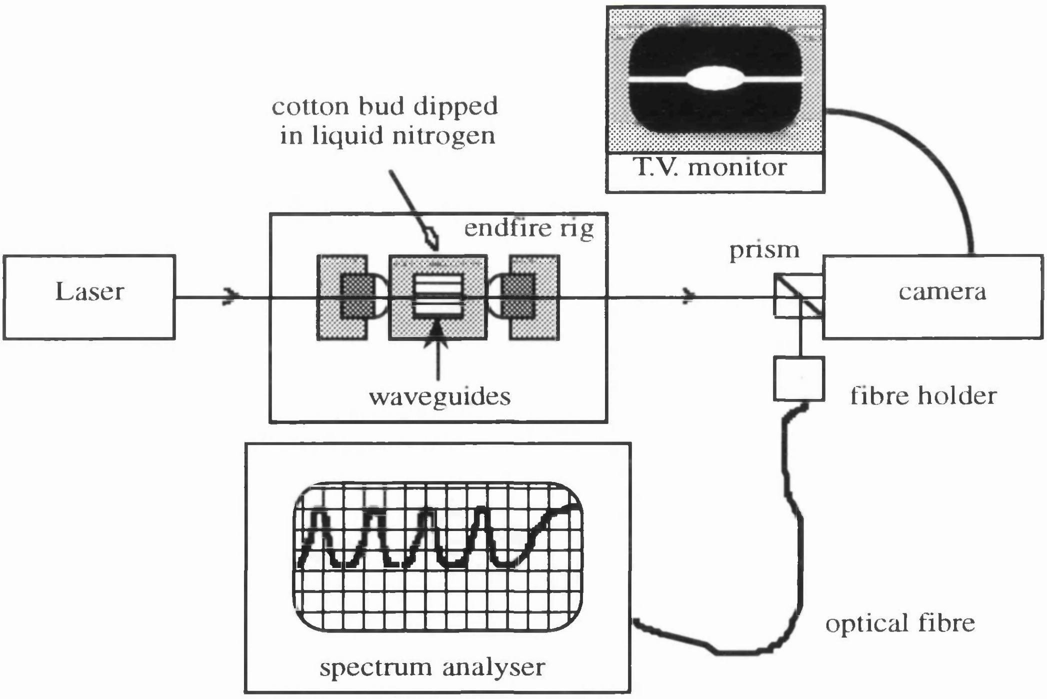

Figure 3.7. Experimental set up used to measure the linear losses of the AlGaAs guides.

Light from a CW semiconductor laser diode operating at a maximum output power of 2 mW at a peak wavelength of 1.556 μm was coupled into the optical waveguides using an endfire rig. Figure 3.8 shows a picture of the rig used. The endfire rig consisted of input and output objective lenses mounted on X-Y-Z translational stages and a sample platform in between the lenses also with X-Y-Z position and sample rotation control.

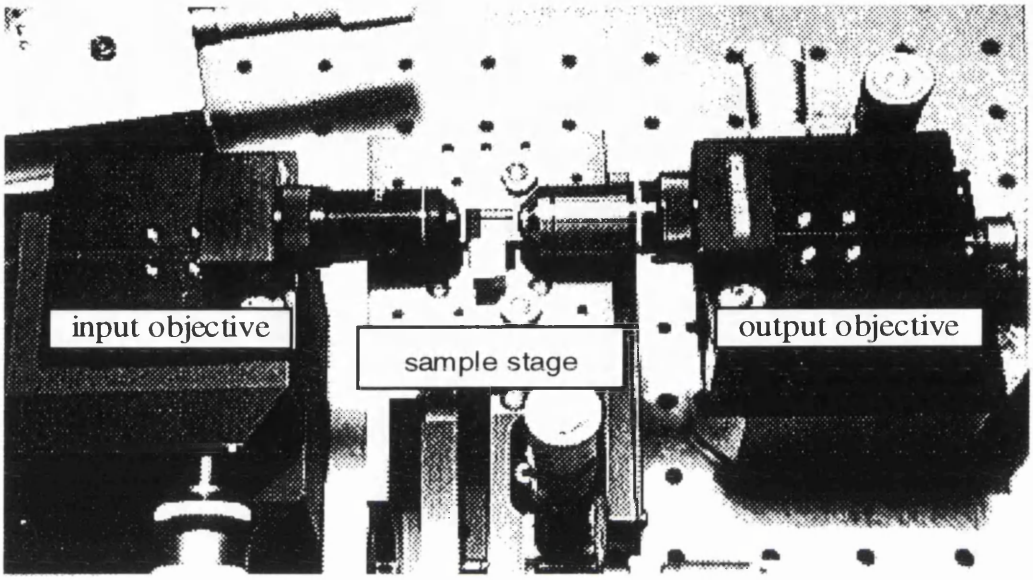

Figure 3.8. Picture of the endfire rig used to couple light in and out of the waveguides.

The magnification strength of both microscopic objective lenses was chosen to be X40 to ensure there was a high overlap between the incident optical field and the waveguide mode. Slab guiding is usually located first before the light can be steered into a single guide. On the TV monitor the waveguide mode looked like a sharp, bright, elliptically shaped spot of light. A beam splitting prism was attached to the camera to allow some of the output power from the guide to be transferred via an optical fibre into a spectrum analyser. The coupling of light into the waveguide was maximised by varying the position of both of the objective lenses until a peak signal was measured on the spectrum analyser.

A cotton bud dipped in liquid nitrogen was used to cool the waveguide. This cooling of the sample alters the cavity length of the guide and hence, fringes are produced in the power transmitted by the guide. Figure 3.9 shows a typical Fabry-Perot fringe pattern that was produced in these experiments. This pattern was produced for 1 cm long, single moded, 4 μm wide guide etched 0.8 μm deep fabricated using the wafer discussed in section 3.4.

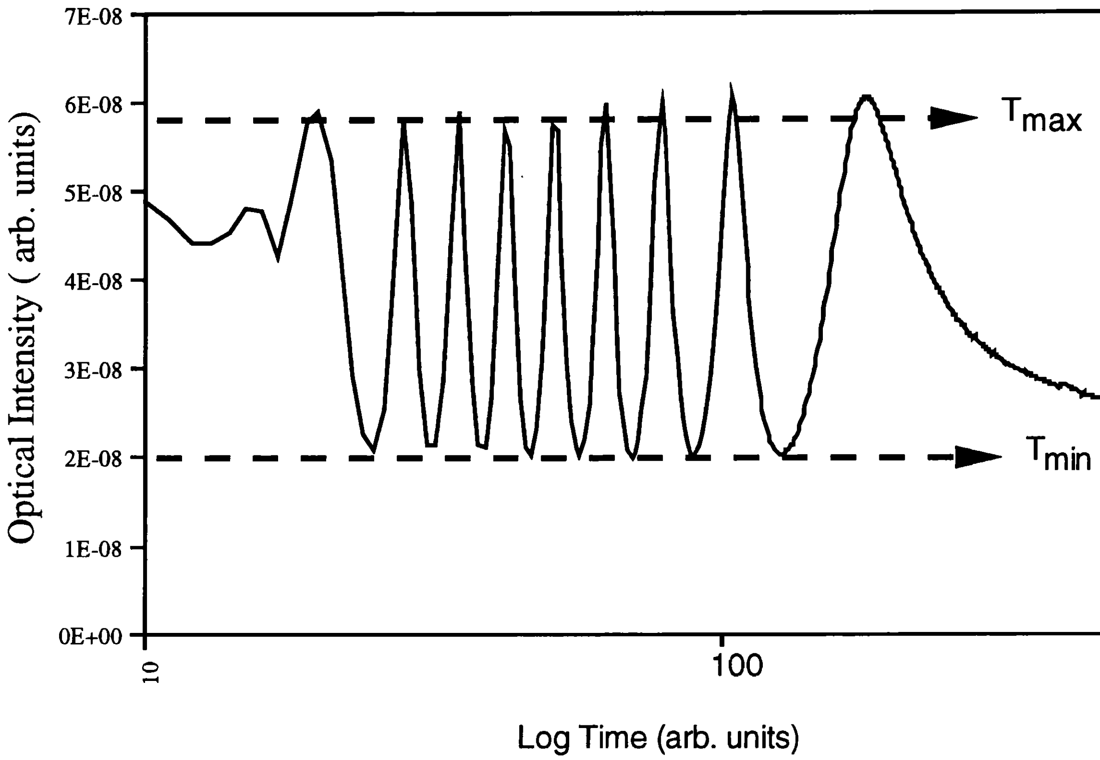

Figure 3.8. Fabry-Perot resonance fringes recorded using a spectrum analyser.

The transmission, T, of the waveguide resonator is given by the equation below, where ϕ is the phase of the guide, α is the linear propagation loss and L is the length of the sample[7].

$$T(\phi) = (1-R^2)e^{-\alpha L} / [(1-r)^2 + 4r\sin^2\phi] \qquad (3.12)$$

where, R is the facet reflectivity which for the wafer used was approximately 30% and r is defined by.

$$r = Re^{-\alpha L} \qquad (3.13)$$

The finesse K of the resonator is calculated from the fringe pattern and is related to r, by the following equation.

$$K=\frac{(T_{max}-T_{min})}{(T_{max}+T_{min})}=2r/(1+r^{2}) \quad (3.14)$$

Hence it follows that the linear loss is related to the fringe contrast, the length and the end facet reflectivity of the guides by the following equation:

$$\ln[1-(1-K^{2})^{\frac{1}{2}}/K]=\ln R-\alpha L \qquad (3.15)$$

Rearranging equation 3.15 gives the following expression for α:

$$\alpha=-\frac{1}{L}\ln\left(\frac{1-(1-K^{2})^{\frac{1}{2}}}{RK}\right) \qquad (3.16)$$

Using equation 3.16 the waveguide losses could be deduced. Throughout this research the losses of the guides fabricated ranged from 0.74 dB/cm up to 2.3 dB/cm.

3.6 Nonlinear Properties of AlGaAs Waveguides.

In this section the experimental set up used to observe the nonlinear behaviour of the waveguide devices is described. In addition the measurement of n_2 and β_2 for the AlGaAs waveguides around the half-band gap spectral region are presented.

3.6.1 Experimental Arrangement Used to Test the Nonlinear Devices.

To produce nonlinear switching in the waveguide devices, very short, high peak powered pulses were required at a wavelength of ~1.50-1.55 µm. These pulses were supplied using a mode-locked colour ,F-centre laser. In the following section the characteristics of the colour centre laser and the mode-locking techniques used in this research are briefly described.

The F-centre lasers used consisted in general of either a NaCl crystal doped with OH$^-$ or a KCl crystal doped with Tl. The KCl crystal absorbs light of wavelength 1.04 μm and can therefore be optically pumped with light from a Nd:YAG or Nd:YLF. The peak emission wavelength is 1.51 μm and it has a tuning range of about 230 nm. The NaCl:OH$^-$ F-centre has a peak absorption band centred at 1.09 μm and an emission band centred around 1.55 μm with a tuning range of 250 nm. It too can be pumped using a neodymium based solid state laser.

Figure 3.9 shows a schematic diagram of the KCl:Tl colour centre laser. The laser cavity is formed between mirrors m_1, m_2, m_3, m_4 and the output coupler m_0. The output wavelength of the light from the crystal was tuned using a birefringent filter to ~1.51 μm. The crystal contains point defects (vacancies) formed during crystal growth which provide the electronic levels required for lasing. The energy levels are broad due to vibrations in the lattice. The crystal is kept at a cryogenic temperature (~77K) to maintain optimum efficiency and to minimise bleaching of the centres.

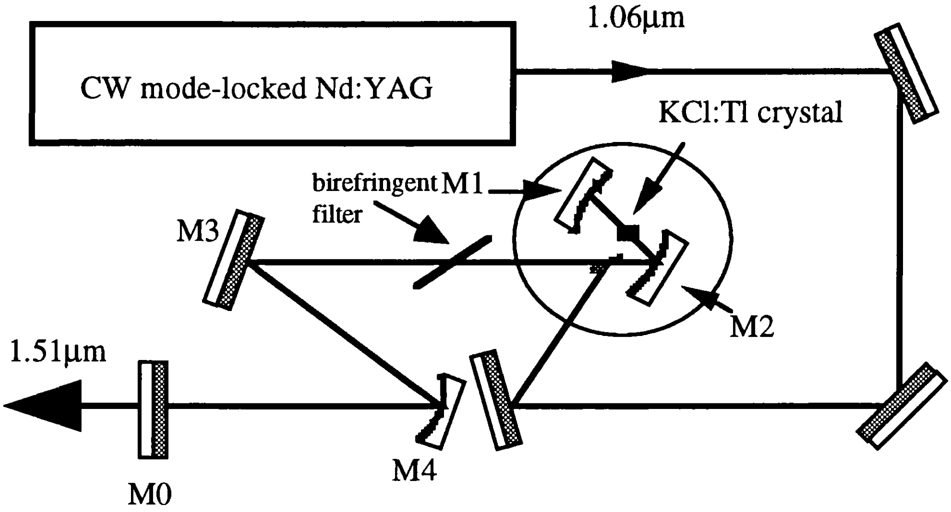

Figure 3.9. Schematic diagram of the KCl:Tl colour centre laser.

3.6.1.1. Mode-Locking.

In general, a laser cavity can support many longitudinal modes. In general the relative phases, frequencies and amplitudes of each mode are random and so the output of the laser varies arbitrarily in time due to the random interference between the various modes. By forcing the relative phases of all modes to be the same, a periodic train of laser pulses is generated at the output. The pulses have a period of the cavity round trip time 2L /C, where L is the cavity length. This technique is called mode-locking and can be achieved either actively or passively. In this research both an active and a passive method of mode-locking were used and these two different methods are described below:

3.6.1.2. Active Mode Locking by Synchronous Pumping.

Active mode-locking involves modulating either the amplitude (loss or gain) or the phase of the light in the cavity. Synchronous pumping is a mode locking method whereby a gain modulation technique is employed. In this case the gain modulation was achieved by mode-locking the pumping laser i.e. the Nd:YAG laser. For this type of mode-locking to take place the cavity length of the F-centre laser has to be an integral multiple of the cavity length of the pumping laser. The pulse shortening is a result of the combined effects of gain saturation and gain modulation due to the pump pulses. In an F-centre laser relatively short pulses, a few tens of pico-seconds can be produced using this technique.

3.6.1.3. Passive Mode-Locking using a Coupled Cavity Mode Locking Technique.

In passive mode-locking an external nonlinear element driven by the mode-locked pulses is used to produce ultra-short pulses[12].

In this research a coupled cavity, or additive-pulse, mode-locking scheme was employed. Basically the coupled cavity scheme consists of two cavities, one formed by the laser and the other is an external cavity that includes an nonlinear element. Figure 3.10 below shows a schematic of one of 3 widely used coupled cavity configurations known as the Fabry-Perot cavity. In this research the nonlinear element used was a length of nonlinear fibre. In this process the pulses produced by the F-centre are fed into the fibre where the band-width of the pulse is broadened through self-phase modulation. The amount of power in the nonlinear cavity is adjusted until the phase across the returning pulse causes constructive interference in the centre and destructive interference in the wings. The result is a redistribution of the energy into a single short pulse. The external cavity must be the same length as the laser cavity for this technique to work.

Using this method femto-second pulses in the kilo-watt peak power range can be formed.

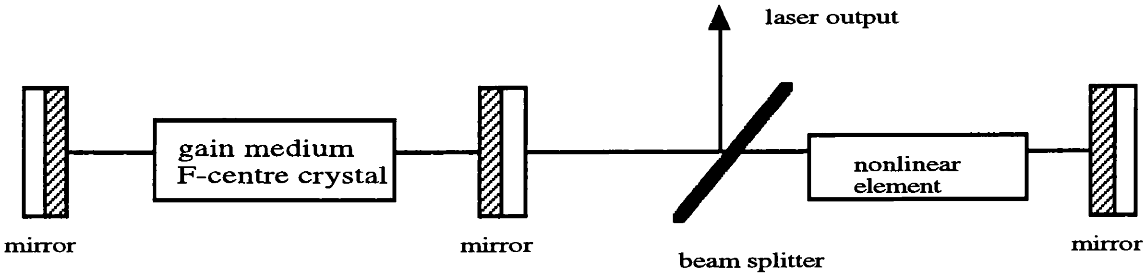

Figure 3.10. Schematic diagram of Fabry-Perot type coupled cavity mode-locked arrangement.

3.6.2: Measurement of the nonlinear refractive index coefficient.

The nonlinear refractive index of a semiconductor material can be estimated, as described in chapter 1, using self-phase modulation.

Figure 3.11 below shows the experimental set which was used to measure the self phase modulation of a 1.6 cm long and 4 μm wide AlGaAs waveguide. The colour centre laser operated at a wavelength of 1.48 μm. A coupled cavity mode-locked arrangement was used to produce 300 fs pulses with a peak pulse power of 950 W. An end-fire rig was used to couple the laser pulses into and out of the waveguides and a spectrum analyser was used to record the spectrum of the input and transmitted pulses of the guides as a function of input light intensity.

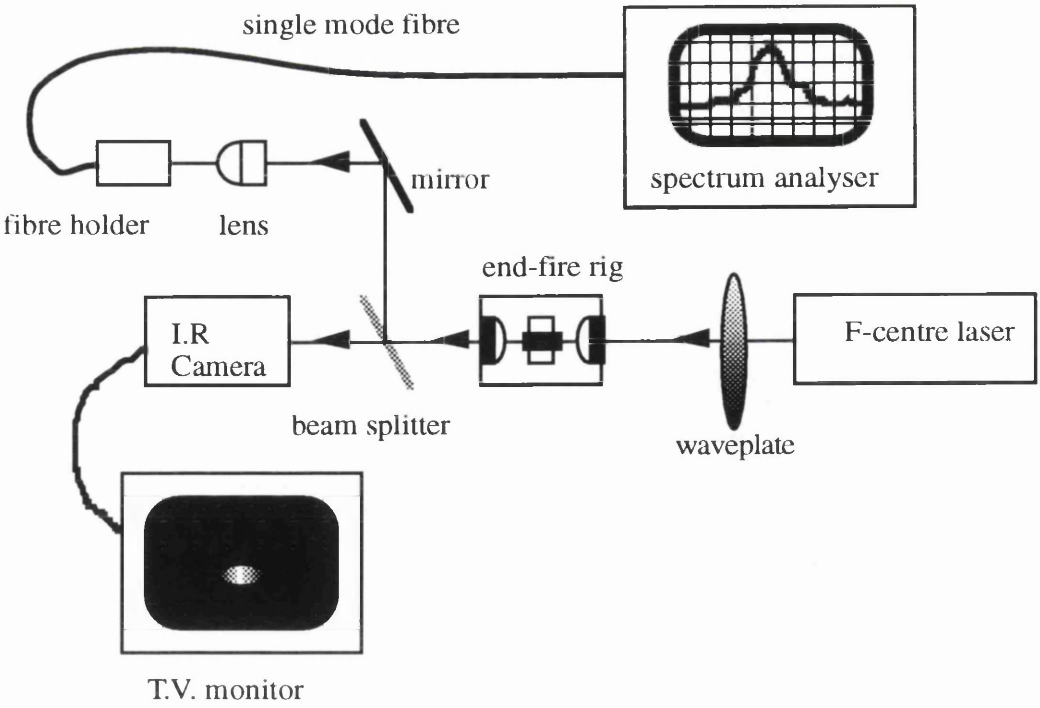

Figure 3.11. Experimental set up used to measure SPM in the optical guides.

Figure 3.12 displays the recorded output spectra of the pulses transmitted from the guides for various input light intensities and also shows for comparison the theoretically predicted spectral changes and the corresponding phase shifts estimated for a Gaussian shaped pulse[13]. The theoretically determined phase shifts compare well with the shifts measured experimentally.

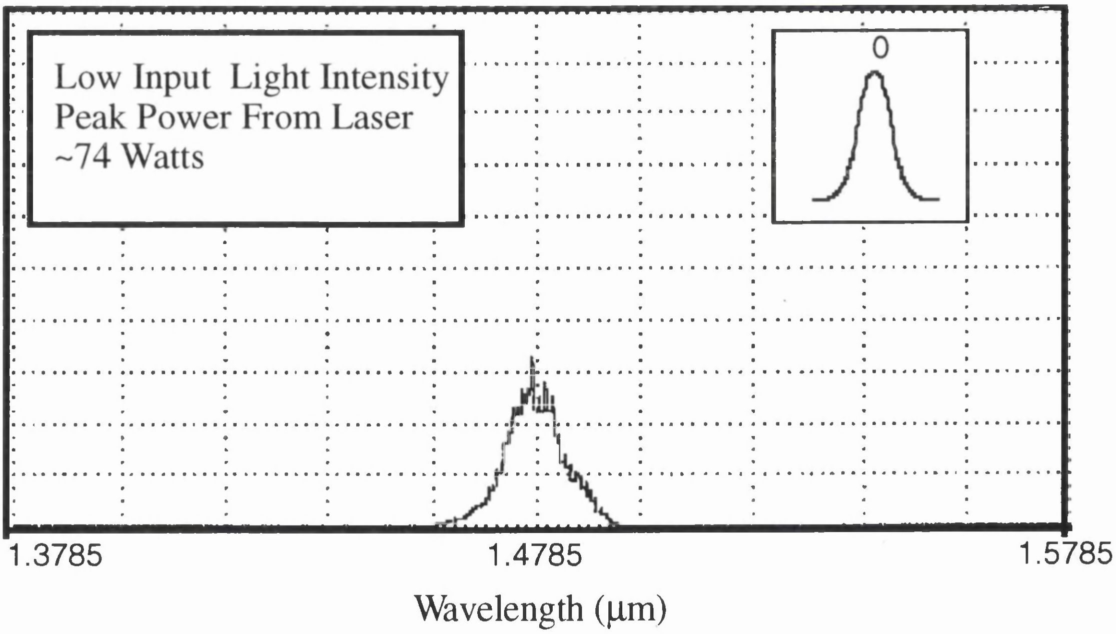

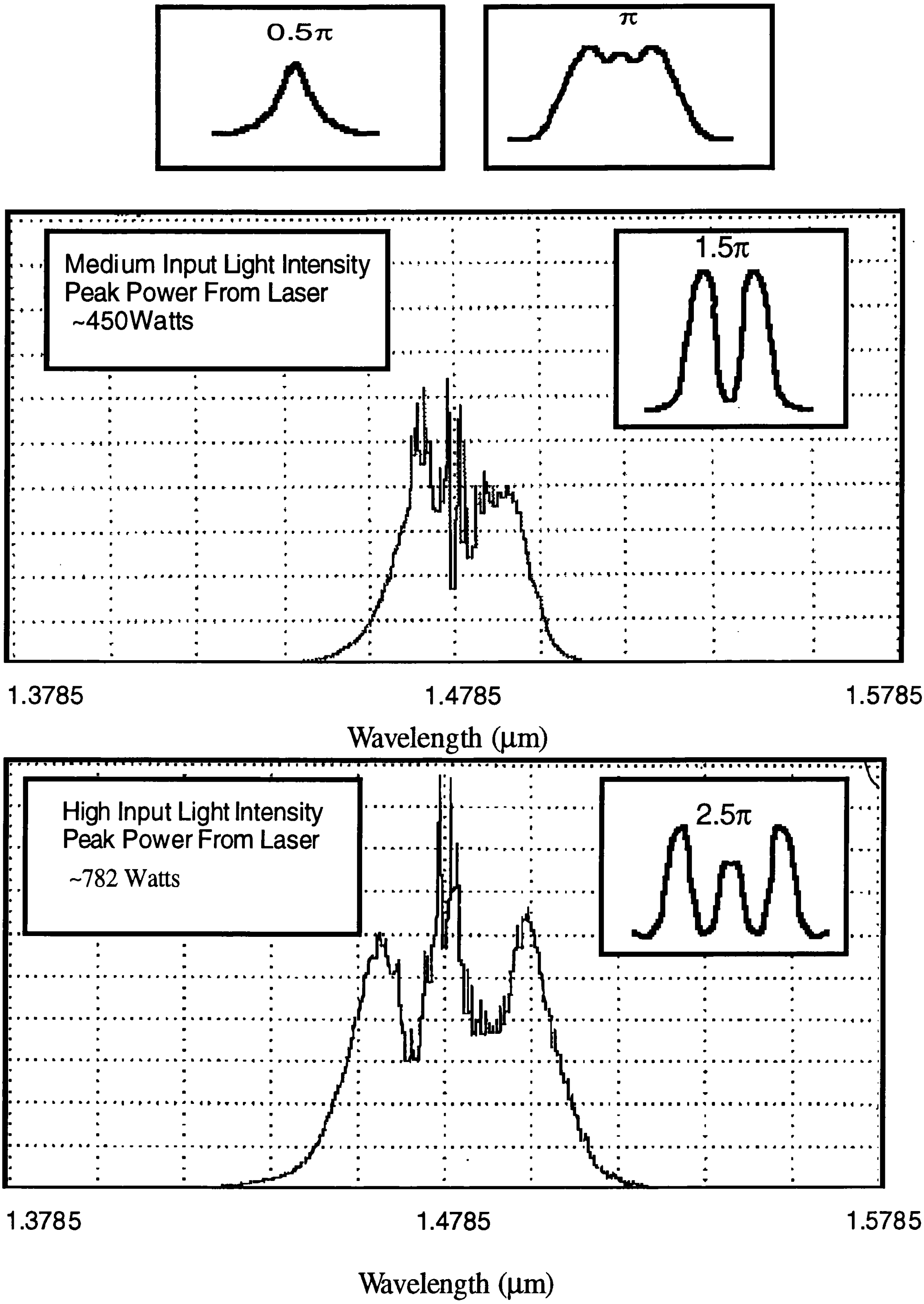

Figure 3.12. Nonlinear phase shifts produced in a laser pulse due to SPM.

From these measurements the value of n_2 can be calculated using equation 1.17:

$$\Delta\phi=\frac{2\pi}{\lambda}\mathrm{L}\mathrm{n}_2\mathrm{I} \qquad (1.17)$$

In this experiment the length, L, of the guide was 1.6 cm and the effective area of the guide was 12 x 10^{-8} cm^2. A phase shift of 1.5π occurred in the output pulse spectrum for an estimated peak power of ~ 50 Watts inside the guide and a phase shift of 2.5π first occurred in the output pulse spectrum for an estimated peak power of ~ 90 Watts within the waveguide. Using these measurements of the phase change and the corresponding peak power in the waveguides, the average value of n_2 was estimated to be ~ (1.5 +/- 0.2) X 10^{-13} cm^2/W. Referring to figure 2.4 this value of n_2 compares well with a previously calculated value of the nonlinear refraction coefficient, for similar AlGaAs waveguides, by Aitchison et al[14].

3.6.3. Nonlinear Loss Measurement.

Chapter 2, explored the subject of multi-photon absorption within semiconductor materials. It was seen that the nonlinear loss associated with a AlGaAs passive waveguide can be estimated by measuring the transmission characteristics of a waveguide for various input powers.

Assuming that only two photon absorption is present then the attenuation of light propagating through a waveguide is given by :

$$\frac{\mathrm{dI}}{\mathrm{dz}}-\alpha\mathrm{I}-\alpha_2\mathrm{I} \qquad (3.17)$$

Using equation (3.17) the inverse transmission factor 1/T can be derived and is given by:[13]

$$\begin{aligned}\frac{1}{T}=\frac{I_{inc}}{I_{trans}}&=\frac{1}{(1-R)^2\eta e^{-\alpha L}}+\frac{\alpha_2\left(1-e^{-\alpha L}\right)}{(1-R)\alpha e^{-\alpha L}}I_{inc}\\&=\frac{1}{T_0}+\frac{\alpha_2\left(1-e^{-\alpha L}\right)}{(1-R)\alpha e^{-\alpha L}}I_{inc}\end{aligned} \qquad (3.18)$$

Where I_{inc} and I_{tran} are the intensity of the light incident and propagating through the waveguide. R is the Fresnel reflectivity of the facets, η is the coupling efficiency into the waveguide. L is the waveguide length and T_0 is the linear transmission factor. It can be seen from equation 3.18 that α_2 can be estimated from the slope, S, of the inverse transmission plotted as a function of the incident light intensity.

$$\alpha_2 = \frac{(1-R)\alpha e^{-\alpha L}}{1-e^{-\alpha L}} S \qquad (3.19)$$

Considering sech^2 pulses the peak light intensity in a waveguide I_p is given by:[13]

$$I_p = \frac{P_{ave}}{1.134\tau_p f_p A_{eff}} \qquad (3.20)$$

where A_{eff} is the effective area of the mode, P_{ave} is the average power in the guide, τ_p is the pulse duration and f_p is the repetition rate of the pulses. Hence, using equation 3.19 and 3.20 and assuming a sech^2 pulse profile, the two photon absorption coefficient can be found by calculating the slope ,S_p, of the plot of the inverse transmission function versus the average incident power and is given by:[13]

$$\alpha_2 = \frac{1.134\tau_p f_p A_{eff}(1-R)\alpha e^{-\alpha L}}{1-e^{-\alpha L}} S_p \qquad (3.21)$$

For this experiment a synchronously pumped mode-locked colour centre was used. The laser produced 11.8 ps pulses at a rep rate of 81.93 MHz and with a peak output power of approximately 420 Watts at a wavelength of 1.54 µm. The experimental set up was the same as that used to measure the SPM of the waveguide as described in section 3.6.1. The input and output powers from the guide were measured using a photodiode. Using the 11.8 ps pulses and also CW light (with the same average power as the pulsed light but with considerably less peak power), both the linear and nonlinear transmission characteristics of a 1.6 cm long semiconductor waveguide were obtained. The transmission characteristics of the guide are shown in figure 3.9 below.

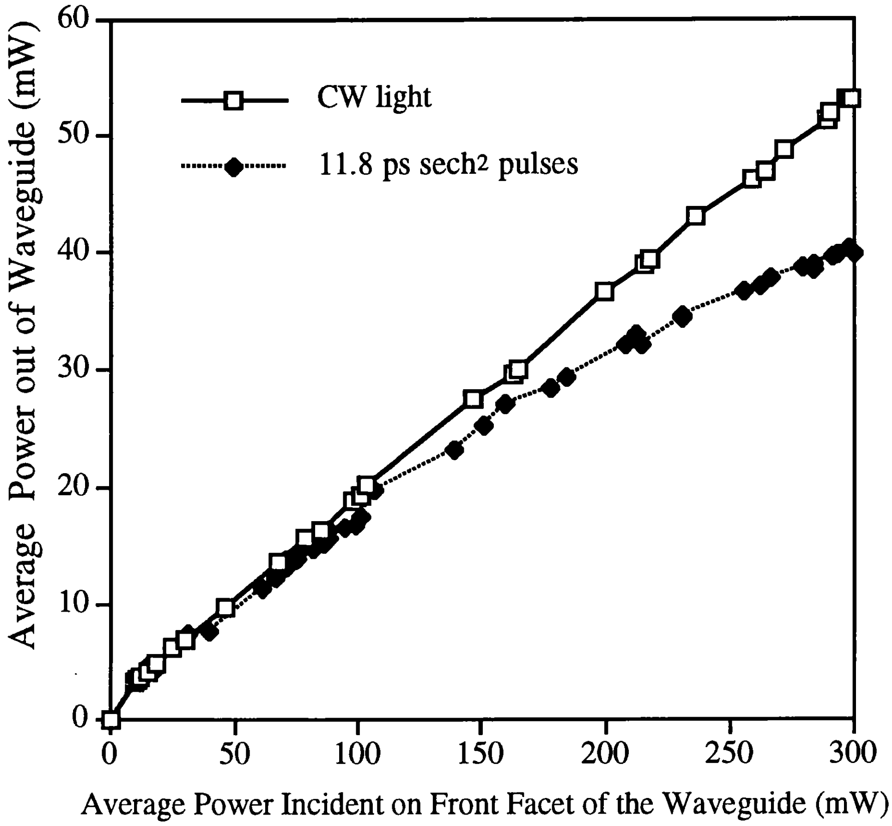

Figure 3.13. The transmission characteristics of a nonlinear waveguide.

It is seen that at low peak powers the transmitted power varies linearly with the input power. However, at high peak power i.e. using the pulsed laser light source, the transmission characteristics of the guide become nonlinear as absorption occurs at high peak powers, which results in power loss. Figure 3.10 shows the graph of the inverse transmission as a function of average power incident onto the guide. The gradient of the slope, S_p, was measured to be 0.01. The slope cut the y axis at 4.6 which, referring to equation 3.18, corresponds to a linear transmission efficiency, T_0, of ~ 21%. This value compares well with the experimentally measured throughput of the waveguide.

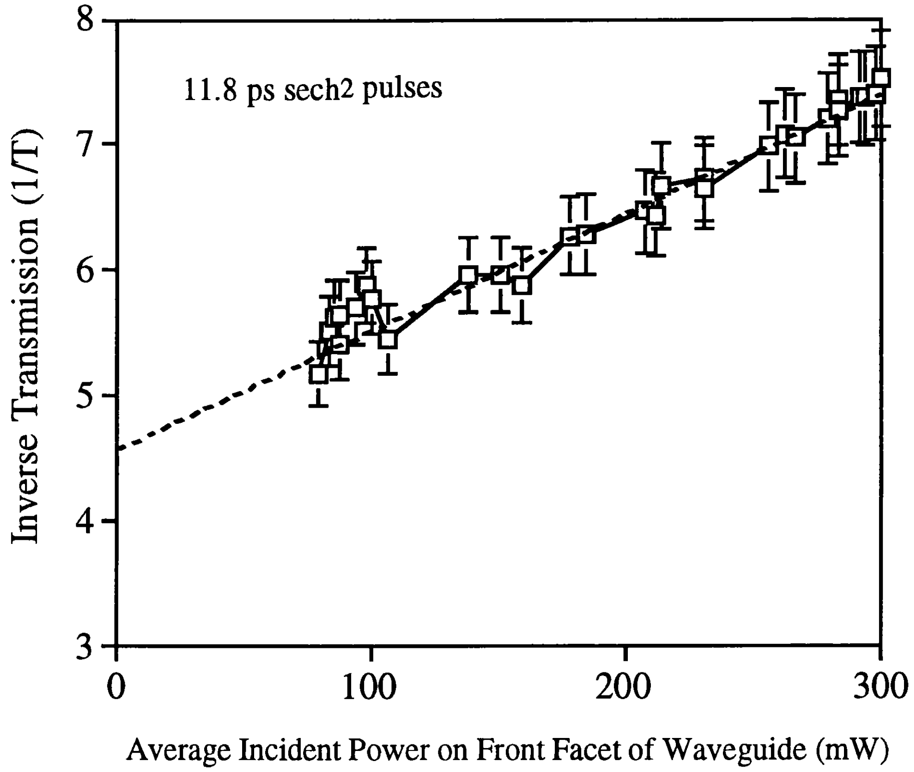

Figure 3.10. Plot of inverse transmission ($1/(P_{tran}/P_{in})$ as a function of incident average input power.

Since the experimental data fall on a straight line, it can be concluded that at this wavelength the major nonlinear loss mechanism was two photon absorption. The presence of three photon absorption would result in a curved feature. Using equation 3.21 and assuming the following waveguide parameters: $A_{eff}=12 \times 10^{-8}$ cm^2, $\alpha=0.53$ cm^{-1}, L=1.6 cm, R=0.3 the value for α_2 was estimated to be ~(0.2 +/- 0.05) cm/GW. Referring to fig. 2.5, this calculated value compares very well to a previous calculation of α_2 as deduced by Aitchison et al[13] for similar AlGaAs waveguides.

3.7 Conclusion.

In this chapter the design, fabrication and characterisation of AlGaAs optical waveguides for ultrafast switching were discussed. In particular, the methods of determining the propagation constants and field profiles of the modes propagating in the guides using an effective index and a finite difference method were outlined. The experimental set up used to examine the waveguides was described. Linear and nonlinear loss measurements were carried out on a single mode waveguide. Linear losses were found to be as low as 0.74 dB/cm. The value of n_2 of the AlGaAs waveguide was measured, using self-phase modulation and found to be ~ $1.5\text{x}10^{-13}$ cm^2/W at a wavelength of 1.4785 µm. The two photon absorption coefficient was also estimated at a wavelength of 1.54 µm to be ~ 0.2 cm/GW. Both estimated nonlinear coefficients compared well with previously published nonlinear experimental measurements by Aitchison et al[14].

References.

1 J.U. Kang, G.I. Stegeman and J.S. Aitchison, "All-optical multiplexing of femtosecond signals using an AlGaAs nonlinear directional coupler", Electron. Lett., **31**, pp 118-119 (1995).

2 K. Al-Hemyari, J.S. Aitchison, C.N. Ironside, G.T. Kennedy, R.S. Grant and W. Sibbett," Ultrafast all-optical switching in a GaAlAs integrated interferometer in the 1.55 μm spectral range", Electron. Lett., **28**, pp 1090-1092 (1992).

3 J.S. Aitchison, A.H. Kean, C.N. Ironside, A. Villeneuve and G.I. Stegeman, " Ultrafast all-optical switching in a $Al_{0.82}Ga_{0.28}As$ directional coupler in the 1.55 μm spectral range", Electron. Lett., **27**, pp 1709-1710 (1991).

4 F. Hernandez-gil, T.L. Koch, U. Koren, R.P. Gnall and C.A. Burrus, "Tunable MQW-DBR laser with monolithically integrated GaInAs/InPdirectional coupler switch", Electron. Lett., **25**, pp 1271-1272 (1989).

5 E. Hecht, "Optics", Addison-Wesley Pub. Comp., 2nd Ed, Chp.4 (1989).

6 A. Yariv, "Optical Electronics" , Saunders College Publ. , 4th ed, chapter 13 (1991).

7 R.J. Deri and E.Kapon, "Low-loss III-V semiconductor optical waveguides" IEE J. of Quant. Elec. , **27**, pp 626-640 (1991).

8 R.J. Deri, E. Kapon and L.M. Schiavone, "Scattering in low-loss GaAs/AlGaAs rib waveguides", Appl. Phys. Lett., **51**, pp 789-791 (1987).

9 S.Adachi,"GaAs,AlAs and $Al_xGa_{1-x}As$", J. of Appl. Phys., **58**,pR1 (1985).

10 G.J.M. Krijnen, H.J.W. M.Hoekstra, P.V. Lambeck, "A new method for the calculation of propagation constants and field profiles of guided modes of channel waveguides based on the effective index method", J. of Lightwave Tech. , **12**, pp 1550-1559 (1994).

11 P. Lüsse, P. Stuwe, J. Schüle and H.G. Unger, "Analysis of vectorial mode fields in optical waveguides by a new finite difference method", J. of lightwave Tech. , **12**, pp 487-493 (1994).

12 R.G. Walker, "Simple and accurate loss measurement technique for semiconductor optical waveguides", Electron. Lett., **21**, pp 581-583 (1985).

13 Z. Su, "Generation and propagation of ultrashort laser pulses using nonlinear waveguides", Ph.D Thesis, University of St Andrews, (1994).

14 R.H. Solen, C. Lin, "Self-phase modulation in silica optical fibers" , Phys. Rev. A., **17**, pp 1448-1453 (1978).

15 J.S. Aitchison, D.C. Hutchings, J.U. Kang, G.I. Stegeman and A. Villeneuve, "The nonlinear optical properties of AlGaAs at the half band gap", IEEE Journal of Quant. Elec., **33**, pp 341-347 (1997).

Chapter 4

Nonlinear Coupled Waveguide Arrays.

Introduction.

There is currently a great deal of interest in all-optical switching and signal processing systems. A number of different device configurations have been investigated. All-optical switching has been experimentally observed in nonlinear directional couplers[1], Mach-Zehnder interferometers[2] and nonlinear X-junctions[3]. Switching has also been theoretically investigated in grating[4] and prism couplers[5]. Optical information processing can be achieved using either a parallel, or serial approach. To date most of the devices discussed have been of a serial nature. In such systems nonlinear couplers promise to play an important role.

In this chapter the use of nonlinear waveguide arrays as switching elements will be discussed. In particular, the experimental and theoretical switching characteristics of several different nonlinear coupled waveguide arrays will be considered.

The chapter is organised as follows: The basic operation of the standard linear directional coupler is described in section 4.1. Section 4.2 discusses the development of the various types of coupled arrays under investigation today. Section 4.3 deals with nonlinear coupler theory and outlines the important features of a nonlinear coupled array. The applications of nonlinear coupled arrays in future soliton systems are described in section 4.4. In section 4.5, the spatial and temporal beam propagation method (BPM) codes and a fourth order Runge-Kutta algorithm used to simulate the transmission characteristics of the waveguide arrays are described. The BPM codes include the effects of dispersion as well as linear and nonlinear loss. Also in this section the switching characteristics of a number of different coupler arrangements are simulated. The design and details of the semiconductor material used to fabricate the arrays are discussed in section 4.6. The experimental results on ultrafast switching in both uniformly and non-uniformly spaced waveguide arrays consisting of three, four and eight waveguides are presented in section 4.7. The experimentally measured transmission characteristics are shown to compare very well to the theoretical simulations using the BPM program. Finally, in section 4.8 the results are summarised and discussed.

4.1. The Linear Directional Coupler.

In this section the underlying principles of the two-core directional coupler are outlined. This model is then extended to the generic N-core case. Linear couplers have been used in wavelength selecting[6], modulating[7], demultiplexing[8] and switching applications[9].

Linear coupled arrays operate on the principle that an exchange of optical power can occur between adjacent guides of an array when the guides are placed in close proximity to one another, such that the evanescent fields / mode tails of the guides overlap. In addition, the guides must also be phase-matched, or have the same propagation constant. The coupling of light between the guides is then a periodic function of the device length. Figure 4.1 shows a cross-sectional view of a typical directional coupler formed by two ridge waveguides etched into a three layer AlGaAs wafer. This figure illustrates the overlapping mode tails of the light fields propagating within the individual guides.

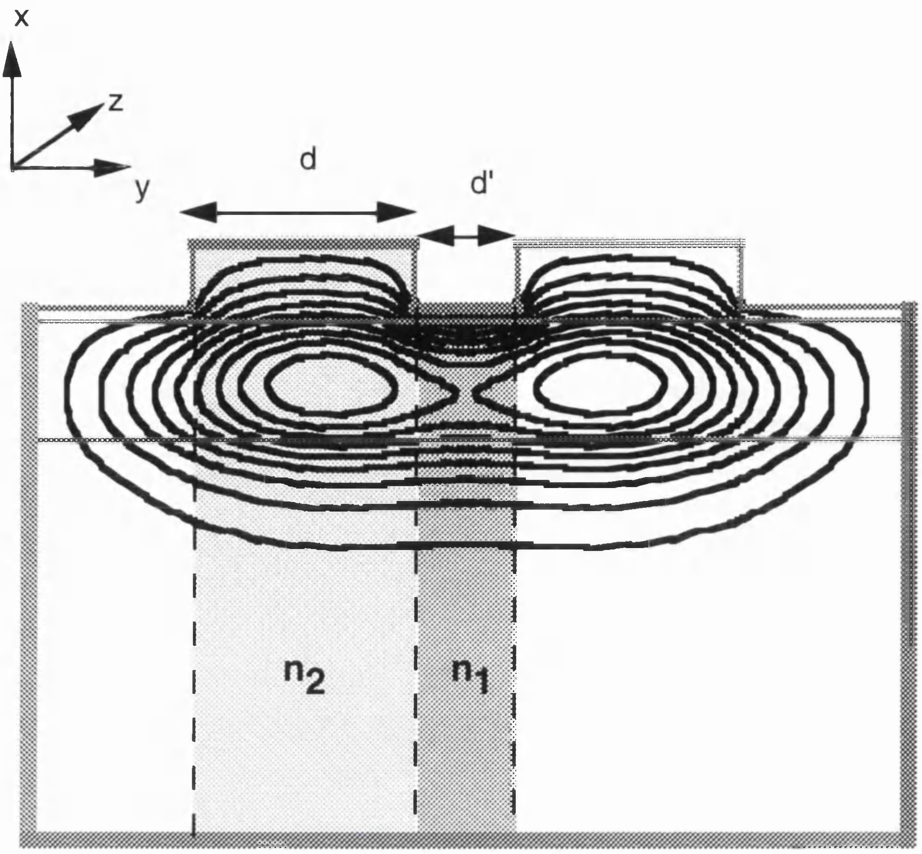

Figure 4.1. Transverse view of a linear two guide directional coupler.

The propagation of light within a linear directional coupler is generally described by coupled mode theory[10]. The evolution of the electric fields along two coupled waveguides can be described by[11]:

$$\frac{dA_1}{dz} = -jC_{21}e^{j\Delta\beta z}A_2(z) \qquad (4.1)$$

$$\frac{dA_2}{dz} = -jC_{12}e^{-j\Delta\beta z}A_1(z) \qquad (4.2)$$

where A_1 and A_2 are the amplitudes of the electric fields in waveguides 1 and 2, C_{12} is the linear coupling strength between the guides, $\Delta\beta$ is the difference in the propagation constant between the two waveguides and z is the propagation length.

The coupling strength between the guides, C_{12}, depends on the coupled waveguide structure and is given by:[12]

$$C_{12} = \frac{2k_o^2(n_2^2 - n_1^2)\alpha_x \cos^2\left(k_{2x}\frac{d}{2}\right)}{\beta d_{eff}\left(\alpha_x^2 + k_{2x}^2\right)} e^{-\alpha_x d'} \qquad (4.3)$$

where n_1 and n_2 are the effective refractive indices of the etched slab region and the unetched region under the guides respectively, as illustrated in fig. 4.1, d' is the edge to edge separation of the two waveguides, k_0 is the wave number given by $2\pi/\lambda$ and d_{eff} is the effective waveguide width given by:[12]

$$d_{eff} = d + 2\left(\frac{1}{\alpha_x}\right) \qquad (4.4)$$

where α_x,k_{2x} are the transverse propagation constants of light travelling within the regions 1 and 2 respectivley, as illustrated in fig. 4.1 and are given by the following equations:

$$\alpha_x = k_o\sqrt{{n_{eff}}^2 - {n_1}^2} \qquad (4.5)$$

$$k_{2x} = k_o\sqrt{n_2^2 - n_{eff}^2} \qquad (4.6)$$

where n_{eff} is the effective index of an individual waveguide.

The coupling length, L_c, is defined as the length over which power is transferred from the input guide to the adjacent guide. This is depicted schematically in figure 4.2. Figure 4.2 also shows a schematic of a 1xN coupler array, where the $C_{N,N+1}$ coefficients are the linear coupling coefficients between the guides. A two guide coupler of the length L_c is known as the half beat length device. A full beat length device has a length $2L_c$ and corresponds to all the power exiting from the input guide.

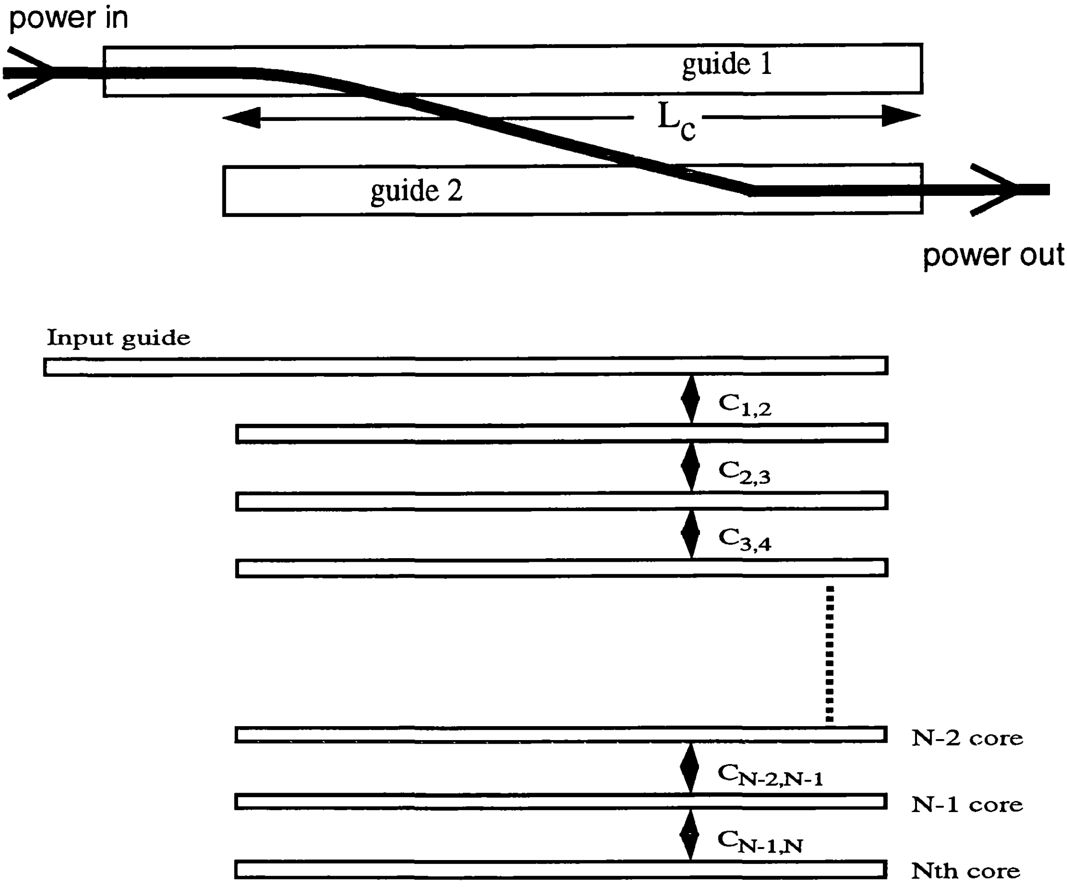

Figure 4.2. Top view of a half beat two guide coupler and a N-core coupled array.

The coupling length is related to the coupling strength by the following equation.

$$L_c = \frac{\pi}{2C_{12}} \qquad (4.7)$$

The same underlying arguments can be used to explain the operation of an N-core coupler. As the number of guides increases the maximum power transfer to the outermost guide decreases. This can be explained by assuming that only nearest neighbour coupling takes place, thus for a waveguide in the centre of the array, power can be transferred both towards the output and the input waveguides. For example in a uniformly spaced, four core coupler a half beat corresponds to a 97% percent power transfer to the outermost guide. Improved, almost complete linear power transfer (approx. 99%) to the outermost guides in multi-guide arrays, consisting of four or more guides, has been theoretically simulated using non-uniformly spaced coupled waveguides. In this case the nearest neighbour coupling is non-uniform and power is preferentially transferred towards the output waveguide.

Theoretically it has been found that the coupling length of a 1x N array , where N is the number of guides, is related to the half beat length of a 1X2 array, L_c, by the following relation[13]:

$$L_N = \sqrt{(N-1)}L_c \quad (4.8)$$

where L_N is the half-beat coupling length of the N-core array. Equation 4.8 shows that the half-beat coupling length of the array ,increases as the number of guides within the array increases.

4.2. Development of the Nonlinear Coupled Array.

Over the past few decades there has been a great deal of research which has led to the development of a diverse range of coupled waveguide devices. In this section these methods are reviewed and the development of the nonlinear waveguide array is discussed in detail. In particular its use as an ultrafast switching element will be examined.

The electro-optic effect is a common method of light control in couplers and has been employed in many systems. In such arrangements the coupling between the guides is controlled by the application of an electric field. Multi-quantum well materials such as GaAs/InGaAsP/InP, which employ the quantum-confined stark effect[14], have produced a variety of electro-optic coupler devices[15-19] and vertical directional couplers[20]. Ti diffused Lithium Niobate is another popular electro-optic material which has been widely investigated and implemented in many coupler configurations[21-23].

The thermo-optic properties of materials have been used to build coupler arrays. In such elements a heater electrode is use to alter the waveguide refractive index, enabling the coupling between the guides to be manipulated.[24] In addition, acoustic waves have been used to control the

refractive index and hence the light propagating in coupled waveguide systems.[25]
More recently coupler devices have been proposed in which active nematic liquid crystals sandwiched between passive couplers were used to control the power exchange between waveguides. Such devices have been fabricated on glass substrates and using polymer films.[26,27] Semiconductor doped / ion exchange glass nonlinear couplers[28,29] have also been studied. An interesting application of the directional coupler has been developed using Ag^+-Na^+ ion exchange in glass, for a detector element which is sensitive to environmental pollutants.[30] Integrated optical directional couplers in silicon-on-insulator[31] are another type of coupler which has been explored and have potential application in silicon integrated circuit technology. Quantum directional couplers which consist of coupled electron waveguides in close proximity to one another are also being investigated.[32] Also there has been great interest recently in coupled waveguide components composed of anti-resonant reflecting waveguides (ARROWS).[33-36]

The experimental work described in this chapter deals with the ultrafast switching properties of nonlinear waveguide arrays fabricated in AlGaAs. AlGaAs and certain organic polymers such as polydiacetylene (12,8)[37] and nonlinear silica fibres[38] exhibit the third order, optical Kerr effect. Therefore, the refractive index of the material depends on the input field intensity and in a nonlinear array this effect can result in a redistribution of the field within the device.

4.3. Nonlinear Coupler Theory.

When optical waveguides are constructed from a nonlinear Kerr material, the refractive index of the medium depends on the input beam intensity, as discussed in chapter 1 and is given by:[39]

$$n = n_0 + n_2 I \quad (4.9)$$

In a waveguide this results in the effective index becoming power dependent. When such guides are used to produce a coupled waveguide array, the coupling coefficient becomes power dependent. As the intensity of the input light is increased the local refractive index changes, breaking the low power phase matching condition and so the guides become detuned, resulting in the light remaining in the input guide at high powers. Thus, the nonlinear coupler exhibits a power dependent transmission characteristic. The propagation of light in a nonlinear, weakly coupled waveguide array can be described by coupled mode theory. For example equation 4.10 below describes the propagation of the envelope of a field E_n travelling in the nth guide of a 1x N waveguide array:[40]

$$i\frac{dE_n}{dZ} = \beta_n E_n - C(E_{n+1} + E_{n-1}) + \chi |E_n|^2 E_n = 0 \quad (4.10)$$

In equation 4.10, C is the linear coupling coefficient, β_n, is the propagation constant of the mode in guide n and $\chi = \omega_0 n_2/(cA_{eff})$ where A_{eff} is the effective area of the modes.

Considering a two guide nonlinear directional coupler. The normalised fields propagating in a half-beat length device, taking into account multi-photon absorption but neglecting group velocity can be described by :[40]

$$\begin{aligned} &i\frac{\partial q_{1,2}}{\partial \zeta} + \left(1 + i\frac{T}{8\pi}\right)|q_{1,2}|^2 q_{1,2} + \\ &i\frac{V}{8\pi^2}|q_{1,2}|^4 q_{1,2} + \frac{\pi}{2} q_{2,1} = 0 \end{aligned} \quad (4.11)$$

here, ζ is the normalised propagation coordinate related to the actual propagation distance, z, by $\zeta=z/L_c$ and $q_{1,2}$ is the normalised complex field amplitude in waveguides 1 and 2 and is expressed as :

$$q_{1,2}=\left(\frac{2\pi a_2 n_2 L_c}{\lambda}\right)^{\frac{1}{2}} \qquad (4.12)$$

Where a_2 represents the overlap integral over the mode profiles in the waveguides for the third order nonlinearity. T is the two photon absorption figure of merit for a coupler defined by :[42]

$$T=\frac{2\alpha_2\lambda}{n_2} \qquad (4.13)$$

where α_2 is the two photon absorption coefficient. V is the three photon figure of merit for a coupler defined by :[41]

$$V=\frac{I_c\alpha_3 a_3\lambda}{a_2 n_2} \qquad (4.14)$$

α_3 is the three photon absorption coefficient. a_3 represents the overlap integral over the mode profiles in the waveguides for the fifth order nonlinearity.I_C, otherwise known as the critical intensity, is the intensity of the input light required to switch a half-beat coupler to the point where 50% of the power exits each waveguide and can be expressed as:

$$I_c=\frac{\lambda}{a_2 L_c n_2} \qquad (4.15)$$

Linear and nonlinear absorption within such a system can cause the switching efficiency of the coupled arrays as well as the throughput to decrease. The presence of multi-photon absorption can also lead to the distortion of the output pulses from the bar and cross states.

Assuming no multi-photon absorption equation 4.11 can be solved analytically in terms of elliptic functions. The intensity of light emerging from the bar (input guide) can be written as :[41]

$$I_b(L) = I(0)\left[1 + \mathrm{cn}\left(\frac{\pi L}{L_c} \middle| m\right)\right]^{1/2} \quad (4.16)$$

were L is the length of the coupling section, $m=[I(0)/I_c]^2$, $I_b(L)$ is the output intensity of the input guide, I(0) is the input intensity and cn(u|m) is a jacobi elliptic function.

When the effects of multi-photon absorption are taken into account then numerical techniques are required to solve equation 4.11. Two such methods, the Runge-Kutta method and the beam propagation method, are discussed in section 4.5.

4.4. Applications of Nonlinear Coupler Devices.

One of the most promising applications of nonlinear coupled arrays is that of a switching element. The implementation of all-optical switches has already been explored theoretically in many broad band switching systems including asynchronous transfer mode (ATM) switching networks,[43] optical TDM switching systems[44] and in other optical photonic switching networks.[45-48]

The nonlinear coupler was initially investigated by Jensen in 1982.[49] This paper considered the operation of a two guide nonlinear coupler, otherwise known as the nonlinear directional coupler and predicted power dependent all-optical switching. Since then research into a number of different coupler configuration has taken place, including the study of an infinite set of couplers constituting a periodic array.[50]

The first observation of switching in a nonlinear directional coupler was reported in a strain induced, GaAs/AlGaAs, multiple quantum well device.[19] In that experiment, partial switching was achieved using an AlGaAs laser diode with an average output power of 1 mW, operating at 850 nm and producing 100 ns pulse at a repetion rate of 1 kHz. Subpicosecond all-optical switching was also reported in a dual-core fused quartz fibre device[51] using 100 ps pulses from a 1.06 μm modelocked Nd:YAG. The critical switching power for this device was 850 W. Since then the critical switching powers of couplers have been improved considerably. Switching has been observed in semiconductor waveguides as a result of the AC Stark effect,[52] in nonlinear semiconductor laser amplifiers[53-54] and devices based on the half band gap nonlinearity of AlGaAs.[55-56] All-optical switching has also been observed in two cascaded nonlinear directional couplers.[42] Mode/polarisation splitters,[21-22] modulators,[52,57] pulse compressor,[58-59] pulse shaping and modelocking[60-61] applications have all been demonstrated using nonlinear couplers.

In computing systems nonlinear couplers have been used to provide optical control,[62] to produce optical counters[63] and used to perform routing and memory implementations.[64] They have also been used as optically controlled bistable latches,[65] optical logic gates,[66] limiters and wavelength selecting / filtering components[25,67,68] which will be useful in future wavelength division multiplexing (WDM) networks. Intensity coded signal multiplexers/demultiplexers of serial data in fibre and planar waveguide systems using nonlinear couplers have also been demonstrated.[29,69,70]

Other interesting devices developed using nonlinear couplers included a multiple wavelength light source fabricated in GaAs/AlAs.[71] A Fabry Perot resonators/ resonant optical reflector laser diodes,[72] a passive fibre optic gyroscope (rotation detector) formed using a 3x3 coupler[73] and fibre amplifiers[73] and Ring lasers /resonators systems[75-76] have also been proposed which employ nonlinear couplers.

4.4.1. Nonlinear Waveguide Arrays and Soliton Switching.

Recent theoretical studies[77-78] of three-core nonlinear couplers have shown that these arrays have sharper switching characteristics than the standard dual-core couplers. The result is that when implemented as a switch they behave more like an ideal, step-like switch. Investigations into the behaviour of inhomogenous nonlinear waveguide arrays have shown that these guides have interesting switching characteristics which could be used to create novel all-optical devices.[79-81] For example Matsumoto et al[81] analysed the switching properties of a waveguide array with a longitudinally decreasing coupling coefficient. They found that this array can induce an adiabatic narrowing of the spatial field distribution propagating in the guides making possible both phase and amplitude-controlled optical switching with a high extinction ratio. In addition theoretical studies into both nonlinear waveguide arrays[79-83] and fibre arrays[83-86] have shown that these structures can support discrete spatial soliton modes in which light is self-trapped in a few guides. Such devices make possible power controlled beam steering and switching.

Using a soliton (either temporal or spatial) based all-optical switch has some potential advantages over a non-soliton configuration. Optical pulses, in general, contain a time depenednt distribution of powers and so the switching characteristics depend on the shape of the pulse and the response of the nonlinearity. Therefore, there is inevitably some pulse distortion in nonlinear switching arrays. In contrast, solitons switch as a single unit and so this distortion is avoided, enabling a switching efficiency of 100% to be achieved.

4.5. Theoretical Modelling of Nonlinear Coupler Arrays.

The numerical simulations used in this research were performed using a split-step Fast-Fourier Transform (FFT) beam propagation method[87] to model the switching of short high powered pulses in the waveguide arrays. A fourth order Runge-Kutta algorithm was also employed to simulate the switching of CW waves in the nonlinear arrays.[88] An explanation of the R-K method is given in appendix A along with the R.K FORTRAN program code used to simulate the C.W. switching within the coupled arrays.

4.5.1. Temporal Beam Propagation Method.

The split-step fourier transform method used in this research is a popular numerical technique commonly utilised in the analysis of the propagation of light pulses within dispersive nonlinear material. The equations describing the propagation of short, high powered, light pulses within the coupled arrays are nonlinear partial differential equations which include the effects of dispersion, linear absorption, nonlinear loss and self-phase modulation. Initially the temporal behaviour of the pulses propagating through the coupler structure was considered. In the case of the three guide coupler the equations describing the propagation of the temporal pulse through the guides were as follows :

$$
\begin{aligned}
&i\frac{dE_1}{dz} = -C_{1,2}E_2 + \frac{D_2}{2}\frac{d^2E_1}{dt^2} - i\frac{\alpha_0}{2}E_1 + \\
&\left(i\frac{\alpha_2}{2} - n_2\kappa_0\right)\frac{|E_1|^2 E_1}{A_{eff}} - i\frac{\alpha_3}{2}\frac{|E_1|^4 E_1}{(A_{eff})^2}
\end{aligned}
\qquad (4.17)
$$

$$
\begin{aligned}
&i\frac{dE_2}{dz} = (-C_{1,2}E_1 - C_{2,3}E_3) + \frac{D_2}{2}\frac{d^2E_2}{dt^2} - i\frac{\alpha_0}{2}E_2 + \\
&\left(i\frac{\alpha_2}{2} - n_2\kappa_0\right)\frac{|E_2|^2 E_2}{A_{eff}} - i\frac{\alpha_3}{2}\frac{|E_2|^4 E_2}{(A_{eff})^2}
\end{aligned}
\qquad (4.18)
$$

$$
\begin{aligned}
&i\frac{dE_3}{dz} = -C_{2,3}E_2 + \frac{D_2}{2}\frac{d^2E_3}{dt^2} - i\frac{\alpha_0}{2}E_3 + \\
&\left(i\frac{\alpha_2}{2} - n_2\kappa_0\right)\frac{|E_3|^2 E_3}{A_{eff}} + i\frac{\alpha_3}{2}\frac{|E_3|^4 E_3}{(A_{eff})^2}
\end{aligned}
\qquad (4.19)
$$

where E_1, E_2 and E_3 are the fields propagating in the input (bar channel), the centre (cross 1) and the end (cross 2) guides respectively, $C_{1,2}$ is the linear coupling coefficient between the input channel and the centre guide and $C_{2,3}$ is the coupling coefficient between the centre and the end guide. The first term on the right hand side of each equation relates to the linear coupling between the guides. Only nearest neighbour interactions are assumed to be important. The second term on the right hand side describes the effect of chromatic dispersion on the pulse, were D_2 is the chromatic dispersion given in units of s^2/m. The remaining terms on the right hand side of the equations describe the linear loss, two-photon absorption, self-phase modulation and three-photon absorption.

The split-step fourier method operates by dividing the propagation distance z, into very small steps, h. Over each small propagation length interval the nonlinear effects and linear effects are considered independent of each other. This method is used because it can be much faster than most finite difference methods. The method is illustrated in figure 4.3.

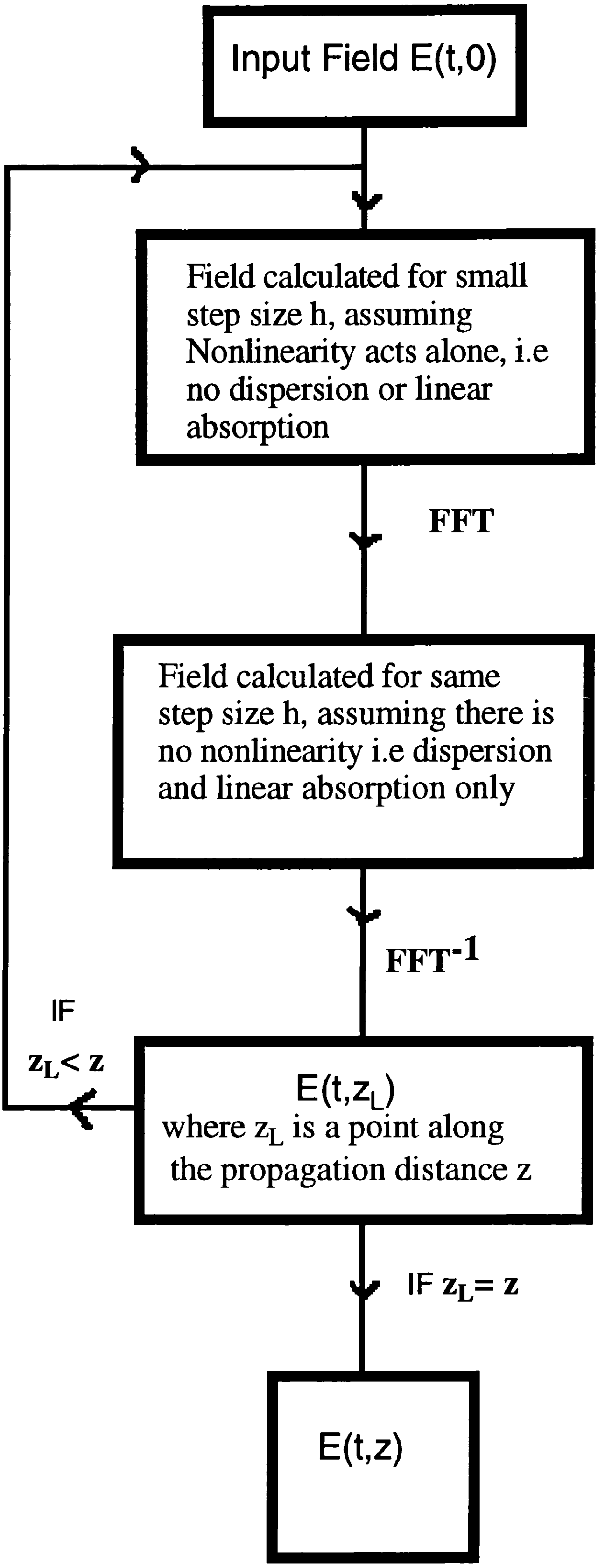

Figure 4.3. Schematic of the BPM process.

Initially the linear and nonlinear terms of the equations describing the field propagating within the coupled structure are grouped together. For example, equations 4.17-19 can be rewritten as:

$$i\frac{\partial E}{\partial z}=\left(\hat{D}+\hat{N}\right)E \quad (4.20)$$

Where $\hat{D}$ is the linear differential operator which includes all the linear terms of the equation, i.e. the dispersion and linear absorption terms. $\hat{N}$ is the nonlinear operator which includes the nonlinear loss and nonlinear refraction terms. The propagation length z, is divided into small step sizes of length, h. The calculation of the Electric field propagating from a point z_L to the z_L+h along the total interaction length, z, is carried out in two stages. In the first stage the linear operator is assumed to be zero. In the second stage the nonlinear operator is assumed to be zero and the field is calculated in the fourier domain as shown in figure 4.3. This process can be expressed mathematically:[87]

$$E(z_L+h,t)=\exp\left(ih\hat{D}\right)\exp\left(ih\hat{N}\right)E\left(z_L,t\right) \quad (4.21)$$

In the theoretical simulations, the initial input pulse shape, E^o_1, was taken to be a sech pulse shape of temporal full width at half maximum equal to $1.763T_O$ and is expressed as :

$$E_1^o=\sqrt{P_{peak}}\,\mathrm{sech}(t/T_0) \quad (4.22)$$

were P_{peak} is the peak power. The initial fields in the cross states were assumed to be zero. After propagation of the pulses through the sample, an integration was performed over the temporal profile of the three pulses to establish the energy exiting each waveguide. This step is similar to that carried out by detection system used in the experiment where the germanium photodiodes measured the average power or energy from each waveguide.

4.5.2. Spatial Beam Propagation Method.

To simulate spatial switching in the device a Gaussian input was propagated through the structure (neglecting the temporal dependence by propagating a CW Gaussian beam). In this case diffraction, instead of dispersion is considered. The equation describing the propagation of the electric field through the devices is given by:

$$-i\frac{dE}{dz}=\frac{1}{2\kappa_o n_{eff}}\frac{d^2E}{dx^2}+ \\ \frac{\kappa_o}{n_{eff}}\left[n^2(x)-n^2{}_{eff}+2n_{eff}n_2|E|^2\right]E \qquad (4.23)$$

where the input beam is chosen as either a waveguide mode or a Gaussian beam. The structure of the device is included in the refractive index profile n(x). It should be noted that equation 4.23 does not included the effects of multiphoton absorption. Thees effects were included when the spatial BPM model was used carry out simulations of the propagation characteristics of the coupler arrays tested.

4.5.3. Theoretical Simulations of the Switching Characteristics of Nonlinear Arrays.

The temporal BPM code, listed in appendix B, was originally developed by Prof. A. Villeneuve. The code simulates the switching behaviour of a three guide nonlinear coupler. It was easily adapted to simulate the switching characteristics of multi-core couplers.

The BPM program contains a changeable data file which enabled an accurate comparison to be made between the experimentally observed and the theoretically simulated switching characteristics of real nonlinear arrays. The data file allowed the following parameters to be adapted: pulse width (FWHM), pulse shape (sech, Gaussian or an input file), the nonlinear refractive index, n_2, the two and three photon absorption coefficients, the effective area of the guides, dispersion, linear absorption and the coupling strengths between the guides.

The Runge Kutta algorithm, was used to simulate the switching characteristics of a nonlinear array were the input light was a CW beam. The R.K. simulations give an insight into the ideal switching characteristics of the nonlinear arrays rather than emulating the experimentally observed switching behaviour of the guides. This is due to the fact that the experimentally observed switching was produced using short high peaked pulses. Therefore, pulse distortion and break up occurs due to the fact that the nonlinearity has an instantaneous response time compared to the temporal width of the pulse and so the switching efficiency/contrast of the guides is lower than the ideal case.

Figure 4.4, produced using the R.K. algorithm, shows the power transmitted by the bar state of a two, three and four guide nonlinear array, one half beat length long, as a function of input field intensity. It can be seen that the three guide and four guide couplers have much sharper switching characteristic compared to the two guide nonlinear coupler. This figure also shows that the switching power increases as the number of guides in the coupler increase.

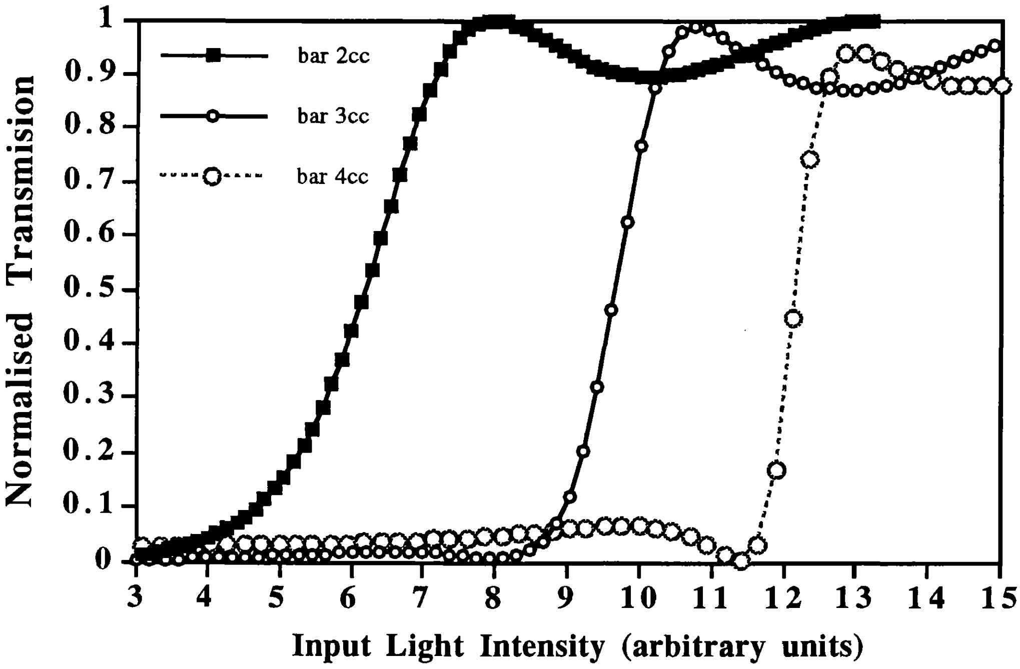

Figure 4.4. Illustration of the switching of the bar state of a half-beat two guide nonlinear coupler labelled 2cc, a half-beat three guide nonlinear coupler labelled 3cc and a half-beat four guide coupler labelled 4cc, as a function of input power into the bar state.

4.5.3.1. Simulation of the Switching Behaviour of a Nonlinear Three-Core Coupler.

Figure 4.5 shows the switching characteristics of a nonlinear three guide coupler simulated using both the Runge-Kutta code and the temporal BPM program. In these simulations the effects of dispersion, linear and nonlinear loss were neglected. Figure 4.5(a) is the switching characteristics of a CW light beam in the three guide coupler. At low powers all the light has linearly coupled over to the cross 2 guide (end guide). As the light intensity is increased most of the power is transferred to the cross 1 (middle guide) guide before switching back to the input (bar) guide. Fig. 4.5 (b) shows the simulated switching characteristics of the same three core coupler, this time using the temporal BPM and a sech type input pulse of 10 ps duration. As shown there is a clear reduction in the switching fraction /efficiency of the nonlinear coupler when using pulses although the actual switching behaviour is essentially the same.

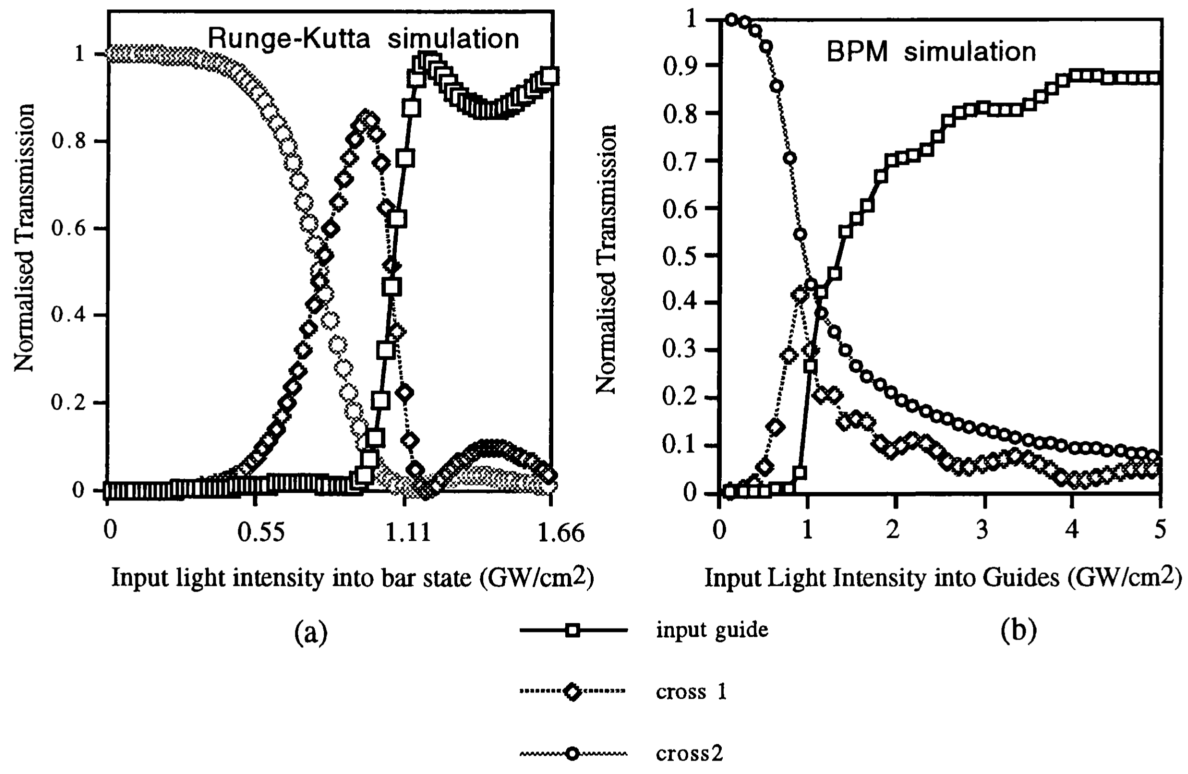

Figure 4.5 Simulations of the switching behaviour of a nonlinear three guide coupler.

4.5.3.2. Simulations of the Switching Behaviour of Nonlinear Four-Core Couplers.

The switching characteristics of a uniformly spaced four guide nonlinear coupler is shown in figure 4.6 for a CW light source using the R.K. algorithm.

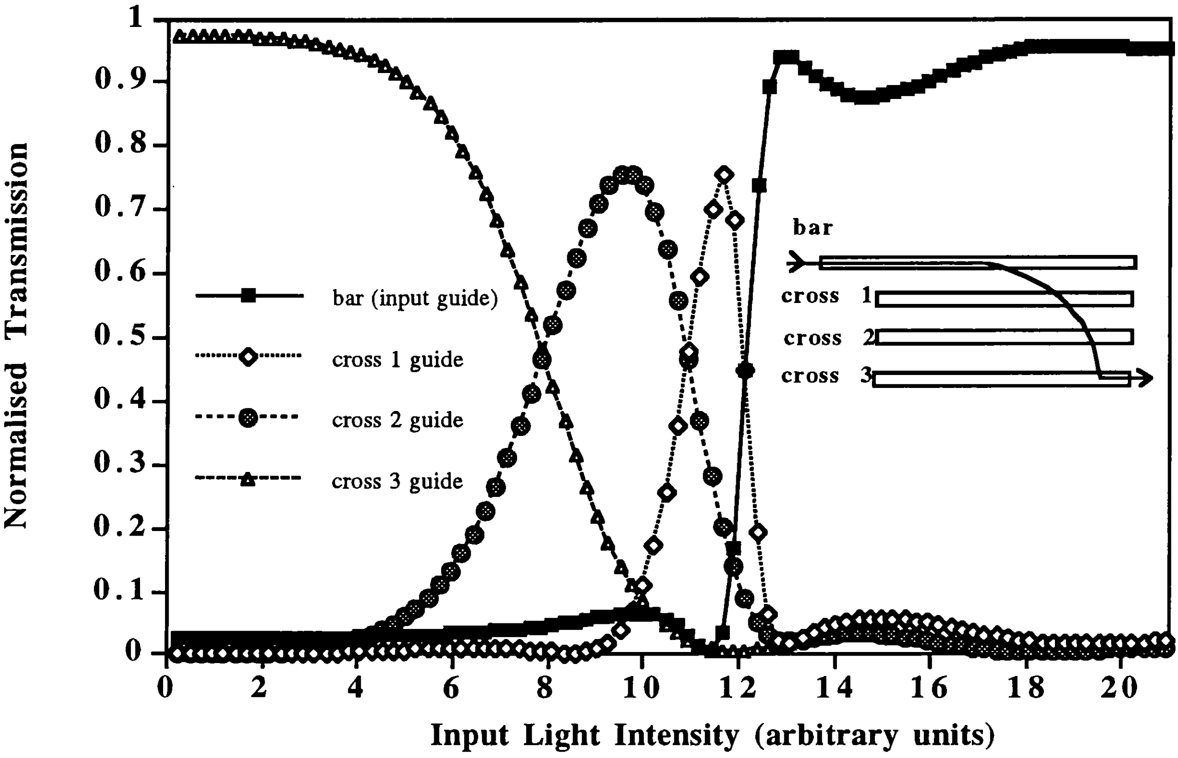

Figure 4.6. simulation of the switching of a CW input beam in a uniformly spaced four guide nonlinear coupler.

Figure 4.6 compares well with the switching behaviour of the same four guide coupler simulated using sech shaped pulses of 1 ps duration as shown in figure 4.7. Again the switching fraction/ efficiency is less when switching pulses. Comparing the simulated switching characteristics of the three and four guide couplers, it is seen that with the four guide couplers the switching to the bar state is sharper but the actual switching fraction is slightly lower that of the three guide coupler.

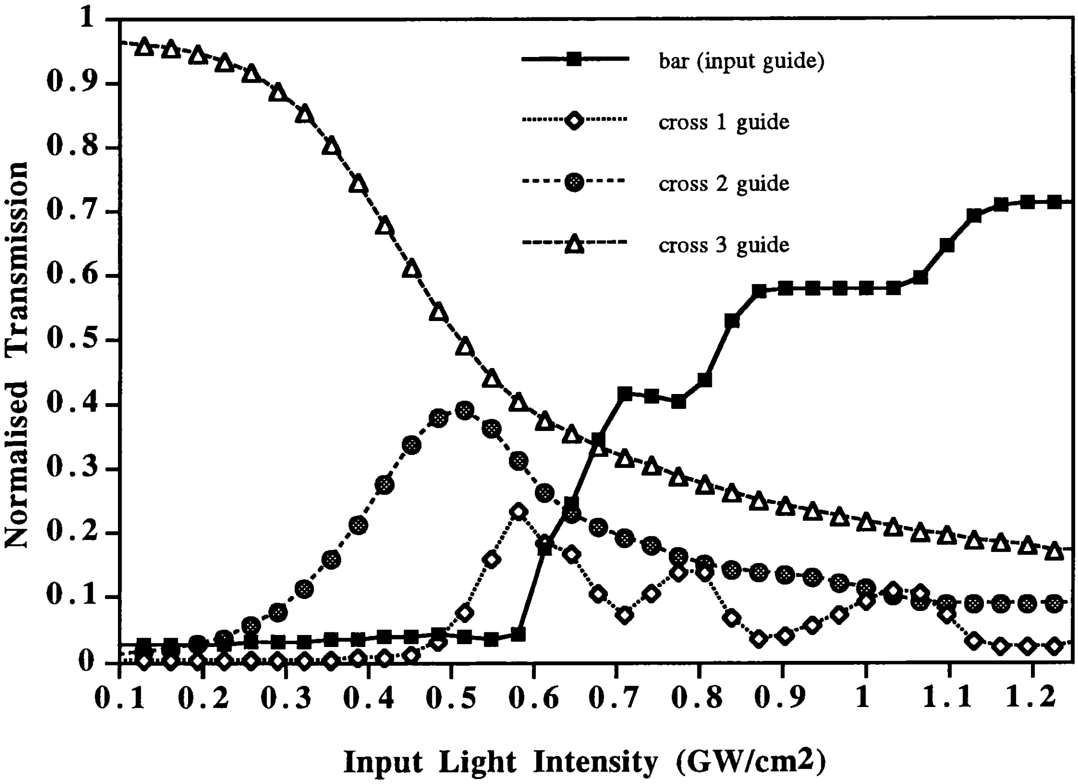

Figure 4.7. The switching characteristics of a uniformly spaced four guide coupler obtained using a pulsed input .

In this section the switching behaviour of several different non-uniformly spaced four guide couplers will be examined. Figure 4.8 illustrates a 1x4 nonlinear array were $C_{1,2}$, $C_{2,3}$, $C_{3,4}$ are the linear coupling coefficients between the guides as shown.

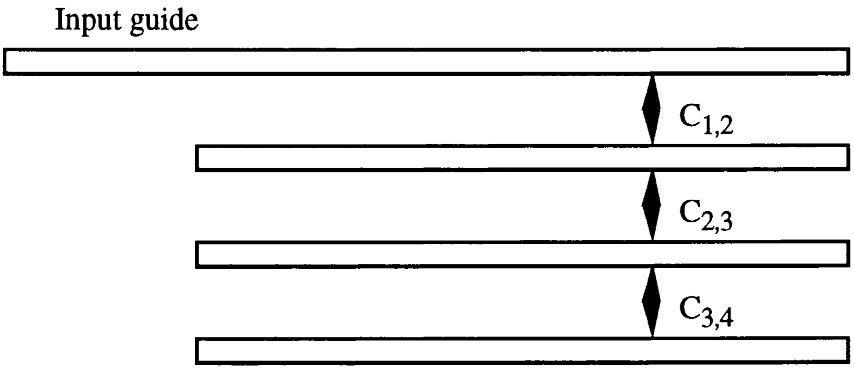

Figure 4.8. Top view of a 1*4 nonlinear array, C denotes the coupling between the guides.

In the first example, a four guide coupler where the coupling coefficients between the guides were as follows $C_{1,2}=C_{3,4}=(0.82) \times C_{2,3}$ was examined. This corresponds to a coupler where the spacing between the input and cross 1 guide and also the spacing between the cross 2 and cross 3 guide is ~ 4.3 μm and the spacing between the cross 1 and cross 2 guide is ~ 4 μm.

Figure 4.9 shows the transmission characteristics of the coupler obtained using the R.K algorithm. Comparing fig. 4.6 and fig. 4.9 it is clear that there is less switching of the light into the cross 1 guide and sharper switching between the cross 2 guide and the bar state in the non-uniformly spaced coupler than for the uniformly spaced coupler.

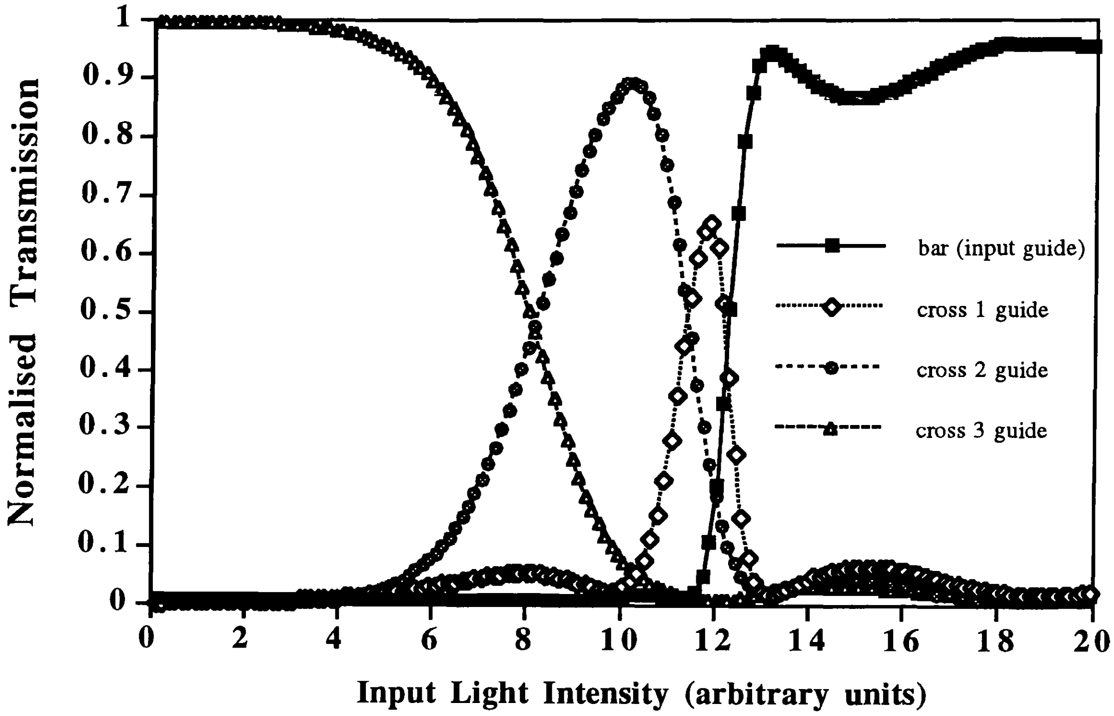

Figure 4.9. R.K, Simulation of the transmission characteristics of a non-uniformly spaced coupler where $C_{1,2}=C_{3,4}=(0.82) \times C_{2,3}$.

This result was echoed by the BPM simulation shown in figure 4.10 of the switching of a 1 ps sech pulse in the coupler array. As shown in this figure ripples occur in the output power of the bar and cross 1 guide at light intensities higher than the critical intensity for switching to occur. These power fluctuations are not evident in the Runge-Kutta simulations of the same couplers and may be due to the fact that pulse break up is accounted for in the BPM simulations. Therefore the wings of the pulse not switched at the critical light intensity play a part in the transmission characteristics of the couplers at higher powers.

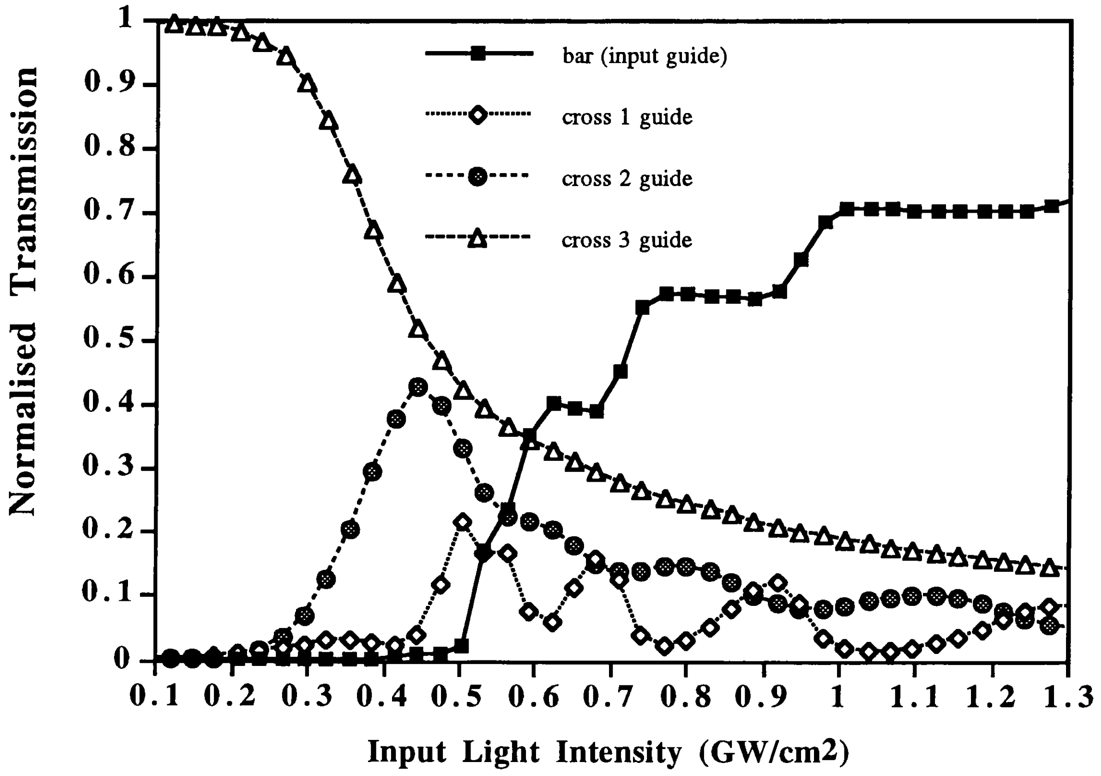

Figure 4.10 . BPM simulation of the transmission characteristics of a non-uniformly spaced coupler, where $C_{1,2}=C_{3,4}=(0.82) \times C_{2,3}$.

Figure 4.11 shows the transmission characteristics of a non-uniformly spaced coupler where the coupling between the guides were $C_{2,3}=C_{3,4}=(0.82) \times C_{1,2}$ using the R.K algorithm. Figure 4.12 is the BPM simulation of the same coupler produced using 1 ps sech shaped pulses.

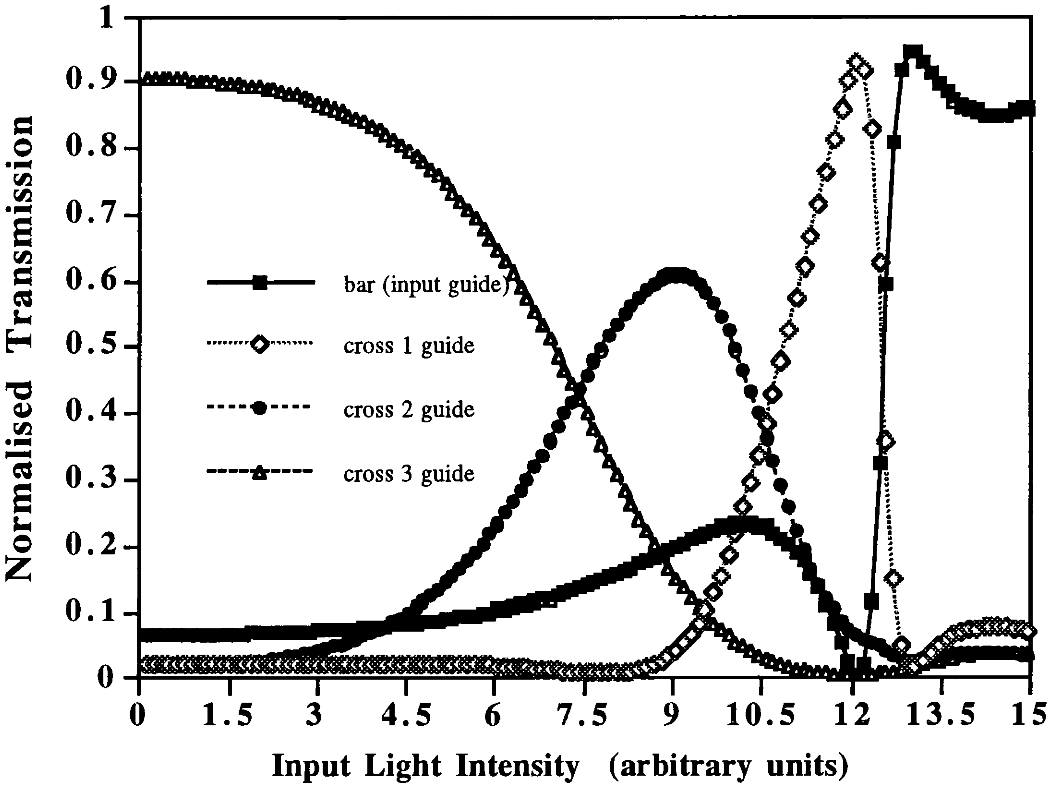

Figure 4.11. R.K simulation of the transmission characteristics of a non-uniformly spaced coupler, where $C_{2,3}=C_{3,4}=(0.82) \times C_{1,2}$.

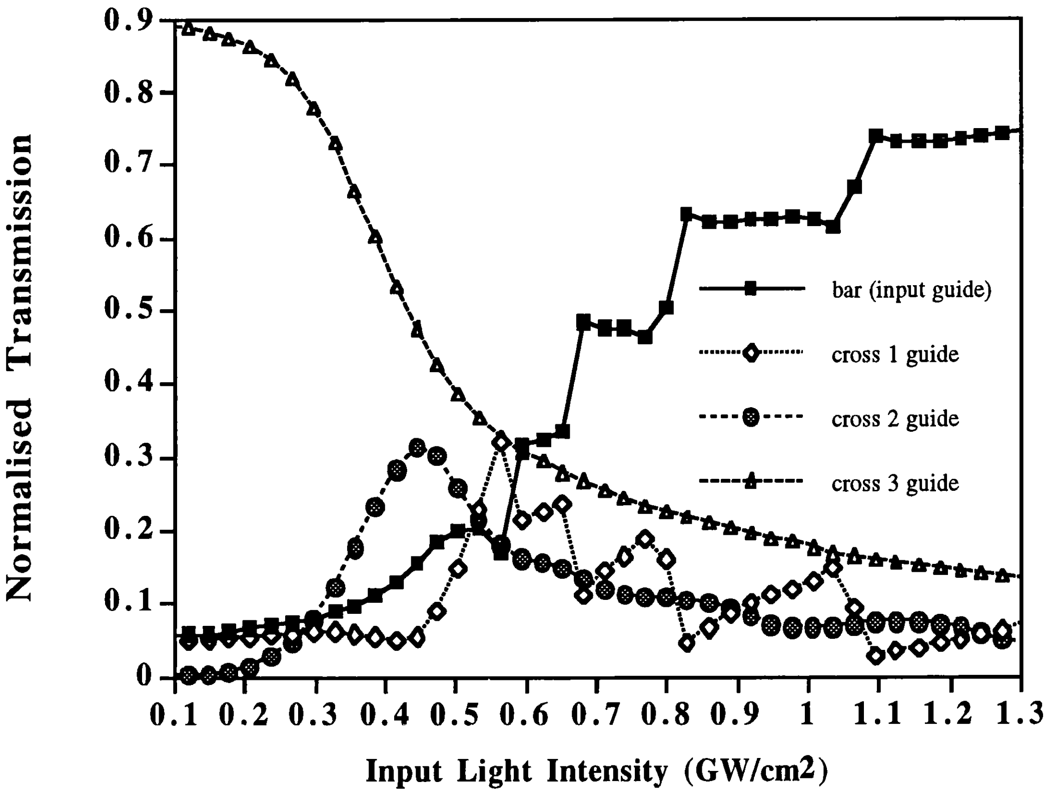

Figure 4.12. BPM simulation of the transmission characteristics of a non-uniformly spaced coupler where $C_{23}=C_{34}=(0.82) \times C_{12}$.

Again the transmission characteristics of this non-uniformly spaced coupler are different from those of the uniformly spaced coupler. As shown in figure 4.12 there is greater power transfer from the cross 2 into the cross 1 before switching back into the input guide.Therefore, it has been shown that the switching characteristics of a nonlinear array can be altered by varying the spacing between the guides. These non-uniformly spaced waveguide couplers could be useful in the development of novel waveguide devices.

4.6. Design and Fabrication of the Arrays.

Efficient ultrafast switching in nonlinear waveguide arrays requires a material with low linear and nonlinear absorption losses. The waveguide's structure must have a good optical confinement factor in order to maintain the high optical intensities required to induce the phase shift necessary for switching. The optical waveguides tested had been fabricated using a reactive ion etching process. It has been shown that this method of fabrication produces well defined, low loss guides. The couplers were fabricated in AlGaAs and operated in the half-bandgap spectral region. The lower cladding layer was 4 μm thick and contained 24% Al, the waveguide layer was 1.5 μm thick and contained 18% Al and finally the upper cladding was 1 μm thick with 24% Al. Guides, 4 μm wide, were etched 0.9 μm into the upper cladding layer, using a combination of standard photo-lithography and reactive ion etching. The lateral optical confinement factor, corresponding to the effective index difference between the rib region and the unetched region outside the rib was calculated to be 2.56×10^{-3}. The input guide was extended by a few mm to ensure that light is initially launched into a single channel. Figure 4.13 shows a photograph, produced using a scanning electron microscope, of a two guide nonlinear coupler. It can be seen that the reactive ion etching process results in well defined waveguide structures. The good quality side walls result in low loss waveguides, where the scattering loss of a typical waveguide is less than 0.1 cm^{-1}.

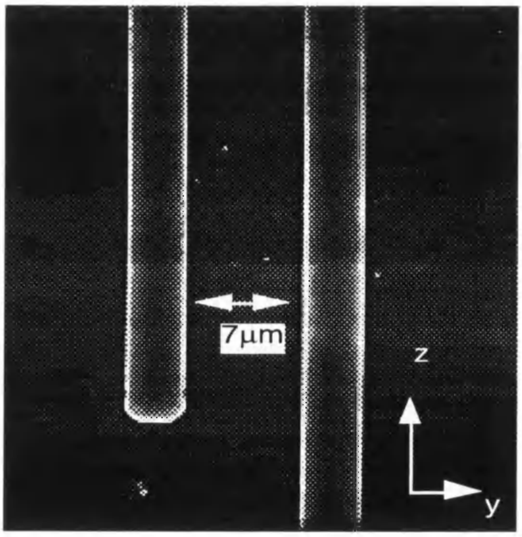

Figure 4.13. SEM photo of a two guide coupler formed using photolithography and reactive ion etching.

4.7. Experimental Investigation of Nonlinear Coupled Arrays.

In this section the experimentally measured switching characteristics of three, four and eight-core couplers are presented. The section begins with a look at the experimental arrangement and procedure. The experimental switching results are then presented and compared to the theoretically simulated transmission characteristics of the devices. It should be noted than in the following experiments each measurement taken was repeated several times to achieve the most accurate results possible.

4.7.1. The Experimental Set-up.

Initially the switching characteristics of several three-core coupler configurations were studied. The experimental set up used to test the coupler is illustrated in figure 4.14.

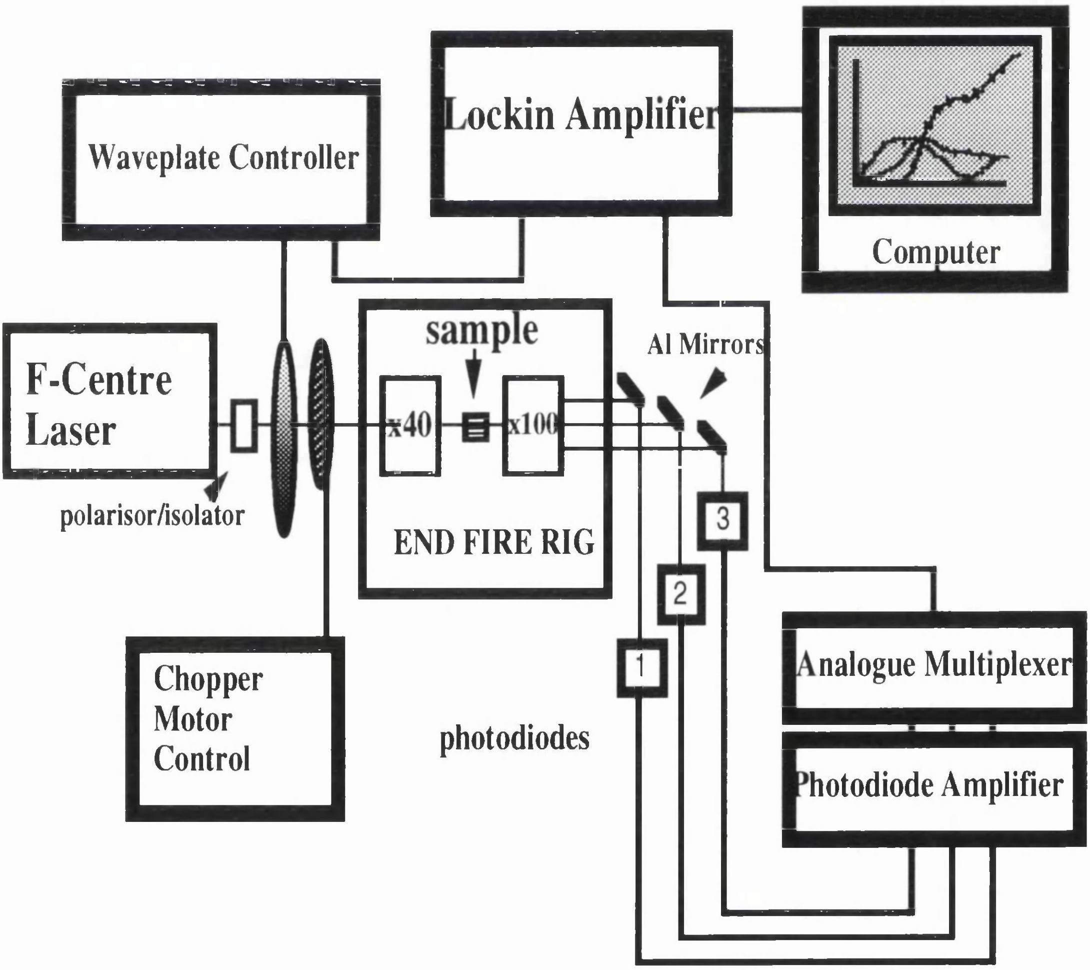

Figure 4.14. The experimental set up used to test the nonlinear arrays.

The experiments were performed with a modelocked colour centre laser as described in chapter 1. The output of the laser beam was end-fire coupled into the guides. The coupling was optimised by monitoring the output of the couplers using an IR camera and a TV monitor. The laser was focused into the guides using a x40 objective and the output of each coupler was separated and focused onto the camera by a x100 objective lens. A polariser / half-wave plate combination was used to select the input polarisation and the chopper served to provide a reference signal to the lockin amplifier. A second wave-plate was used to control the amount of power coupled into the guides. The output of each guide was imaged onto three separate Ge detectors via three plane aluminium mirrors and the input power was also measured using a Ge detector. Maximum coupling was obtained by monitoring the total output power of all the guides until it reached its greatest value. The outputs of the 4 photodiodes were individually monitored by separate lockin amplifiers. The position /speed of the waveplate and the lockin measurements were computer controlled using a Macintosh with a GPBI interface. This software control allowed measurement of the output power of each of the guides as a function of input power.

4.8. Experimental Results.

4.8.1. Three Guide Nonlinear Couplers Experiments.

4.8.1.1. The Centre Launched Three Guide Coupler.

Figure 4.15 shows a SEM picture of one of the centre launched couplers that was tested.

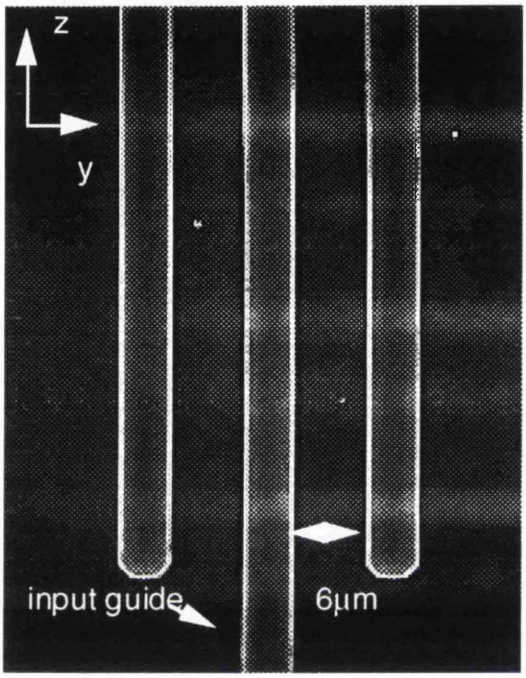

Figure 4.15 . SEM photograph of a three guide coupler were the input guide is the centre core.

The light used to test these couplers was from a synchronously pumped laser arrangement which produced 10.5 ps sech^2 pulses of 620 mW average power at a pulse repetition rate of ~ 80 Mhz, corresponding to a peak power of ~ 600 W, at a wavelength of 1540 nm. The peak power into the guides was approximately 300 W. This coupler comprised 4 μm wide waveguides, separated by 6 μm. The length of the coupler was chosen to be 1.5 cm to approximate a half-beat coupler. The experimentally measured normalised transmission for a uniformly spaced three-core coupler where the input beam was applied to the centre waveguide (bar channel) is shown in fig. 4.16 below. It is seen that at lower powers approximately 75% of the light was linearly coupled into the outermost (cross) guides, as the input power was increased the nonlinear phase shift induced detuned the guides resulting in the light switching back to the input (centre) guide. The linear throughput of the guides was measured to be 18%.

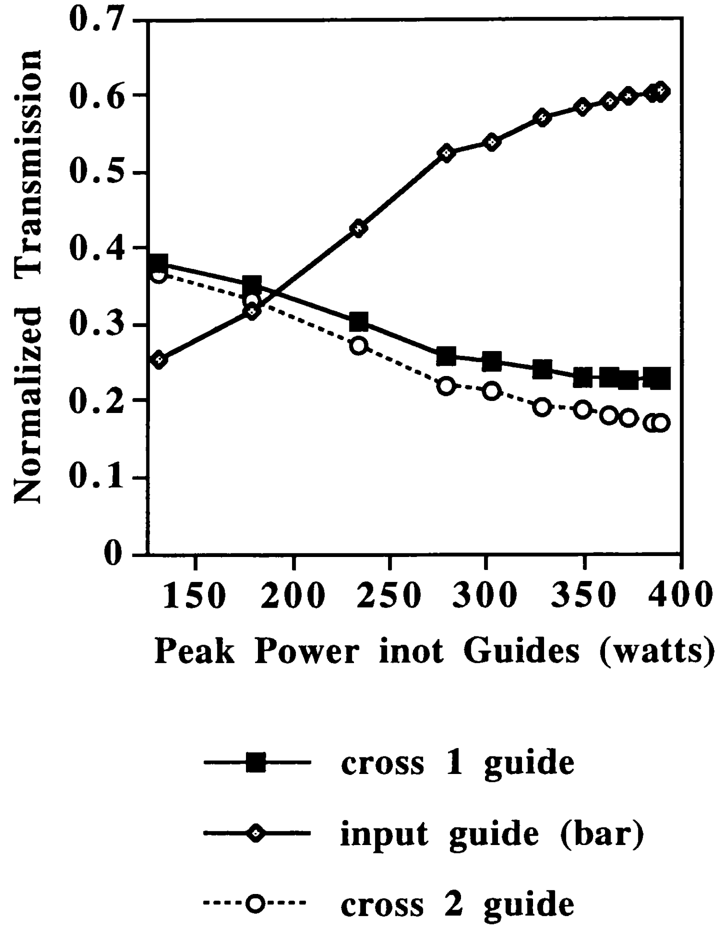

Figure 4.16. The experimental switching characteristics of a centre launched nonlinear three core coupler.

Theoretical simulations of the transmission characteristics of the centre launched nonlinear coupler were performed using the temporal, fast fourier transform BPM. It should be noted that in the theoretical simulations of the following experiments the following values for multiphoton absorption coefficients were used: For the devices tested at an operating wavelength of 1.556 μm, it was assumed that dominant multi-photon absorption present within the was due to three photon absorption as it has been shown that two photon absorption in AlGaAs operated at this wavelength is negligible.[89]. The value for the three photon absorption used was $5.5\text{x}10^{-20}$ cm^3/W^2, this number is based on previous experimental measurements.[90] At an operating wavelength of

1.54 μm, the value for TPA was taken to be 0.16 cm/W as measured in chapter 3. Figure 4.17 shows the theoretically predicted switching characteristics of the three-core coupler. As shown the experimentally measured transmission result was in good agreement with the theoretical predicted switching function. One difference to note is that the theoretical simulation predicts that at high powers the light remaining in the outermost guides (cross 1 and cross 2) are equal. Experimentally a slight difference in the power levels in the outermost guides was observed. This was attributed to small defects which resulted in a slight asymmetry between the guides.

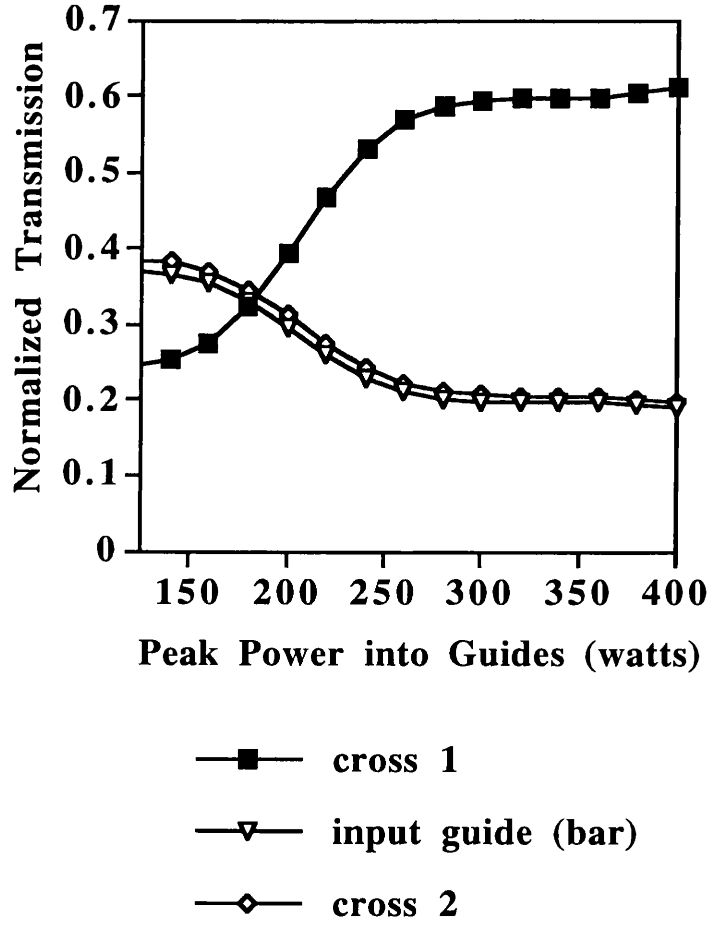

Figure 4.17. Theoretical simulation of the switching characteristics of a centre launched three guide coupler

4.8.1.2. The Side Launched Uniformly Spaced Three Guide Coupler.

The same experimental arrangement was used to characterise a uniformly spaced three guide coupler were the light was initially launched into one of the outermost guides. Figure 4.18 below is an SEM of one such device that was examined.

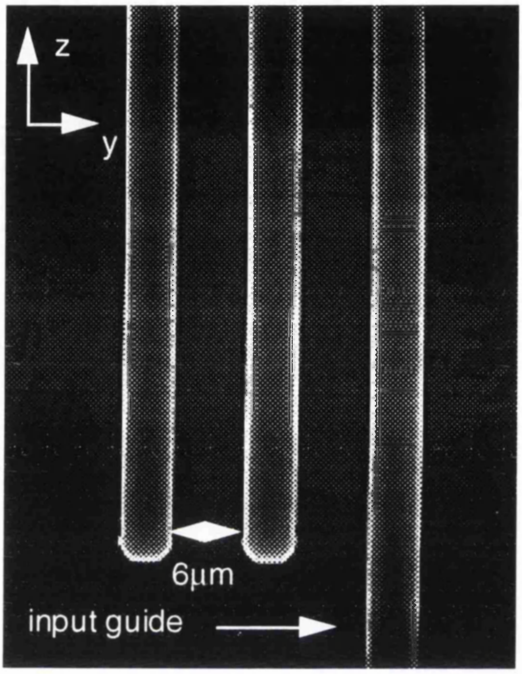

Figure 4.18 . SEM photograph of a three guide coupler with an extended length , side guide.

At low and high input light intensities the power distribution within the coupled waveguides were seen to change as shown in figure 4.19, which are photographs taken from the TV monitor of the output power from each of the guides at low and high input beam intensities.

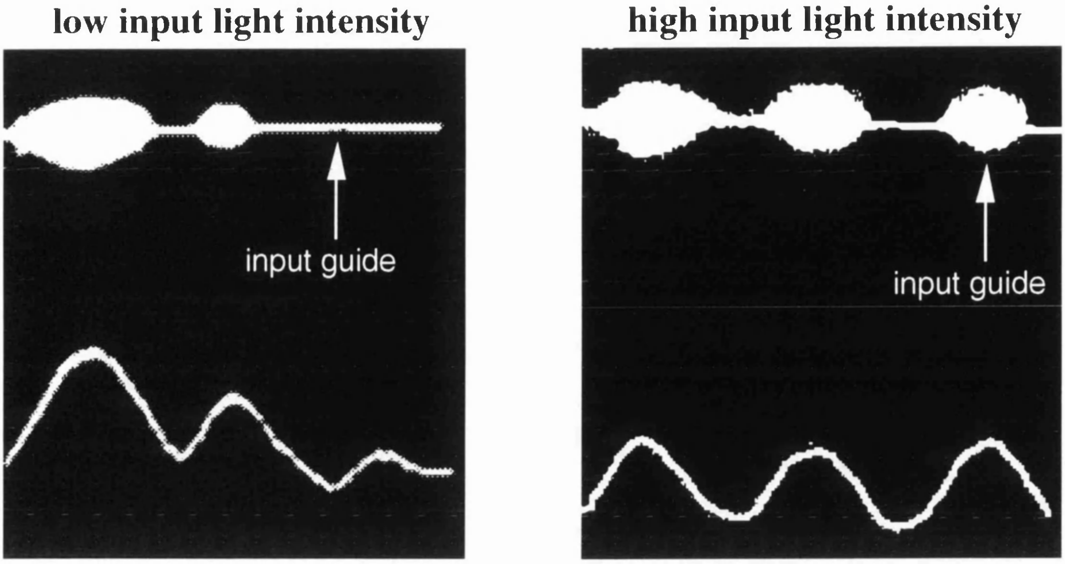

Figure 4.19. The observed light distribution in a nonlinear three guide coupler at low and high input beam intensity. The lower traces on each photograph are lines scans measured across the centre of the guides and indicate the power distribution within each guide.

The experimental switching characteristic of a side launched, three guide coupler are shown in fig .4.20. As before the guides were 4 μm wide and with a coupler length of 1.5 cm. The spacings between the guides were 6 μm. It should be noted that the etch depth of the guides on this sample was shallower and hence the coupling strength between the guides was stronger, than those for the three guide centre launch device tested previously. Therefore the half-beat length for the two devices was approximately the same. It was shown that at low powers most of the light remains in the end guide and at high powers due to the nonlinearity the linear coupling between the guides is broken resulting in the light switching back to the input guide via the middle core. Figure 4.21 displays the theoretical simulation of the switching behaviour of this device.

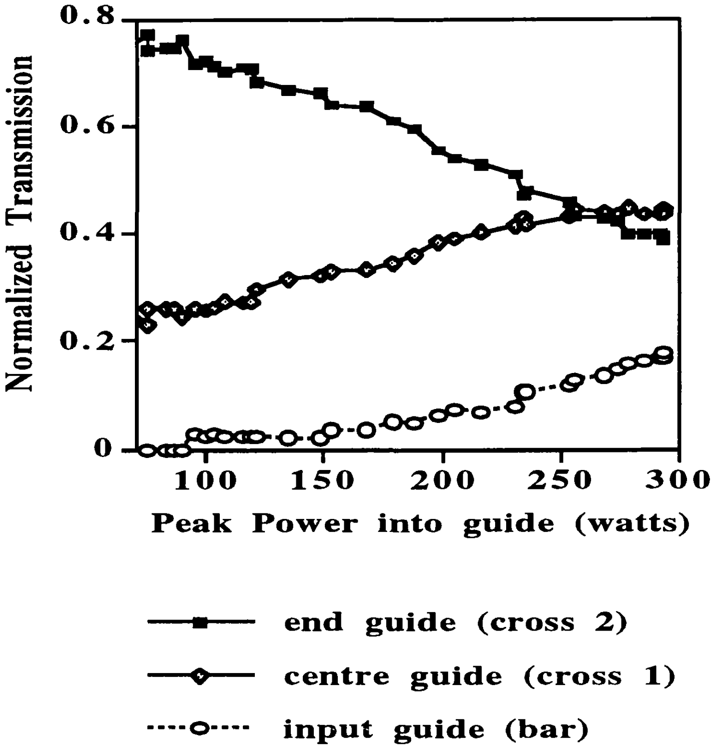

Figure 4.20. The experimental switching characteristic of a uniformly spaced side launched three guide coupler.

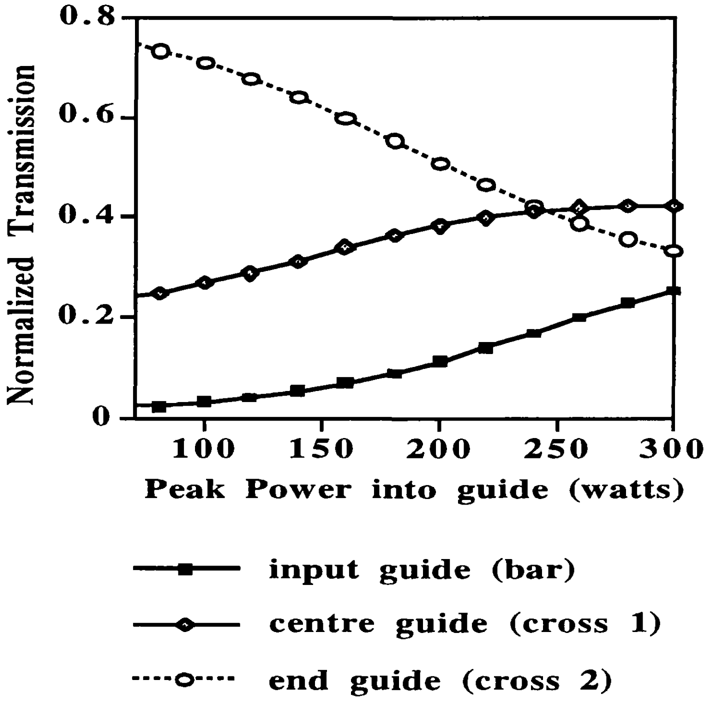

Figure 4.21 . The theoretical switching characteristic of a uniformly spaced side launched three guide coupler.

By comparing figures 4.20 and 4.21 it is seen that there is good agreement between the theoretical switching behaviour and the experimentally obtained switching characteristics of the uniformly spaced, side launched three guide coupler.

4.8.1.3. The side launched non-uniformly spaced three guide coupler.

The final three core coupler tested was a non uniformly spaced coupler. Figure 4.22 illustrate the switching behaviour of this coupler. A coupled cavity mode locked arrangement was used in this experiment. This laser arrangement was used to reduce the risk of damage to the front facet of the guides due to high average powers. The coupled-cavity mode-locked laser used was a NaCl:OH$^-$ colour centre laser which was modified using an actively stabilised external nonlinear fibre cavity to produce 0.5-1 ps pulses with an average power of 200 mW, at a wavelength centred on 1556 nm. The length of the coupler was again 1.5 cm and the width of the coupler was 4 μm. The spacing between the input and middle guide was 7.2 μm and the spacing between the middle and end guide was 7 μm.

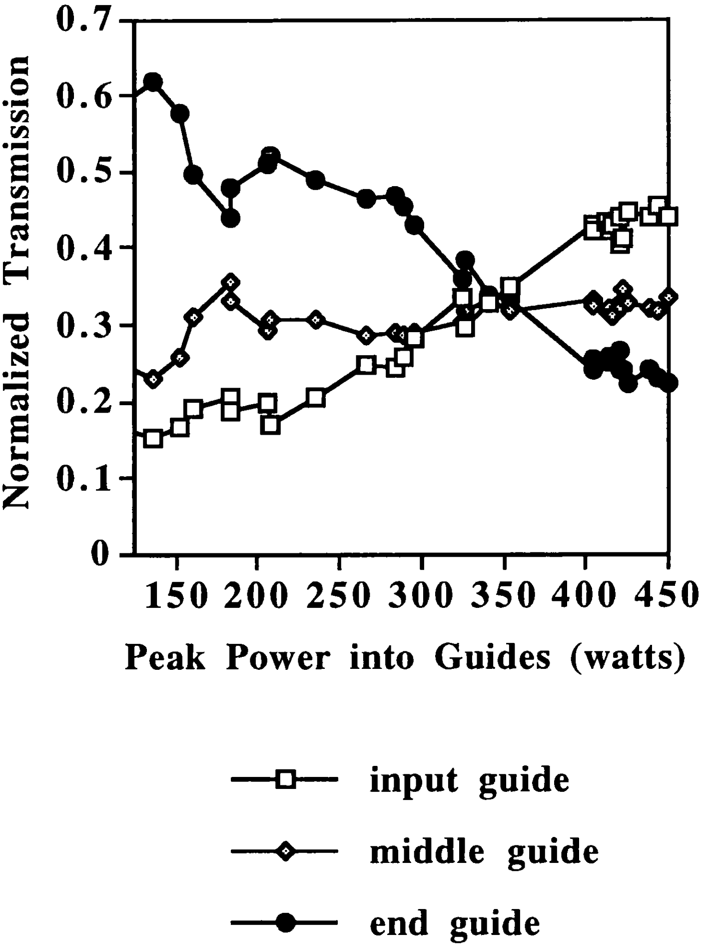

Figure 4.22. The experimental switching characteristics of a non-uniformly spaced , side-launched ,three guide coupler.

Below the critical power at around 170 W peak power there appears to be a small dip in the power transmitted by the end (or cross 2) guide. This was attributed to the instability of the laser used in the test which caused a false reading of peak input power to be calculated. The instability of the laser momentarily caused a change in the pulse width of the laser light which was not taken into account when the peak input power into the guides was estimated.

The switching characteristics of the uniformly and non-uniformly spaced couplers are compared in fig. 4.23. As can be seen, the switching behaviour of the uniform and non uniformly spaced three guide couplers are distinctly different.

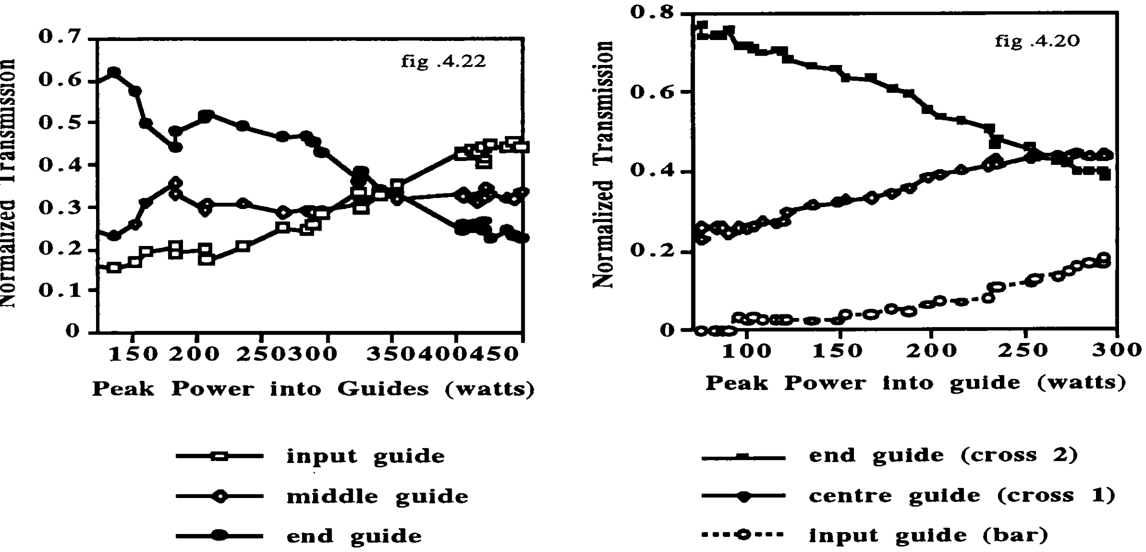

Figure 4.23. comparison of figure 4.22 and figure 4.20.

In the case of the non uniformly spaced coupler there is less power transference into the middle guide and sharper power exchange between the end and input guide than in the uniformly spaced array. This result was confirmed by the simulated switching behaviour of the non uniformly spaced guides as shown in figure 4.24 were the temporal switching behaviour is illustrated.

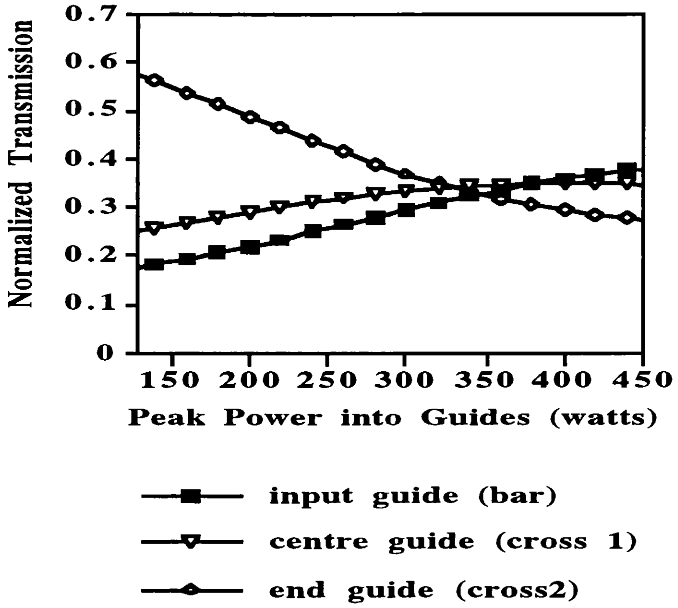

Figure 4.24. The theoretical switching characteristics of a non-uniformly spaced , side-launched ,three guide coupler.

4.8.2. Multi-guide nonlinear coupler experiments.

Waveguide arrays with a greater number of waveguides were studied next. In particular transmission characteristics of a four guide and an eight guide array were measured. These nonlinear couplers were excited by end-fire coupling the output of the coupled-cavity mode-locked, NaCl:OH^- colour centre laser producing 0.5-1 ps pulses with a peak output power of 1.5 kW, at a wavelength centred on 1556 nm. The output of the guides were imaged onto an IR camera and line scans of the output beam profiles were recorded at different power levels. These were then corrected for the nonlinear response of the camera.

4.8.2.1. The Four guide nonlinear coupler experiment.

For the four core device, the spacing between the guides was 6 µm and the coupler length was 2.32 cm. Figure 4.25 shows a SEM photo of the four guide coupler.

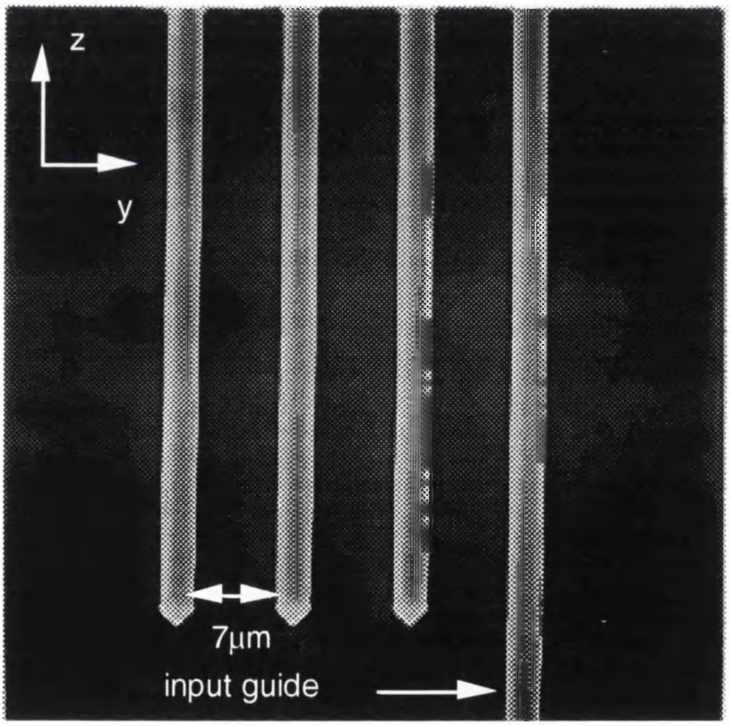

Figure 4.25. SEM photograph of a 1x4 nonlinear directional coupler.

The linear throughput of the guides was 10%. Figure 4.26 shows the experimentally obtained line scans of the output of the four guide coupler measured at low power and at the high peak power of 1.5 kW. In both cases, the average power was the same, however the pulse widths were different approximately 6 ps and 0.6 ps for the low and high power states respectively. It is clear that at low intensity levels the power is transferring to the opposite side of the sample, while at high input intensities the coupling is being broken and the power remains in the input waveguide. The high power line scan represents the time averaged output from the sample and hence, some of the switching contrast is lost.

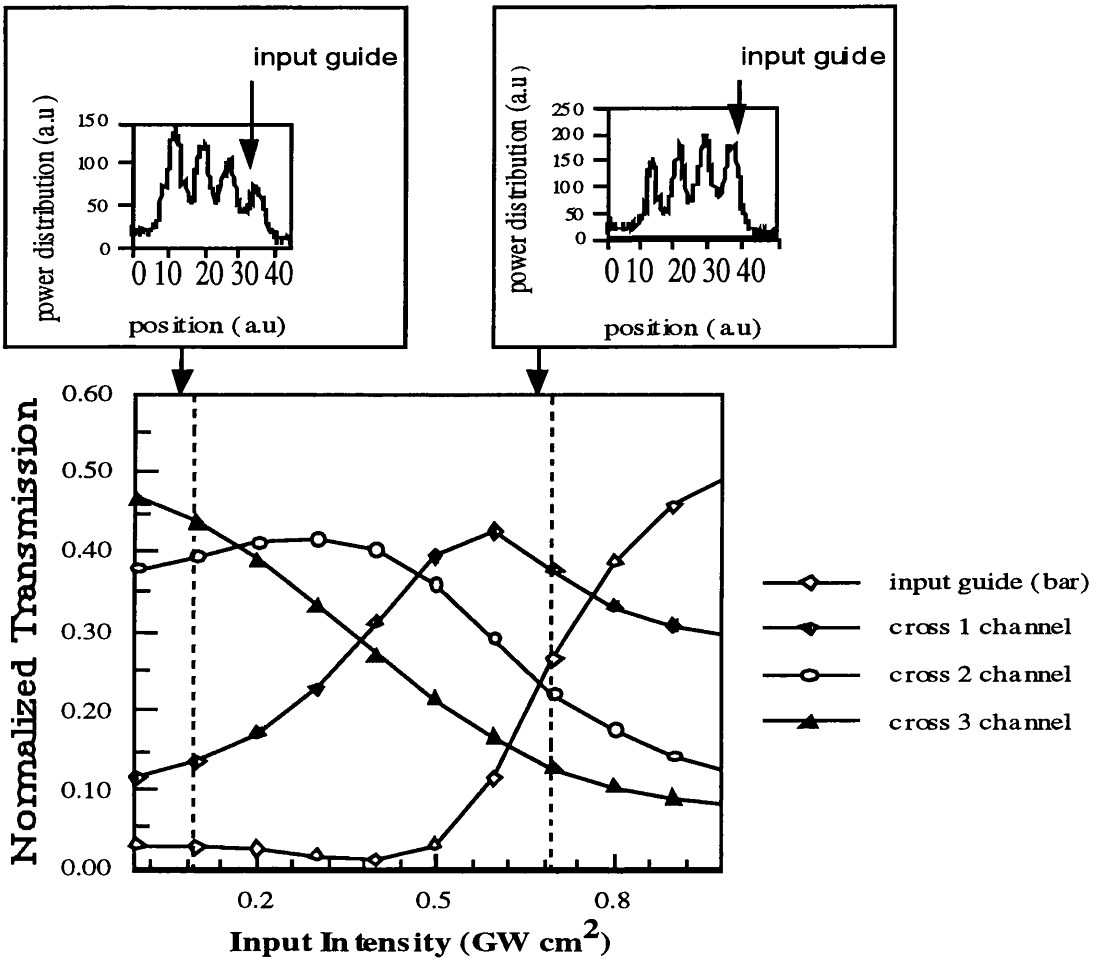

Figure 4.26. Comparison of the theoretically predicted switching characteristics of a four guide nonlinear coupler and the experimentally observed power distributions in a four core coupler at high and low light intensities.

Figure 4.26 also shows the theoretically simulated transmission characteristics of a four guide coupler. The dotted lines indicate the power ratios corresponding to the experimentally measured power distribution in the guides as indicated by the line scans. The experimental switching behaviour of the four guide coupler compares well with that of theoretically predicted switching characteristics.

4.8.2.2. The Eight Guide Nonlinear Coupler Experiment.

The final coupler to be tested was an eight guide coupler. Figure 4.27 is a photograph of the eight guide coupler tested.

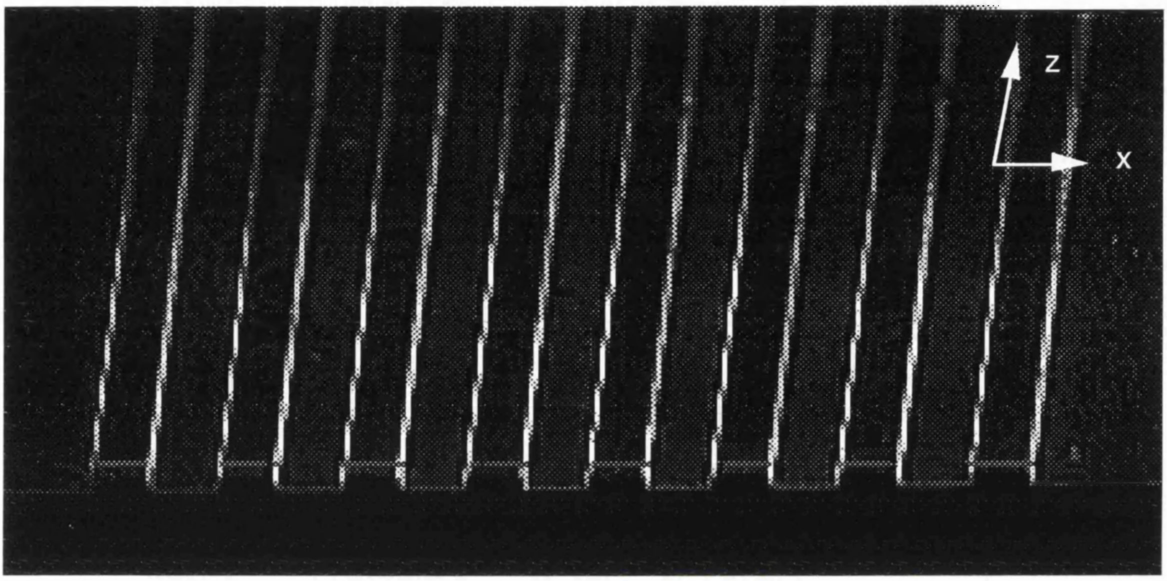

Figure 4.27. SEM showing the output facet of the eight guide coupler.

Figure 4.28 shows line scan pictures depicting the experimentally obtained switching observed in an initially over coupled one by eight directional coupler. This coupler was 3.24 cm long and the spacing between the guides was 7 μm.

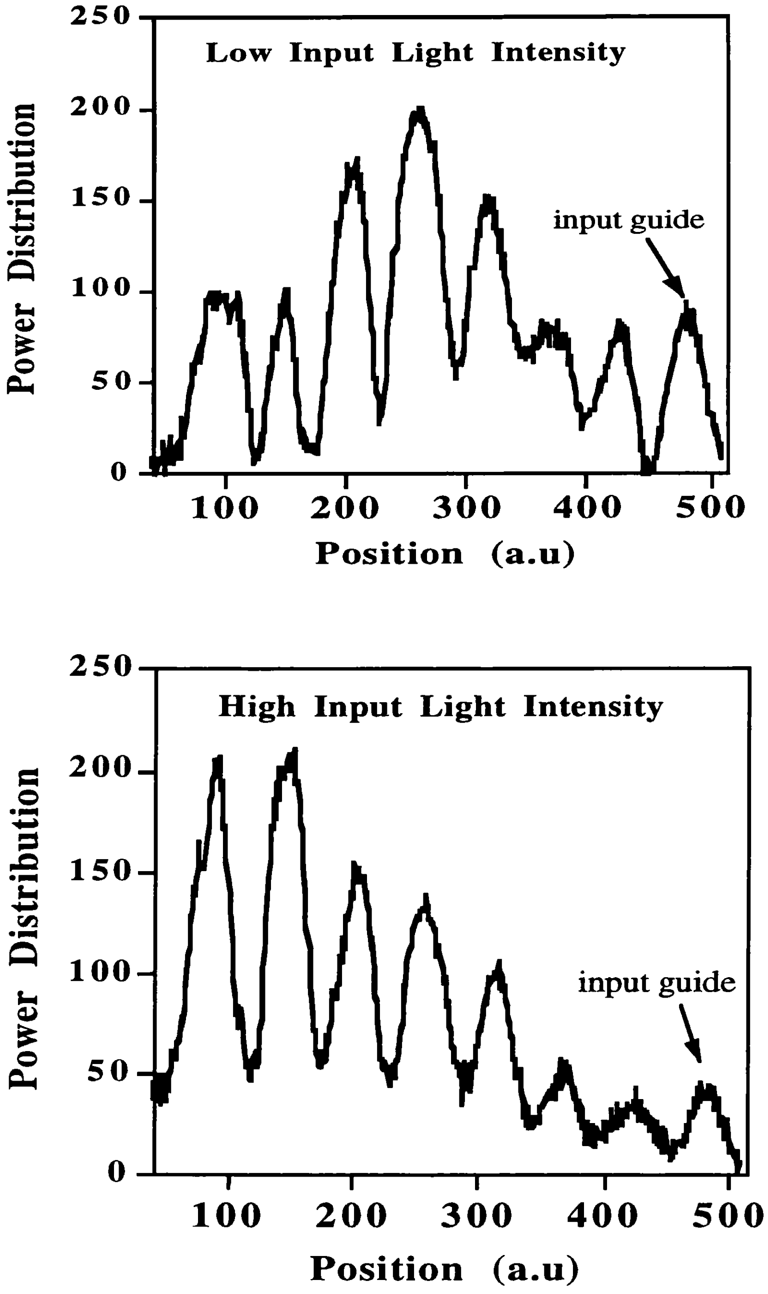

Figure 4.28. The power distribution in a 1x8 guide nonlinear array at low and high light intensities.

Again it is clear that switching is taking place in the sample at high intensities and power is transferring from one side of the sample to the other. This type of coupler has applications as an all-optical interconnect.

4.9. Conclusion.

In conclusion, all-optical switching in nonlinear three, four couplers and eight guide couplers has been observed for the first time. The experimental results agree well with numerical simulations based on a beam propagation code. It was seen that the switching characteristics of the uniformly spaced coupler and the non uniformly spaced coupler were different as accurately predicted by the BPM program. This result suggests that the switching characteristic of a multi-guide coupler can be controlled by altering the spacing between the guides in the array. Complete switching between the guides was not observed and this was attributed to the fact that a pulsed light source was used and so an intensity dependent nonlinear phase shift is acquired over the pulse envelope which results in pulse break up at the output. Multi-photon absorption can further distort the output pulses of the bar and cross states. However it is envisaged that these types of waveguide array will be useful in future all-optical switching and routing operations as work is being done to reduce the switching power requirements and losses within these devices. In particular the multi-guide couplers will have great potential for soliton power steering and switching applications.

References.

1. J.U. Kang, G.I. Stegeman and J.S. Aitchison,"All-optical multiplexing of femtosecond signals using an AlGaAs nonlinear directional coupler" Electron. Lett., **31**, pp 118-119 (1995).
2. K. Al-Hemyari, J.S. Aitchison, C.N. Ironside, G.T. Kennedy, R.S. Grant and W. Sibbett," Ultrafast all-optical switching in a GaAlAs integrated interferometer in the 1.55 μm spectral range", Electron. Lett., **28**, pp 1090-1092 (1992).
3. J.S. Aitchison, A.H. Kean, C.N. Ironside, A. Villeneuve and G.I. Stegeman, " Ultrafast all-optical switching in a $Al_{0.82}Ga_{0.28}As$ directional coupler in the 1.55 μm spectral range", Electron. Lett., **27**, pp 1709-1710 (1991).
4. S. Trillo, S. Wabnitz and G.I. Stegeman, " Nonlinear codirectional guided wave mode conversion in grating structures" J. Lightwave Tech., **6**, pp 971-976 (1988).
5. J. Fick, G. Vitrant, "Fast optical switching in nonlinear prism couplers", Opt. Lett., **20**, pp 1462-1467 (1995).
6. Y. Shibata, S. Oku, Y. Kondo, and T. Tamamura, "Semiconductor monlithic wavelength-selective router using grating switch integrated with directional coupler", Electron. Lett., **11**, pp 966-967 (1995).
7. R.C. Alferness, L.L. Buhl and M.D. Divino, "Low loss fibre coupled waveguide directional coupler modulator", Electron. Lett., **18**, pp 490-491 (1982).
8. K. Kiyoshi, "Novel three waveguide demultiplexer utilizing the two and three guide couplers", J. of Lightwave Tech., **11**, pp 234-240 (1993).
9. H. Inoue, K. Hiruma, K. Ishida, H. Sato and H. Matsumura, " Switching characteristics of GaAs directional coupler optical switches", Appl. Opt. ,**25**, pp 1484-1490 (1986).
10. H.A. Haus, L. Molter-Orr, "Coupled multiple waveguide systems ", IEEE J. of Quant. Elec., **19**, pp 840-844 (1983).
11. A. Yariv, "Optical Electronics ", Saunder College Publishing, 4th edit., chp. 13.8, pp 519-529 (1991).
12. A.Villeneuve, "Optical nonlinearities and applications of semiconductors near half-band gap", Phd Thesis, University ofArizona (1992).
13. Y. Chen, A.W. Snyder, D.J. Mitchell, "Ideal optical switching by nonlinear multiple (parasitic) core couplers ", Electron. Lett., **26**, pp 77-78 (1990).
14. A.C. Walker, "A comparison of optically nonlinear phenomena in the context of optical information processing", Optical Computing and processing ,**1**, pp 91--106 (1991).

15. M. Cada, B.P. Keyworth, J.M. Glnski, A.J. Springthorpe, C. Rolland and K.O. Hill, "Electro-optic switching in a P-I-N doped multi-quantum well directional coupler", J. of Appl. Phy. , **69**, pp 1760-1762 (1991).

16. S.G. Lee, B.P. McGinnis, R. Jin, J. Yumoto, G. Khitrova, H.M. Gibbs, R. Binder, S.W. Koch, N. Peyghambarian, "Subpicosecond switching in a current injected GaAs/AlGaAs multiple-quantum-well nonlinear directional coupler"Appl. Phy. Lett. , **64**, pp 454-456 (1994).

17. H. Takeuchi, Y. Hasumi, S. Kondo, Y. Noguchi, "Directional couplers switch matrix with an InGaAlAs/InAlAs multiquantum-well structure", Electron. Lett. , **29**, pp 523-524 (1993).

18. Y.H. Jan, M.E. Heimbuch, L.A. Coldren and S.P. Denbaars, "Wavelength tuning range of an InP/InGaAsP photonic integrated tunable receiver", Appl. Phy. Lett., **69**, pp 3131-3133 (1996).

19. P. Li Kam Wa, J.E. Sitch, N.J. Mason, J.S. Roberts and P.N. Robson,"All-optical MQW waveguide switch ", Electron. Lett. , **21**, pp 26-28 (1985).

20. F. Dollinger, M. Vonborcke, G. Bohm, G. Trankle, G. Weimann,"Ultrashort low-loss optical multi-quantum-well GaAs/GaAsAl vertical directional coupler switch" Electron. Lett., **32**, pp 1509-1510 (1996).

21. H. Maruyama, M. Haruna, H. Nishihara, "TE-TM mode splitter using directional coupling between heterogeneous waveguides in LiNbO3", J. of lightwave Tech., **13**, pp 1550-1554 (1995).

22. A.N. Milliou, R. Srivastava and R.V. Ramaswamy, "A 1.3 μm directional coupler polarisation splitter by ion exchange", J. of Lightwave Tech., **11**, pp 220-225 (1993).

23. S.S. Lee, M.C. Oh, Y.K. Jhee, S.Y. Shin, "Y-cut LiNbO3 directional coupler with a self-aligned electrode", J. of lightwave Tech. , **12**, pp 872-875 (1994).

24. N. Keil, H.H. Yao, C. Zawadzi, B. Sterbel, "4x4 polymer thermooptic directional coupler switch at 1.55 μm", Electron. Lett. , **30**, pp 639-640 (1994).

25. H. Herrman, K. Schafer, W. Sohler, "Polarisation-independent, integrated optical, acoustically tunable wavelength filters switches with tapered acoustical directional coupler", IEEE Photonics Tech. Lett, **6**, pp 1335-1337 (1994).

26. M.A. Karpierz, T.R. Wolinski, M. Sierakowski, "Liquid-crystalline directional coupler with asymmetrical nonlinearity", Molecular crystals and liquid crystals science and technology section A-molecular crystals and liquid crystals, **261**, pp 217-223 (1995).

27. WY. Lee, J.S. Lin and W.C. Chuang, "SSFLC optical directional coupler switch with a short device length-a proposal", J. of Light Wave Tech. ,**13**, pp 2236--2243 (1995).

28. M. Guntau, R. Muller, A. Brauer, W. Karthe, "Performance and limits of nonlinear optical waveguide couplers on the basis of CDS1-XseX-doped glasses", J. of Lightwave Tech., **13**, pp 67-72 (1995).
29. A. Tervonen, S. Honkanen, S.I. Najafi, "Analysis of symmetrical directional couplers and asymmetrical Mach-Zehnder interferometers as 1.30 μm and 1.55 μm dual-wavelength demultiplexers/ multiplexers" Opt. Eng. , **32**, pp 2083-2091 (1993).
30. B.J. Luff, R.D. Harris, J.S. Wilkison, D.J. Schiffrin, "Integrated-optical directional coupler biosensor", Opt. Lett. , **21**, pp 618-620 (1996).
31. B. Pezeshki, F. Agahi, J.A.Kash, J.J.Welser, W.K. Wang, "Wavelength-selective waveguide photodetectors in silicon on insulator", Appl. Phy. Lett. ,**68**, pp 741-743 (1996).
32. N. Dagli, G. Snider, J. Waldam, E. Hu, "An electron wave directional coupler and its analysis", J. of Appl. Phy. , **69**, pp 1047-1051 (1991).
33. M.A. Duguay, V. delisle, U. Trurschel and F. Lederer, "High finesse wavelength-selective coupler based on arrows", IEEE Photonics Tech. Lett. , **8**, pp 791-793, (1996).
34. Z.M. Mao, W.P. Huang, "An arrow optical wavelength filter-design and analysis", J. of light wave tech. , **11**, pp 1183-1188 (1993).
35. U. Trutschel, M. Croningolomb, G. Forgarty, F. Lederer and M. Abraham, " Analysis of metal-clad antiresonant reflecting optical waveguide for polarisation applications", IEEE Photonics Tech. Lett. , **5**, pp 336-339 (1993).
36. J. Gehler, A. Bräuer, W. Karthe, U. Truschel and M.A. Duguay, "Arrow based optical wavelength filter in silica", Electron. Lett. , **31**, pp 547-548 (1995).
37. A. Kaneko, T. Kuwabara, T. Wada, H. Sasabe and K. Sasaki, "All-optical switching phenomenon in polydiacetylene (12,8) based nonlinear directional couplers", IEICE Trans. on Electron. , **E77C**, pp 704-708 (1994).
38. G.P.Agrawal, " Nonlinear Fiber Optics ", 2nd ed., Acedemic Press (1989).
39. G.I. Stegeman, E.M. Wright, N. Finlayson, R. Zanoni and C.T. Seaton, "3rd-order nonlinear integrated optics ", J.Lightwave Technol. , **6**, pp 953-970 (1988).
40. A.B. Aceves, C. De Angelis, S. Trillo and S. Wabnitz, "Storage and steering of self-trapped discrete solitons in nonlinear waveguide arrays ", Opt. Lett. , **19**, pp 332-334 (1994).
41. C.C. Yang, A. Villeneuve, G.I. Stegeman and J.S. Aitchison, "Effects of 3-photon absorption on nonlinear directional coupling ", Opt. Lett., **17**, pp 710-712 (1992).
42. J.S. Aitchison, A.Villeneuve, G.I. Stegeman, "All-optical switching in 2-cascaded nonlinear directional coupler ", Opt. Lett. , **20**, pp 98-100 (1995).

43. M. Cada, G. muller, A. Greil, L. Stoll and U. Wolff, "Dynamic switching characteristics of a 4x4 InP/InGaAsP matrix switch", Electron. Lett. , **28**, pp 2149-2150 (1992).
44. D.K. Hunter, I. Andonovic, D.G. Smith and B.Culshaw, "Architecture for optical TDM switching", Electron. Lett. , **28**, pp 1746-1747 (1992).
45. D.J. Blumenthal, P.R. Prucnal and J.R. Sauer, "Photonic packet switches :architectures and experimental implementations ", Proc. of the IEEE, **82**, pp 1650-1667 (1994).
46. I.G. Voitenko andT. Yatagai, "Integrated-optic comutator for high speed local communication network with cross talk minimisation in optical directional couplers", Institute of Physics Conf. Series, **139**, pp 637-640 (1995).
47. E.J. Murphy, T.O. Murphy, A.F. Ambrose, R.W. Irvin, B.H. Lee and P .Peng, "16*16 strictly nonblocking guide-wave optical switching systems", J. of Light Wave Tech. , **14**, pp 352-358, (1996).
48. A. Jajszczyk, "A class of directional coupler based photonic switching networks", IEEE Trans. on Comm., **41**, pp 599-603 (1993).
49. S.M. Jensen, "The non-linear coherent coupler ", IEEE J. Quantum Electron. , **18**, pp 1580-1583 (1982).
50. D.N. Christodoulides, R.I. Joseph, "Discrete self-focusing in nonlinear arrays of coupled waveguides", Opt. Lett. , **13**, pp 794-796 (1988).
51. S.R. Friberg, Y. Silberberg, M.K. Andrejco, M.A. saifi and P.W Smith, "Ultrafast all-optical switching in dual core fiber nonlinear coupler ", Appl. Phys. Lett.,**51**, pp 1135-1137 (1987).
52. R. Lin, J.P. Sokoloff, P.A. Harten, C.L. Chuang, C.G. Lee, M. Warren, H.M. Gibbs, N. Payghambarian, J.N. Polky and G.A. Pubanz, "Ultrafast modulation with subpicosecond recovery time in a GaAs/AlGaAs nonlinear directional coupler ", Appl. Phys. Lett. , **56**, pp 993-995 (1990).
53. D.A.O. Davies, M.A. Fisher, D.J. Elton, S.D. Perrin, M.J. Adams, G.T. Kennedy, R.S. Grant, P.D. Roberts and W. Sibbett , "Nonlinear switching in InGaAsP laser amplifier directional coupler biased at transparency ", Electron. Lett. **29**, pp 1710-1711 (1993).
54. S.G. Lee, B.P. McGinnis, R. Jin, J. Yumoto, G. Khitrova, H. M. Gibbs, R. Binder, S. W. Koch and N. Peyghambarian, "Subpicosecond switching in a current injected GaAs/AlGaAs MQW nonlinear directional coupler ", Appl. Phys., **64**, pp 454-456, (1994).
55. A. Villeneuve, C.C. Yang, P.G.J. Wigley, G.I. Stegeman, J.S. Aitchison and C.N. Ironside, "Ultrafast all-optical switching in a semiconductor nonlinear directional coulper at half the band-gap", Appl. Phys. Lett. , **61**, pp 147-149 (1992).

56. J.S. Aitchison, A. Villeneuve and G.I. Stegeman, "Nonlinear directional couplers in AlGaAs", J. Nonlinear Opt. Phys and Matter, **4** , pp 871-880 (1995).

57. R. Jin, J.P. Sokoloff, P.A. Harten, C.L. Chuang, S.G. Lee, M. Warren, H.M. Gibbs, N. Peyghambarian, N.J. Polky and G.A. Pubanz, "Ultrafast modulation with subpicosecond recovery time in a GaAs/AlGaAs nonlinear directional coupler", Appl. Phy. Lett., **56**, pp 993-995 (1990).

58. K. Kitayama, S. Wang, "Optical pulse compression by nonlinear coupling", Appl. Phy. Lett, **43**, pp 17-19 (1983).

59. H. Izadpanah, "Short optical pulse generation from laser-diodes with directional coupler external cavity", Fiber and Integrated Optics, **9**, pp 163-170 (1990).

60. D.T. Walton, H.G. Winful, "Passive modelocking with an active nonlinear directional coupler-positve group velocity dispersion ", Opt. Lett. , **18**, pp 720--722 (1993).

61. C.W. Hsu, C.C. Yang, "Passive mode-locking of semiconductor laser based on nonlinear directional couplers", Opt. Lett. , **21**, pp 878-880 (1996).

62. T. Main, R.J. Feurestein, H.F. Jordan, V.P. Heuring, J. Feehrer and C.E. Love,"Implementation of a general purpose stored-program digital optical computer", Appl. Opt. , **33**, pp 1619-1628 (1994).

63. R.J. Feurestein, T. Soukup, V.P. Heuring, "100 MHz optical counter that uses directional couplers switches", Opt. Lett. , **16**, pp 1599-1601 (1991).

64. H.F. Jordan, V.P. Heuring and R. Feuertein, "Optoelectronic time of flight design and the demonstration of an all-optical stored program, digital computer", Proc. of the IEEE, **82**, pp 1678-1689 (1994).

65. R.T. Sahara, S.G. Hummel, W.H. Steier and P.D. Dapkus, "AlGaAs waveguide optically controlled directional coupler latch", J. of light wave tech. , **11**, pp 1533-1538 (1993).

66. C.C. Yang, "All-optical ultrafast logic gates that used asymmetric nonlinear directional couplers", Opt. Lett. ,**16**, pp 1641-1643 (1991).

67. Y. shibata, S. Oku, Y. Kondo, T. Tamamura, "Semiconductor monolithic wavelength-selective router using grating switch integrated with directional coupler", Electron. Lett. , **31**, pp 966-967 (1995).

68. A. Wakatsuki, K. Okamoto, O. Mikami, "Proposed semiconductor narrow band wavelength filter using a directional coupler", Electron. Lett. , **26**, pp 1573-1575 (1990).

69. J.U. Kang, G.I. Stegeman and J.S. Aitchison, "All-optical multiplexing of femtosecond signals using an AlGaAs nonlinear directional coupler " Electron. Lett. , **31**, pp 118-119 (1995).

70. A. Villeneuve, P. Mamyshev, J.U. Kang, G.I. Stegeman, J.S. Aitchison and C.N. Ironside, " Time-domain all-optical demultiplexing with a semiconductor directional coupler", Appl. Phy. Lett. , **66**, pp 1668-1670 (1995).
71. B. Pezeshki, J.A. Kash, D.W. Kisher, F. Tong, "Multiple wavelength light source using asymmetric waveguide coupler", Appl. Phy. Lett., **65**, pp 138-140 (1994).
72. T. Hirata, M. Suehiro, M. Maeda, M. Hirara and H. Hosomatsu,"Monolithic resonant optical reflector laser-diodes", Electron. Lett. , **27**, pp 2050-2051 (1991).
73. G.F. Trommer, H. Poisel, W. Buhler, E. Harl and R. Muller, "Passive fiberoptic gyroscope ", App. Optics, **29**, pp 5360-5365 (1990).
74. C.W. Barnard, J. Chrostowski and M. Kavehrad, "Bidirectional fiber amplifiers" IEEE Photonics Lett. , **4**, pp 911-913 (1992).
75. M.A. Karpierz, A.K ujawski, P. Szczepanski, "Analysis of waveguide ring lasers with nonlinear directional output coupler", J. of Mod. Optics, **42**, pp 1079-1091 (1995).
76. Y.H. Ja, "A single-mode optical fiber ring-resonator using planar 3x3 fiber coupler and a sagnac loop", J. of Lightwave Tech. ,**12**, pp 1348-1354 (1994).
77. N. Finlayson and G.I. Stegeman,"Spatial switching, instabilities and chaos in a 3 waveguide nonlinear directional coupler ", Appl. Phys. Lett.,**56**, pp 2276-2278 (1990).
78. D.J. Mitchell, A.W. Snyder and Y. Chen, "Nonlinear triple core couplers" Electron. Lett., **26**, pp 1164-1166 (1990).
79. R. Muschall, C. Schmidthattenberger and F. Lederer, "Spatially solitary waves in arrays of non-linear waveguides ", Opt. Lett. ,**19**, pp 323-325 (1994).
80. W. Królikowski, Y.S. Kivshar, "Soliton-based optical switching in waveguide arrays ", J. Opt. Soc. Am. B, **13**, pp 876-880 (1996).
81. M. Matsumoto, S. Katayama and A. Hasegawa, "Optical switching in nonlinear waveguide arrays with a longitudinally decreasing coupling coeficient ", Opt. Lett., **20** , pp 1758-1760 (1995).
82. A.B. Aceves, I.S.C. Deangel, T. Peschel, R. Mushall , F. Lederer and S. Trillo, "Discrete self-trapping, soliton interactions and beam steering in non-linear waveguide arrays ", Physical Rev. , E **53**, pp 1172-1189 (1996).
83. F. Lederer, W. Biehlig, "Bright spatial solitons and light bullets in semiconductor waveguides", Electron. Lett. , **30**, pp 1871-1872 (1994).
84. N.J. Doran and D. Wood, "Soliton processing element for all-optical switching and logic ", J.Opt. Soc. Am. B, **4**, pp 1843-1846 (1987).

85. W. Królikowski, U. Trutschel, M. Cronin-Golomb and C. Schmidt-Hattenberger, "Soliton-like switching in a circular fiber array ", Opt. Lett., **19**, pp 320-322 (1994).
86. A.B. Aceves, C.De. Angelis, A.M. Rubenchik, " Multi-dimensional solitons in fibre arrays ", Opt. Lett. ,**19**, pp 329-331 (1994).
87. G.P. Agrawal, " Nonlinear Fiber Optics ", 2nd ed., Acedemic Press (1989).
88. C. Martijn de sterke, K.R. Jackson and B.D. Robert, " Nonlinear coupled-mode equations on a finite interval; a numerical procedure", J.of the Opt. Soc. Am.B, **8**, pp 403-412 (1991).
89. J.S. Aitchison, D.C. Hutchings, J.U. Kang, G.I. Stegeman and A. Villeneuve, IEEE "The nonlinear optical propeties of AlGaAs at the half band gap", J. of Quant. Elec., **33**, pp 341-347 (1997).
90. J.U. Kang, A. Villeneuve, M. Shek-Bahae, G.I. Stegeman, K. Al-Hemyari, J.S. Aitchison and C.N. Ironside, "Limitation due to 3-photon absorption on the usual spectral range for nonlinear optics in AlGaAs below half band gap ", Appl. Phys. Lett., **65**, pp 147-149 (1994).

Chapter 5

Nonlinear Grating Structures in AlGaAs.

Introduction.

In this chapter the design, fabrication and characterisation of an all-optical switch based on a nonlinear distributed feedback (DFB) grating will be considered. The grating filter is formed in a AlGaAs optical waveguide structure using electron beam writing. The application of such filters for use as a solitonic switching element will be described.

The chapter begins with an overview of the development and application of grating devices in intergrated optics. The basic linear and nonlinear theory of the Bragg grating is presented in section 5.2. Theoretical simulations of the transmission characteristics of a nonlinear grating are presented in section 5.3. This is followed by a description of the device design in section 5.4 and an outline of the device fabrication process in section 5.5. The experimental work, including the linear characterisation of the gratings and preliminary nonlinear experiments conducted is given in section 5.6. Section 5.7 explores the design and fabrication of chirped gratings and finally in section 5.8 the conclusion of the chapter and suggested further work is discussed.

5.1. Grating Structures and their Applications.

An integrated grating consists of a corrugation, or periodic variation, in the dielectric constant of a waveguide which provides a mechanism for the selective coupling of the modes of the structure. Gratings can bring about complete power transfer between different waveguide modes. There is a great deal of flexibility concerning the choice of interaction length required for coupling and the selection of the modes to be coupled. In linear materials gratings have been used to provide co-directional and counter-propagating mode conversion. They have also been used in laser systems[1], to form filters, input/output couplers, multiplexers[2] and demultiplexers.

The key concept on which the nonlinear grating coupler is based is that the local intensity in the structure controls the wave-vector of the guided mode. Hence, the intensity dependent wave-vector can be used to tune a grating towards, or away, from the Bragg condition through self or cross-phase modulation. Thus the amount of light reflected by the grating is dependent on the intensity of the input beam.

Numerical studies of nonlinear DFB gratings have predicted bistability and self-pulsing effects[3] and unstable chaotic behaviour at high intensities[4]. The nonlinearity may also lead to the temporal reshaping, compression[5] and break up of intense light pulses[6]. Furthermore, the transmission function of a grating structure is a very sharp function of wavelength. The filter like transmission function of a grating-based device is very sensitive to a change in refractive index, or phase change, which can, in theory, lead to low power switching requirements for such a device. For example in a theoretical study of a nonlinear co-directional mode converter[7] it was estimated that the inclusion of a grating into the mode converting component could potentially result in a switching power 100 times lower than that of the devices in the absence of the grating. This reduction in switching power is attributed to the fact that the grating can serve to offset the phase velocity difference between two coupled modes and hence, reduces the change in refractive index required to observe switching between them.

Grating structures have found widespread applications in nonlinear optics. For example, nonlinear DFBs formed using colloidal crystal solutions, where the nonlinearity is thermal in nature, have been used to observe optical limiting [8], as well as bistability, switching and even multistability.[9] Thermal nonlinearities have also been used to produce wavelength tuning of a Bragg grating in an InSb planar structure.[10] Pulse self-switching and pulse break up have also been experimentally demonstrated in a nonlinear DFB formed in a silicon-on-insulator waveguide[11] and nonlinear gratings have been used for phase-matching in second harmonic generation optical waveguides.[12]

Other proposed devices include optical switches, optical limiters[3] as well as optical logic gates, spatial scanners and tunable optical filters.[13] In fibers a distributed feedback pulse generator has been proposed which is based on a nonlinear fiber grating.[14]

More recently, research has been undertaken into the existence of optical solitons within nonlinear grating structures as mentioned in chapter 1. Suggested applications of gap and Bragg solitons include low-velocity energy transport[15], modal-dispersion cancellation in fibres[16], optically controlled delay lines and all-optical switching applications[17].

5.2. Grating Theory.

In the following section the propagation of light within grating structures both in the linear and nonlinear regime are described.

5.2.1. Linear Grating Theory.

In a linear grating the field of the incident wave is perturbed by the periodic index modulation. The result is the production of modulated components known as space harmonics, or sidebands, in the incident field. These sidebands can couple to fields with similar propagation constants.

There are two conditions that must be satisfied in order to achieve coupling between two counter-propagating modes in a linear grating. First of all the longitudinal phase matching, or Bragg condition, must be satisfied. This requires that the grating must take up the wave vector mismatch between the 2 waveguide modes. This rule can be expressed in the following equation:

$$k_s = k_f + k \quad (5.1)$$

where k_s and k_f are the wave vectors of the reflected and forward propagating modes respectively and k is the wave vector of the grating structure. The second requirement is that the product of the transverse profiles of the two interacting modes and the perturbation which couples them must not be zero.

The propagation of two counter-propagating light beams within a waveguide structure with a periodic grating can be described by the following differential equations[18]:

$$\frac{\partial A}{\partial z} = -i\kappa B e^{i2\Delta\beta z} \quad (5.2)$$

$$\frac{\partial B}{\partial z} = i\kappa A e^{-i2\Delta\beta z} \quad (5.3)$$

where the propagation constant β is given by : $\beta = kn_{eff}$.

A and B are the mode amplitudes of the forward and backward propagating fields respectively. κ is the coupling strength between the two modes and depends on the waveguide and grating structure and $\Delta\beta$ is a detuning factor which describes the difference in propagation constants between the grating and the incident field and z is the propagation distance.

Figure 5.1, illustrates the counter-propagating light fields which can exist within a linear rectangular shaped grating structure. At each interface a small fraction of the incident field is reflected. If $\Delta\beta = 0$ these reflections are all in phase.

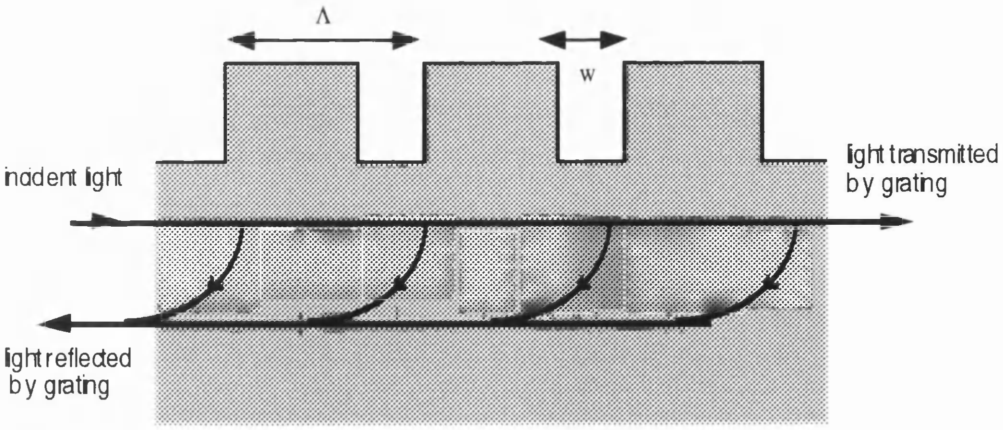

Figure 5.1. The counter-propagating light fields which can exist in a grating structure.

In the fig. 5.1, w is the width of the etched (trough) region of the grating and Λ is the grating period.

For the rectangular grating, illustrated in fig. 5.1. the coupling efficiency κ is given by:

$$\kappa = (\frac{2\Delta n_{eff}}{m\lambda_0})\sin\left\{\frac{\pi m w}{\Lambda}\right\} \qquad (5.4)$$

were Δn_{eff} is the difference in the effective indices of the unetched and etched regions of the grating structure, m is the order of the grating and, λ_0, is the Bragg wavelength of the periodic structure. The grating period Λ, is defined as:[19]

$$\Lambda = \frac{m\lambda_0}{2\tilde{n}_{eff}} \qquad (5.5)$$

where $\tilde{n}_{eff}$ is the average effective index of the structure and w is given by:

$$w = \frac{(2L - 1)\lambda_0}{4\tilde{n}_{eff}} \qquad (5.6)$$

where L is a positive integer: L=1,2,3....

Light with a wavelength near the Bragg wavelength λ_0 will be almost entirely reflected by the grating if it lies within a spectral region commonly known as the stop gap of the grating. In the spectrum the stop gap is centred symmetrically around λ_0. The reflection efficiency R, of the grating is given by the equation below where L is the length of the grating:[19]

$$R = \tanh^2(\kappa L) \qquad (5.7)$$

The width of the gap $\Delta\lambda$ is defined as:[19]

$$\Delta\lambda = \frac{\kappa\lambda_0^{\;2}}{\pi\tilde{n}_{\mathrm{eff}}L}\left[(\kappa L)^2 + \pi^2\right]^{\frac{1}{2}} \qquad (5.8)$$

5.2.2. Nonlinear Grating Theory.

The behaviour of light pulse propagating within a nonlinear grating structure with a positive nonlinear refractive index can be understood as follows: The grating introduces dispersion by coupling the forward and backward propagating waves. Considering light with a wavelength outside but close to the upper band edge of the photonic band gap (short wavelength side of gap). This light has a propagation constant with negative (anomalous) group velocity dispersion. At low light intensities the light pulse has a group velocity lower than that of the uniform medium but the pulse is broadened as it propagates through the grating. If the intensity of the input light increases, then the average refractive index will increase and the nonlinearity counterbalances the effect of the negative dispersion and hence a soliton-like field known as a Bragg soliton can be formed. Considering light with a frequency within the stop band of the grating ,at low light intensities the field is strongly reflected. However at high light intensities the refractive index of the grating can be altered through the nonlinearity which results in a shift in the position of the stop-band. Hence the light can be effectively tuned out of the grating. For light with a wavelength outside but close to the lower edge of the band gap (long wavelength side of the stop band). The dispersion is normal and so the effect of increasing the light intensity can result in pulse broadening.

The evolution of the fields in a nonlinear grating can be described by[20].

$$
\begin{aligned}
i\frac{\partial A}{\partial z} &= \kappa B e^{i2\Delta\beta z} + Q(|A|^2 + 2|B|^2)A \\
-i\frac{\partial B}{\partial z} &= \kappa A e^{-i2\Delta\beta z} + Q(|B|^2 + 2|A|^2)B
\end{aligned}
\qquad (5.9)
$$

where Q is a nonlinear coefficient and is related to the transverse field distribution $E_0(x)$ by the following equation[20]:

$$Q = \frac{\omega}{4}\int_{-\infty}^{\infty} n_2(x)|E_0(x)|^4 dx \qquad (5.10)$$

Equations 5.9 do not take into account the periodic variation in the nonlinear refractive index. The nonlinear refractive index of rectangular shaped grating taking into account the background nonlinear coefficient $n_{20}(x)$, and $n_{21}(x)$ which is a nonlinear refractive index contribution due to the presence of the grating and can be expressed as:

$$n_2(x,z) = n_{20}(x) + n_{21}\sum C_k e^{in2\pi z/\Lambda} \qquad (5.11)$$

For a detailed coupled mode analysis of the nonlinear DFB including the periodically varying n_2 see ref. 10. Theoretically it has been shown that the switching power depends on the coupling strength and the wave-vector mismatch.

5.3. Theoretical Modelling of the Nonlinear DFB.

A Fortran program, based on a Runge-Kutta algorithm, was used to simulate the C.W. switching characteristics of the nonlinear grating.

Figure 5.2 is a theoretical simulation of the transmission efficiency of a nonlinear grating as a function of the input power in the grating structure. In this simulation the grating length was selected such that at low powers the reflection from the grating was almost 100% and the wavelength of the input light was chosen to be that of the central Bragg frequency.

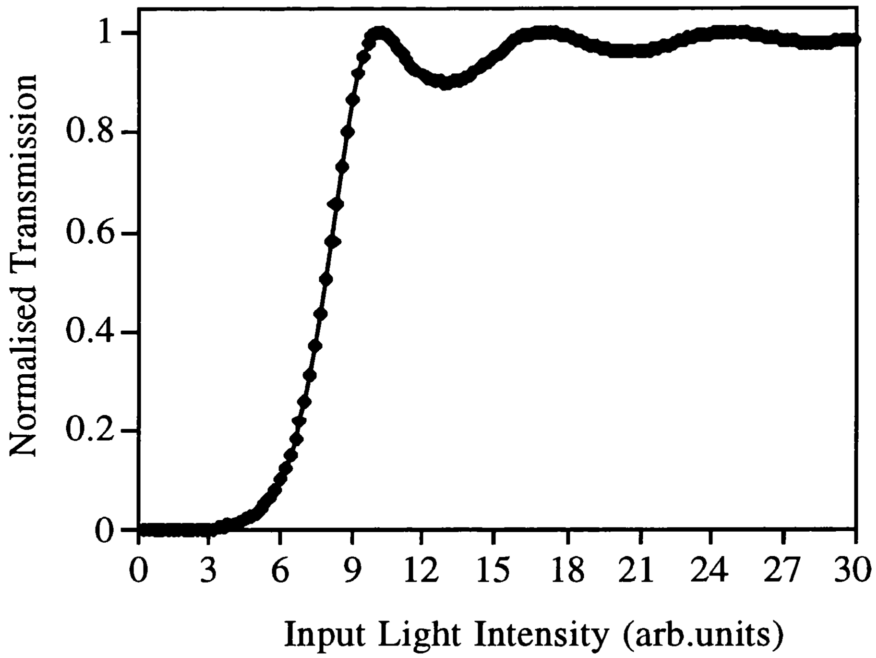

Figure 5.2. Theoretical simulation of the transmission of light with a frequency centred within the stopband of a nonlinear Bragg DFB grating.

At low powers all the light incident on the grating is reflected by the grating, since the grating takes up the phase mismatch between the counter-propagating light modes. As the intensity of the input light increases so too does the effect of the nonlinear refraction coefficient, which locally changes the propagation constant. Hence, at high powers the light is effectively tuned out of the stop-band and so the grating becomes transmitting. Figure 5.3. below shows the transmission efficiency of the nonlinear DFB grating when the incident wavelength is tuned to wavelengths slightly higher than the Bragg central wavelength, but still within the stop-band, where $\Delta\beta$ is the detuning parameter. It is clear from this graph that the switching power of the grating can be reduced by detuning the wavelength of light to slightly higher wavelength than that of the Bragg central wavelength. This type of structure can therefore be used to create an all-optical power dependent switch which at low powers reflects the light and at high powers allows the light to pass through the grating.

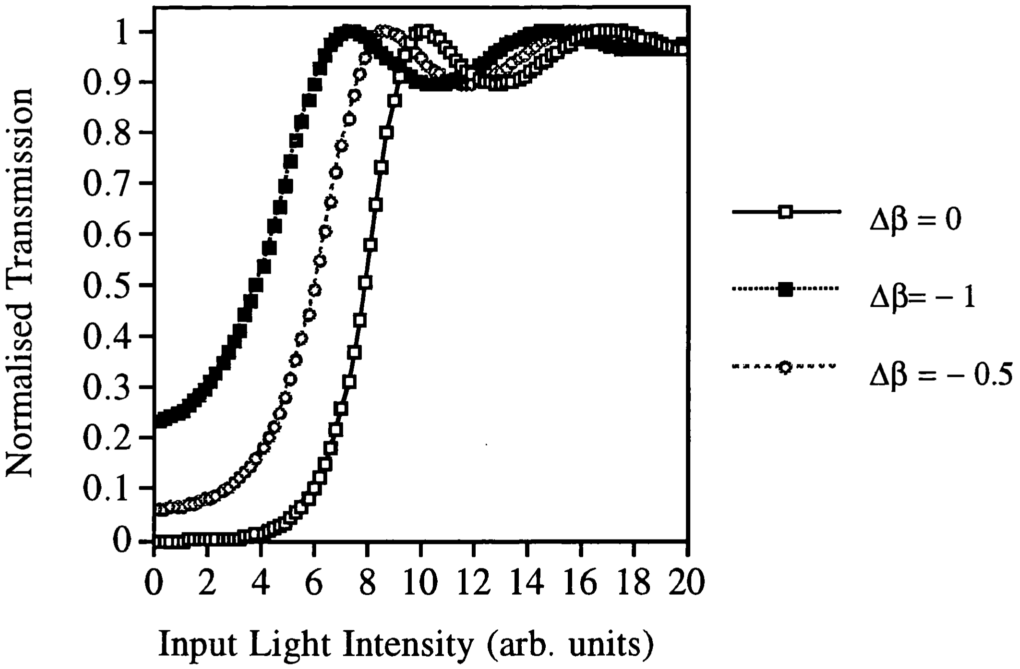

Figure 5.3. The transmission efficiency of a nonlinear DFB grating when the light is initially detuned to slightly higher wavelengths than that of the Bragg central wavelength.

The effect of detuning the light to lower wavelengths than that of the Bragg central wavelength were also simulated as shown in fig. 5.4 This figure shows that for large detunings from the Bragg resonance the switching efficiency of the grating is reduced. But for small detunings, an efficient power dependent switching effect is produced. This effect can be explained as follows: at low powers the grating transmits the incident light as the wavelength of the incident light is outwith the stop-band region. At a certain critical input power the incident light is efficiently reflected by the grating, as the nonlinear refractive index tunes the light into the Bragg reflecting region. For higher powers the light is tuned out of the reflection band and is again transmitted by the grating.

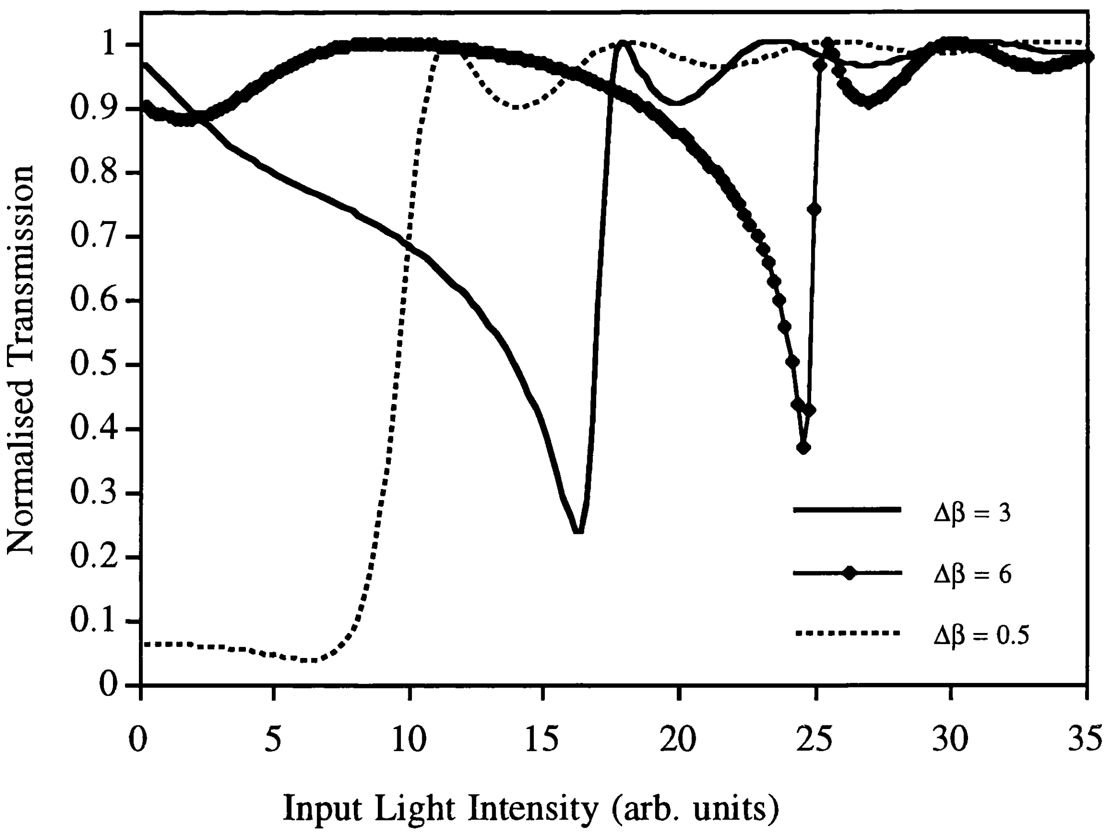

Figure 5.4. The transmission efficiency of a nonlinear DFB grating when the light is initially detuned to slightly lower wavelengths than that of the Bragg central wavelength.

5.4. Design of the Nonlinear Grating Switch.

The aim of this research was to produce a nonlinear DFB grating filter on AlGaAs waveguides which could be used to show all-optical switching. In designing the grating structure the following factors were taken into account.

1. The composition and structure of the AlGaAs wafer.
2. The width and etch depth of the waveguides.
3. The operating wavelength of the laser employed to test the devices.
4. The peak power and pulse width of the laser pulses used.

The AlGaAs wafer used to fabricate the waveguide/grating filters had the following structure. The lower cladding layer was 4 μm thick and contained 24% Al, the waveguide layer was 1.5 μm thick and contained 18% Al, finally the upper cladding was 1 μm thick with 24% Al. The AlGaAs wafer was cut into 1 x 1.3 cm rectangles to incorporate several waveguides. To ensure the optical waveguides were single moded the etch depths of the guides were chosen to be approximae 0.8 μm and the widths of the guides were selected to be 4 μm. A schematic of the designed waveguide and grating filter structure is shown in fig. 5.5.

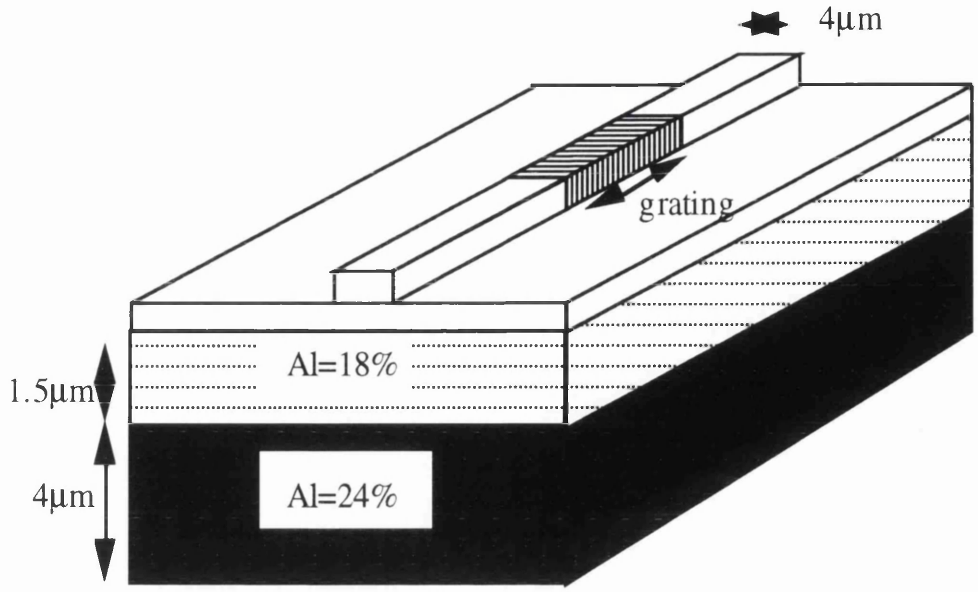

Figure 5.5. Schematic of the grating filter structure.

The Bragg wavelength for the grating was chosen to be approximately 1.50 μm. This corresponds to the half-band-gap of the AlGaAs waveguides. Both first order and second order gratings were designed with periods of 235 nm and 435 nm respectivley. The peak power and pulse width chosen to test these devices will be discussed later on in the chapter.

5.5. Device Fabrication.

In this research two different methods were employed for the fabrication of the optical waveguide grating filters. The first method used was a two-step holographic technique and the other method employed was a one step electron beam writing process. In this section both methods are described and compared with each other.

5.5.1. Fabrication of the Waveguide Grating Filters using a Holographic Process.

This holographic process was carried out in two stages. First the optical waveguides were fabricated using a combination of standard photolithography and reactive ion etching as described in chapter 3. The waveguides were designed to be single mode with a rib width of 4 μm and etch depth around 0.8 μm. The grating structures were then fabricated onto the guides using a holographic process which is described in the folllowing section.

In the holographic process a fringe pattern was produced by the interference of two coherent laser beams. This pattern was written into a thin layer of photoresist which had been coated onto the surface of the sample. Dry etching was used to transfer this pattern into the semiconductor. The stages in this process are summarised in figure 5.6.

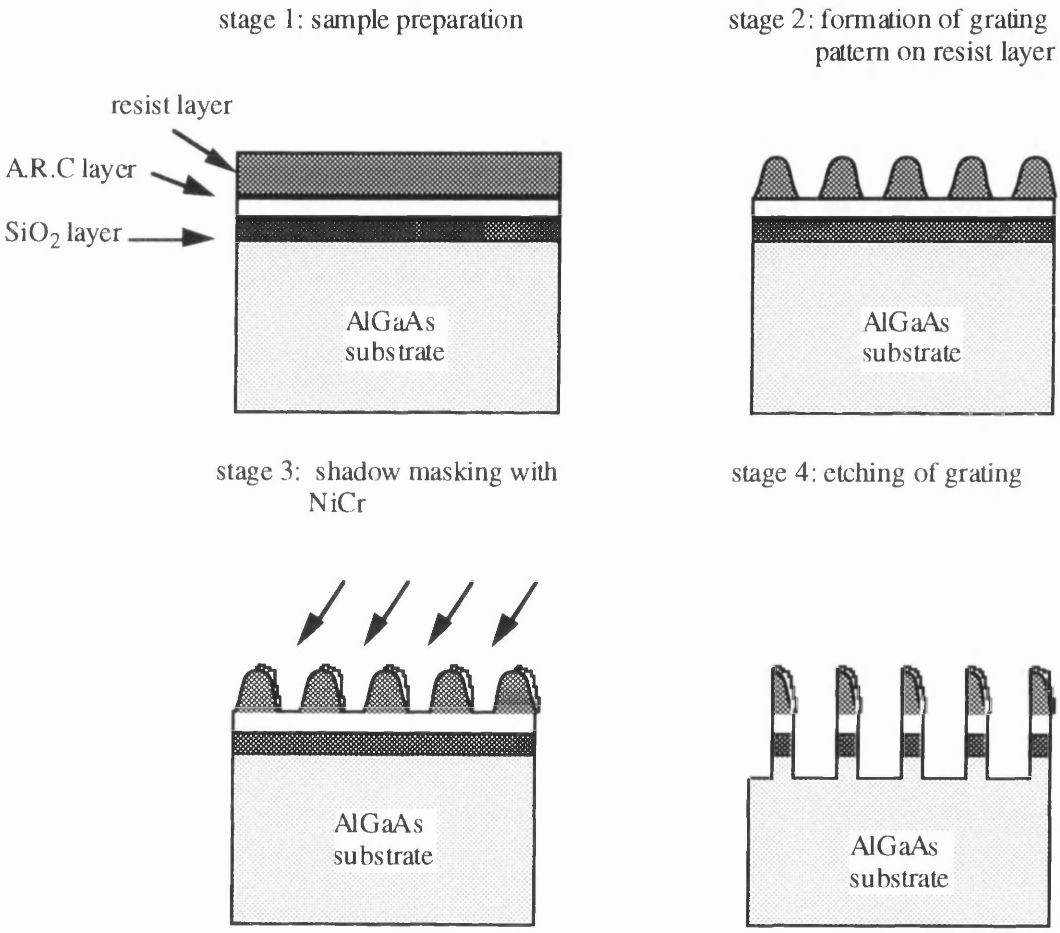

Figure 5.6. Stages in the holographic process.

Stage 1: Sample Preparation.

The AlGaAs sample was thoroughly cleaned in the usual manner as described in chapter 3. Resist can be spun directly onto the sample. However, vertical standing waves can be formed between the resist layer and the highly reflective AlGaAs surface. This results in irregularities and incomplete exposure of the grating pattern. To prevent this from happening a layer of anti-reflection coating (ARC) was applied to the AlGaAs substrate before the resist coating was spun. The ARC used was a polymide substance which curbed the production of standing waves by efficiently absorbing the light used to write the grating. Before applying the ARC layer to the AlGaAs substrate a 50 nm thick layer of SiO_2 was deposited onto the AlGaAs substrate first to ensure that the ARC coating would stick to the sample as adhesion between ARC and AlGaAs can be very poor. The samples were then baked at 130°C to remove any moisture that could affect the adhesion of the ARC to the SiO_2 layer. The ARC was then spun onto the samples at 4000 rpm for 60 seconds and the samples were baked again at 130 °C for 30 minutes. A 0.2 μm thick layer of thinned resist, S1400-31 (33%), was spun onto the samples and they were baked at 90°C for 30 minutes. This thickness of resist is recommended for the production grating structures with periods of approximately 400 nm.

Stage 2: Formation of Grating on Resist Layer.

In this experiment a symmetrical interferometer arrangement was used as depicted in figure 5.7. Light from a Spectra Physics 165 Argon ion laser at a wavelength of 457.9 nm was split into two identical beams using a 50-50 beam splitter. The output power of the light at this wavelength was approximately 200 mW. An aperture was used to select only the TEM_{00} mode thus ensuring the spatial coherence necessary to achieve the holographic interference pattern. The two beams, traversing equal path lengths, were then deflected by two equally spaced mirrors to produce an interference pattern on the surface of the waveguide sample, placed on the sample holder. A spatial filter and lens arrangement was placed along the path of both beams between the mirror and the sample stage. The function of the lens was to expand the laser beam to ensure the interference pattern covered the whole of the sample. The spatial filter was used to cut out any unwanted noise and wave-front imperfections by blocking out the higher frequency components in the beams by effectively acting as low band pass filters.

The period Λ, of the resulting fringe pattern can be calculated from the Bragg condition:

$$\Lambda = \frac{\lambda}{2n\sin\theta} \qquad (5.12)$$

The smallest grating period fabricated was limited by the experimental set up to second order gratings of magnitude 435 nm. This corresponds to a second order grating in the 1.5 μm spectral region.

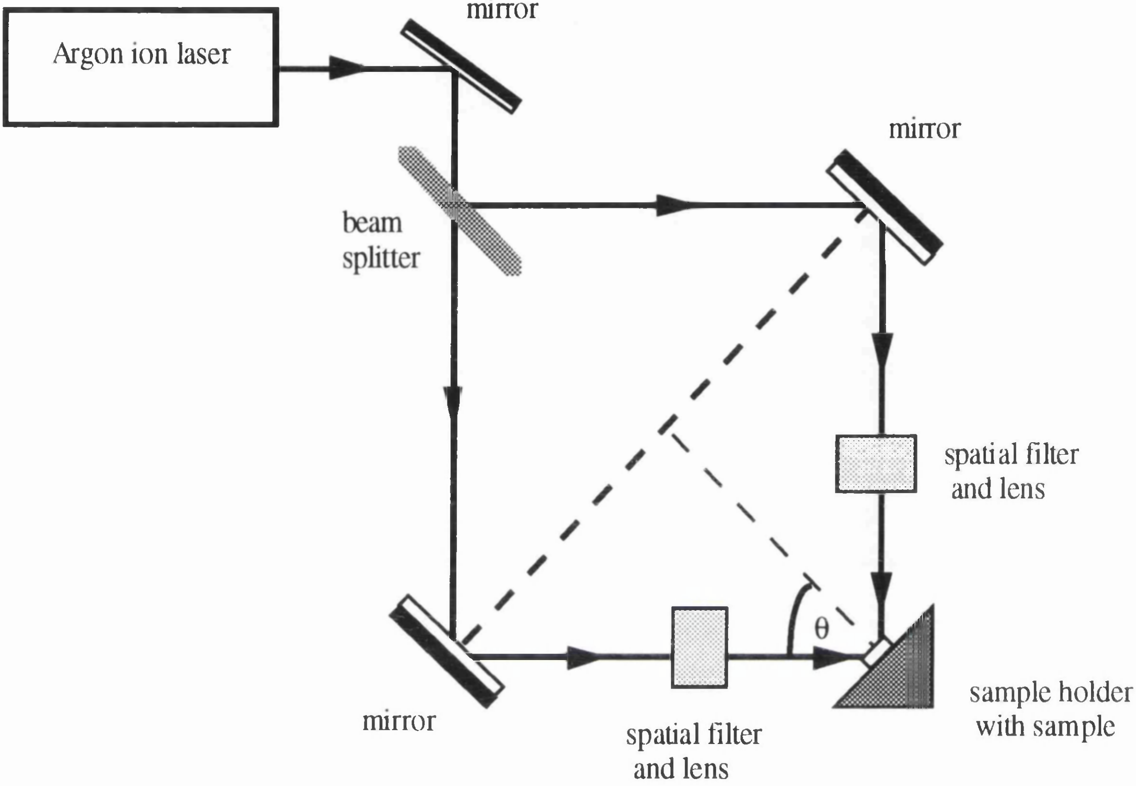

Figure 5.7. Schematic of the holographic experimental set up.

The powers in each of the beams were checked before exposure to make sure they were equal. If the power is not equal in each light beam then incomplete cancellation of the field intensity will occur when the two beams deconstructively interfere to produce the dark fringes of the pattern. Hence an ill defined grating pattern is produced. The exposure time used varied between 30 seconds and 60 seconds depending on the thickness of resist used. A 2:1 concentration of deionised water and AZ Developer was used to develop the resist pattern. The best results were achieved using a development time of twenty seconds. Figure 5.8 below is an SEM picture of the developed pattern produced on a AlGaAs sample after holographic exposure.

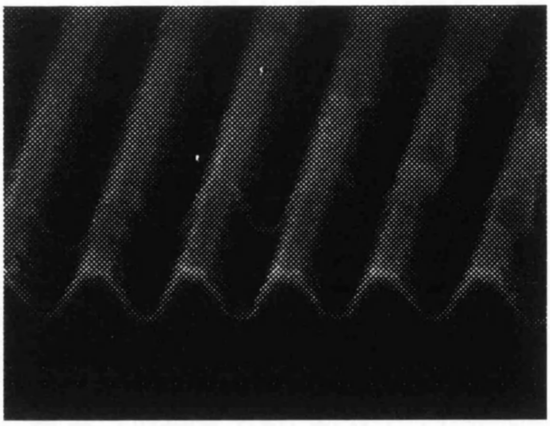

Figure 5.8. SEM picture of a developed grating pattern with a 435 nm period produced on a AlGaAs sample after holographic exposure.

Stage 3 : Shadow Masking with NiCr.

A 15 nm thick layer of Nichrome (NiCr) was evaporated onto the resist mask at an angle to produce a shadow affect. Using an angle of 60° the NiCr layer covers the top and one side of each grating crest, so that the areas of the resist not covered by the NiCr can be etched away leaving a square grating with a mark to space ratio of 1:1. An angle of approximately 45° was used to give a mark to space ratio of 1:3.

Stage 4 : Etching of the Pattern into the Sample.

The resist and ARC were etched using oxygen plasma and the SiO_2 was etched using SF_6 . Finally the AlGaAs was etched using $SiCl_4$. Figure 5.9 shows an SEM photo of the grating profile of an etched grating produced in AlGaAs using the holographic process.

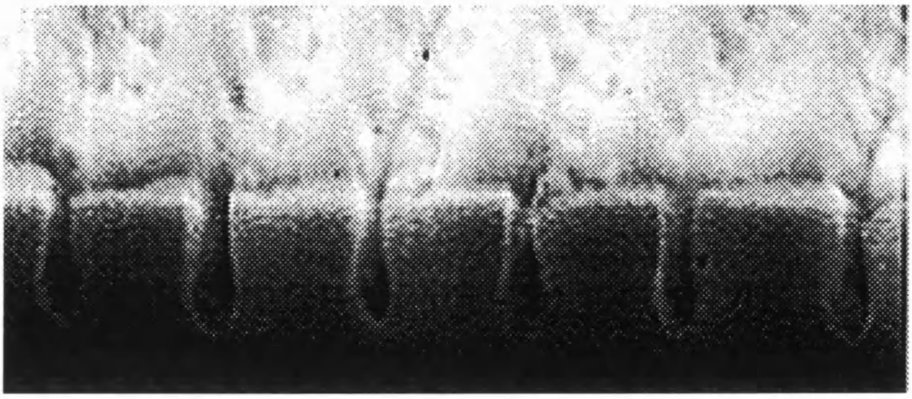

Figure 5.9. SEM picture of an etched grating produced in AlGaAs using the holographic method.The period of the grating is 435 nm.

Figure 5.10 below shows a SEM picture of a typical grating formed on a AlGaAs waveguide. As shown in figure 5.9 the grating was not only formed on the ridges of the guide structure, as desired, but over the entire surface of the wafer. In an attempt to avoid grating pattern production between the ridges, different spin speeds for the A.R.C and resist layers were tried without much success.

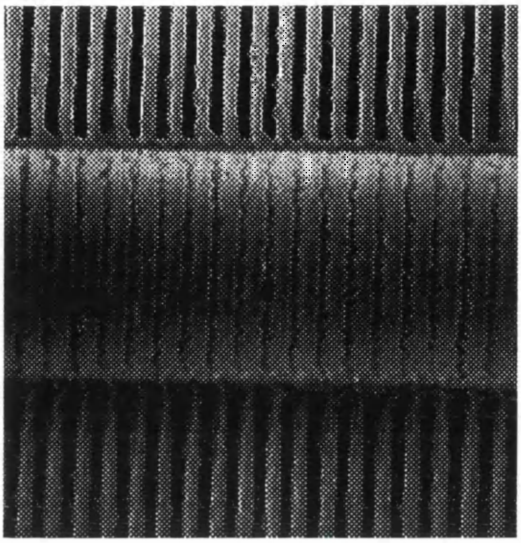

Figure 5.10. SEM showing a 4 μm wide AlGaAs optical waveguide with second order grating with a period of 435 nm etched onto the guide.

5.5.2. E-Beam Lithography.

In this section a single step, electron beam based approach, where the grating and waveguide were defined simultaneously is described. The filters were based on a weak grating on a strip loaded waveguide, to minimise excess scattering losses. Similar single step processes have been used to define 500-800 μm strong gratings on InP/InGaAsP waveguides[21] and short 3 μm long 1-D photonic band gap filters[22]. The stages in the beam writing process are illustrated in figure 5.11 and are also outlined below.

Stage 1: Preparation of AlGaAs Sample Before E-beam Exposure.

The AlGaAs substrate, after cleaning, was initially coated with a electron beam sensitive resist. A standard bi-layer resist recipe consisting of 4%

BDH followed by 4% ELV which is recommended for grating patterns with periods as small as 120 nm was used. The BDH layer was spun onto the sample at 5000 rpm for 60 seconds giving a resist thickness of 69 nm and baked at 180 °C for 2 hrs before the ELV coating was spun on at 5000 rpm for 60 seconds giving a coating thickness of 100 nm. The sample was then baked at 180°C for at least another 4 hours.

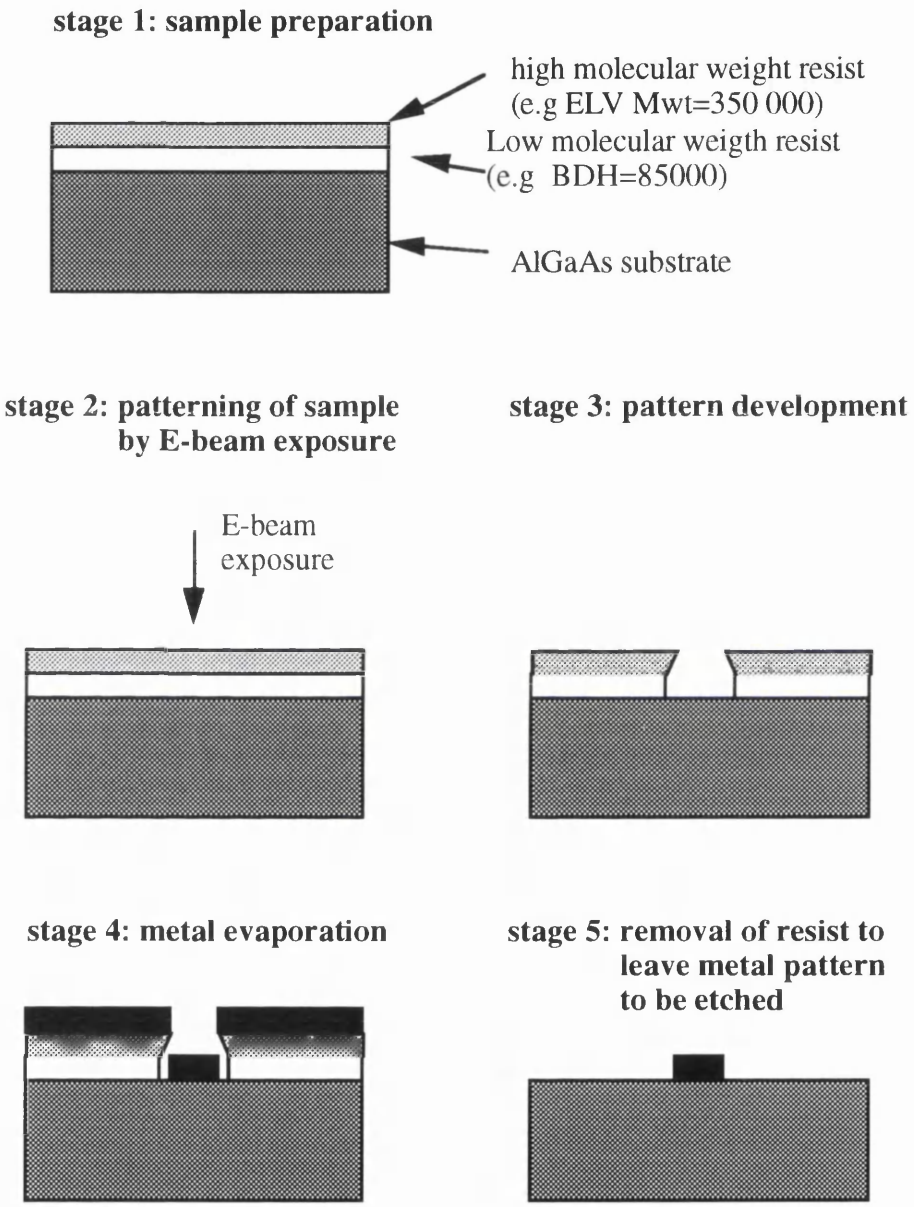

Figure 5.11. Stages in the electron beam writing process.

Stage 2: Patterning of the Sample.

The writing of the pattern by the electron beam is software controlled. First the pattern is design using a software package called WAM. The electrons are focused into a beam with a gaussian shaped cross-sectional profile. The beam is only scanned over the areas specified and not the entire sample. The exposure dose quantified by the number of electrons in the beam incident on the sample, is measured in C/cm^2. It is important to provide the correct exposure dose to ensure that any unwanted resist is removed efficiently at the development stage. Initially a series of exposure test were undertaken to obtain the correct exposure dose for the grating pattern. The exposure doses in this test ranged between 300 and 600 C/cm^2.

Figure 5.12(a) shows the grating pattern which was produced at a very high exposure. In this case at the development stage too much of the resist, and hence, the grating pattern has been removed. Figure 5.12(b) shows the grating pattern produced when the exposure dose was too low. In this case too much of the resist has remained after development and the duty cycle is incorrect. The correct dose for a 1.1 contrast ratio grating pattern was found to be 430 C/cm^2.

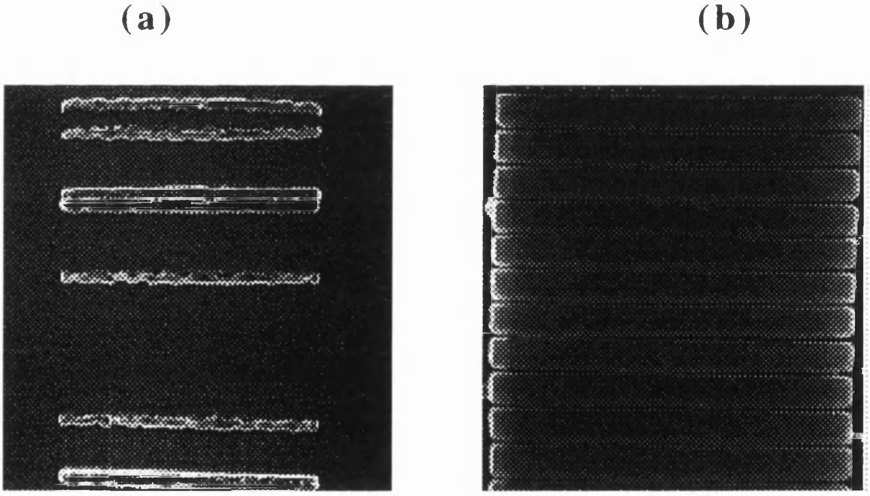

Figure 5.12. SEM photos showing grating patterns produced at different exposure doses : (a) High exposure E-beam pattern , (b) Low exposure E-beam pattern.

Stage 3: Development of Pattern.

A 3:1 concentration of IPA:MiBK developer was used to develop the pattern. The pattern was developed at 23.1°C for 30 seconds.

Stage 4: Evaporation.

A 30 nm thick layer of NiCr was then evaporated onto the top of the sample.

Stage 5: Removal of Resist from Sample.

Acetone was used in a lift-off process to remove the areas where the resist remained, leaving a metal copy of the pattern as the dry etch mask. Figure 5.13, shows an electron beam written waveguide grating structure which was formed on top of an AlGaAs wafer. This sample was then etched using $SiCl_4$ in the final stage of the device fabrication process.

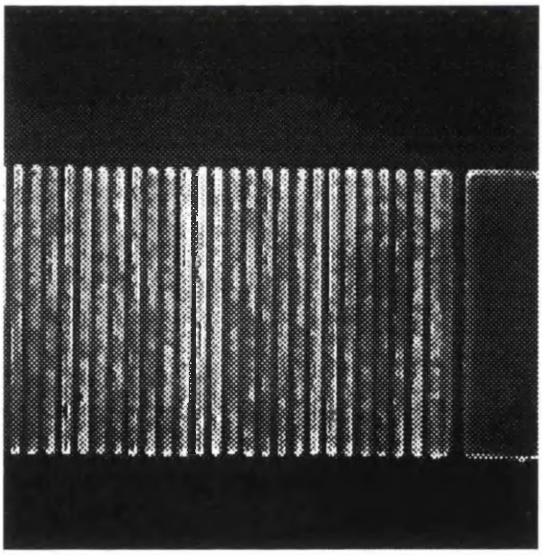

Figure 5.13. SEM showing both the uniform waveguide and the first order grating with a period of 235 nm.

The length of gratings ranged from 3 mm to 0.2 mm on 1.5 cm long waveguides. The width of the guides and hence, the width gratings were 4 μm. The period of the gratings was chosen to be 235 nm with a six to one mark to space ratio.

5.6. Experimental Results.

5.6.1. Linear Characterisation of the Holographic Grating.

The holographic gratings were characterised using a colour centre laser. The transmission was measured as a function of the input wavelength in the range 1.4 - 1.7 μm. The experimental set up used to locate the stop-band of the gratings is shown in Figure 5.14. Initially the light from the laser was coupled into an individual guide using the endfire rig and monitored using an IR camera connected to a T.V. monitor. The power coupled into the guide was maximised and the input and output power transmitted by the guide was monitored using a spectrum analyser, as the wavelength of the input light was altered.

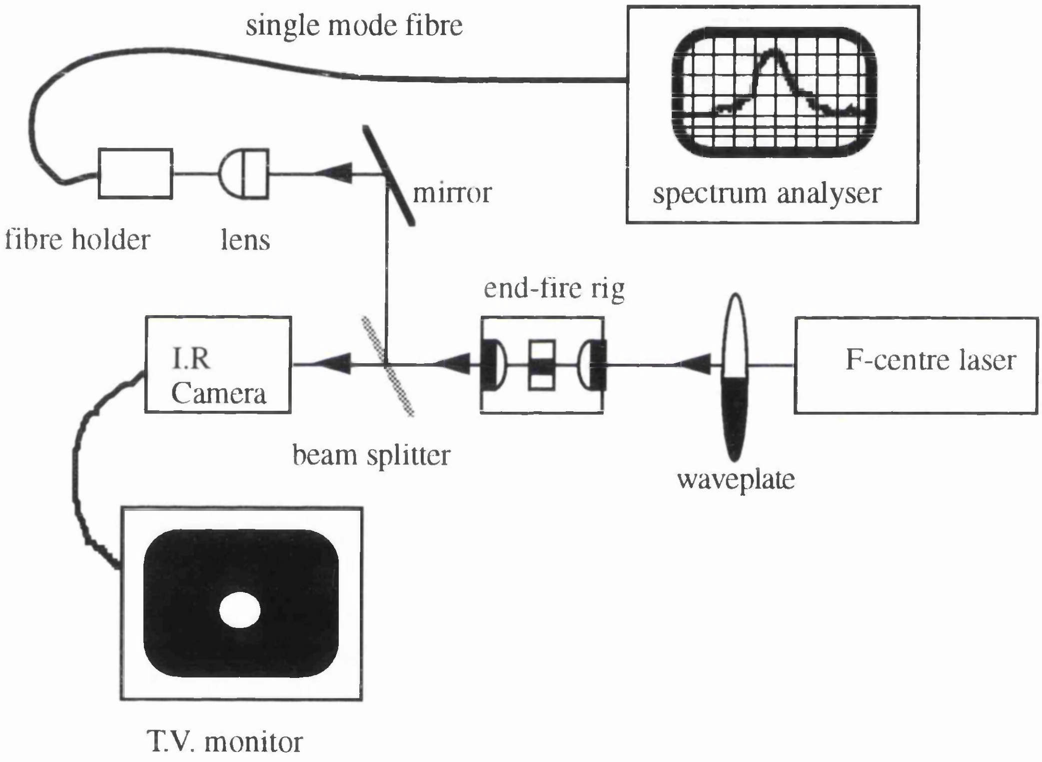

Figure 5.14. The experimental set up used to measure the stop-band of the grating device.

A typical result for a 3 mm long grating, with a mark to space ratio of 6:1 and period of 0.435 μm, is shown in fig. 5.15. The stop-band was located at a wavelength of 1.482 μm, and had a reflection efficiency of ~40%. The actual width of the stopband was difficult to measure as the laser did not tune smoothly but it was estimated to be no more than 2 nm.

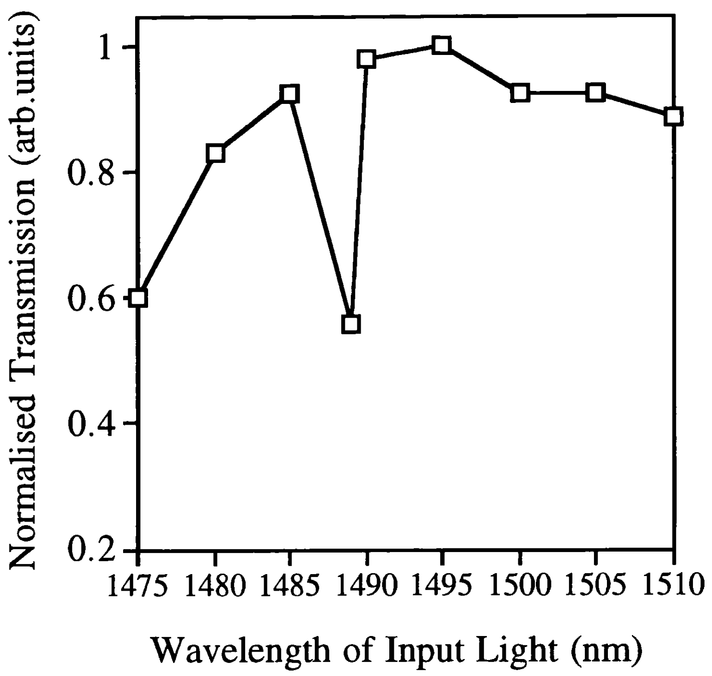

Figure 5.15. The transmission characteristics of a 3 mm long, holographically fabricated grating as a function of wavelength.

5.6.2. Linear Loss Measurements of the Holographic Gratings.

The Fabry-Perot technique discussed in chapter 3 was used to measure the linear absorption losses of the AlGaAs waveguides both before the gratings were formed and after the gratings were etched onto the waveguides. Light from a narrow line width, semiconductor laser operating at 1.556 μm was end-fire coupled into the waveguide. The output power from the guide was coupled into a spectrum analyser via a optical fibre. The sample was then cooled using a cotton bud dipped in liquid nitrogen and the Fabry-Perot fringes recorded as the sample returned to room temperature. From the contrast of the fringe pattern the losses were calculated.

The average linear loss for the uniform waveguides, without gratings was measured to be ~ 1.9 dB/cm. The introduction of a 3 mm long grating section resulted in an increase in the measured linear loss to 3.5 dB/cm. The increase in loss was attributed to the poor definition of the gratings.

5.6.3. Linear Characterisation of the Beam Written Grating Structures.

The experimental set up as depicted in fig 5.14 was used to locate the stop-band of the beam written gratings. Figure 5.16 shows the transmission profile of a typical 3 mm long grating as a function of wavelength over **a)** a long wavelength range and **b)** at around the stopband region. The stop-band was located at a wavelength of 1.502 μm, had a width of ~0.9 nm and reflection efficiency of ~70%. This reflection efficiency could have been greater as the limited resolution of most optical spectrum analysers leads to an underestimation of the reflectivity.

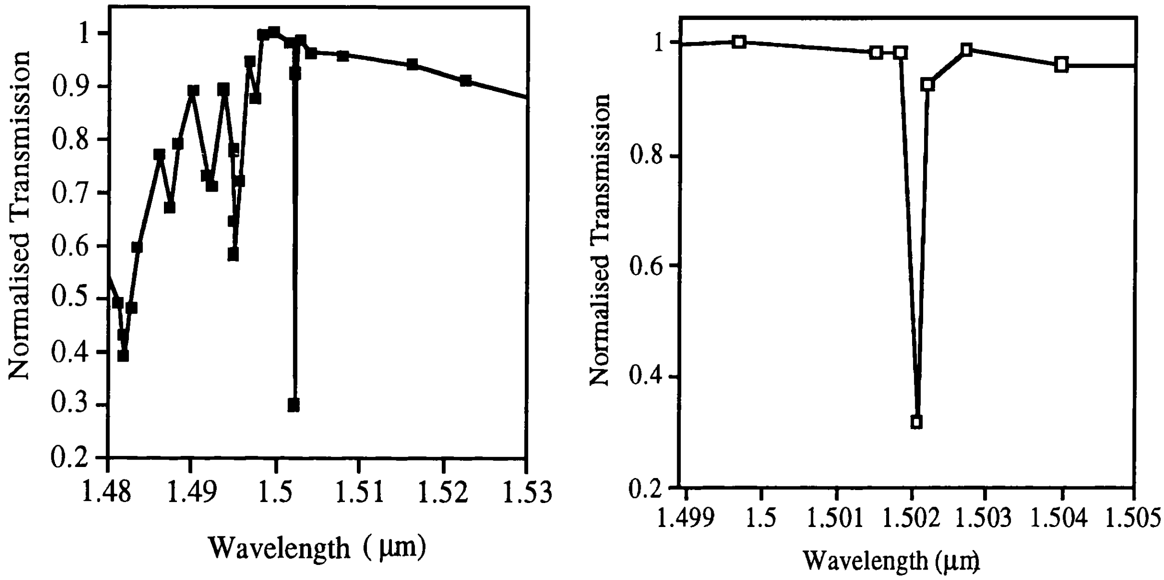

Figure 5.16. The Transmission profile of a 3mm long, e-beam written grating (a) transmission profile over a wavelength span from 1.48-1.53 μm and (b) profile around stop-band.

It is evident from figure 5.16(a) that the transmission profile exhibits significant loss with multiple sharp peaks on the short wavelength side of the bragg wavelength. This behaviour is the result of coupling to the cladding and radiation modes of the waveguide and has been characterised by Mizrahi and Sipe[23].

The average linear loss, measured for various 3 mm long gratings, with a mark to space ratio of 6:1 and period of 0.235 μm was 2.2 dB/cm. The linear scattering losses were also measured for several uniform guides without gratings and the average losses were again measured to be 2.2 dB/cm.

5.6.4. Comparison Between the Two Fabrication Processes.

The holographic fabrication process allows uniform gratings to be produced over large areas and the pitch of the grating can be accurately controlled. Another advantage of employing this technique is that the actual fabrication process time is extremely short with exposure times being approximatley 60 seconds. In contrast the E-beam process is very slow with exposure times being several hours and with the added problem of possible stitching errors occurring which limit the uniformity of the grating over large areas. However, the grating structures produced by the holographic method were seen to be poorly defined when compared to those produced by the beam writer as illustrated in fig. 5.17 which shows SEM photos of the profile of a grating produced by the holographic method (a) and compares it to the profile of a grating fabricated by the beam writer method (b).

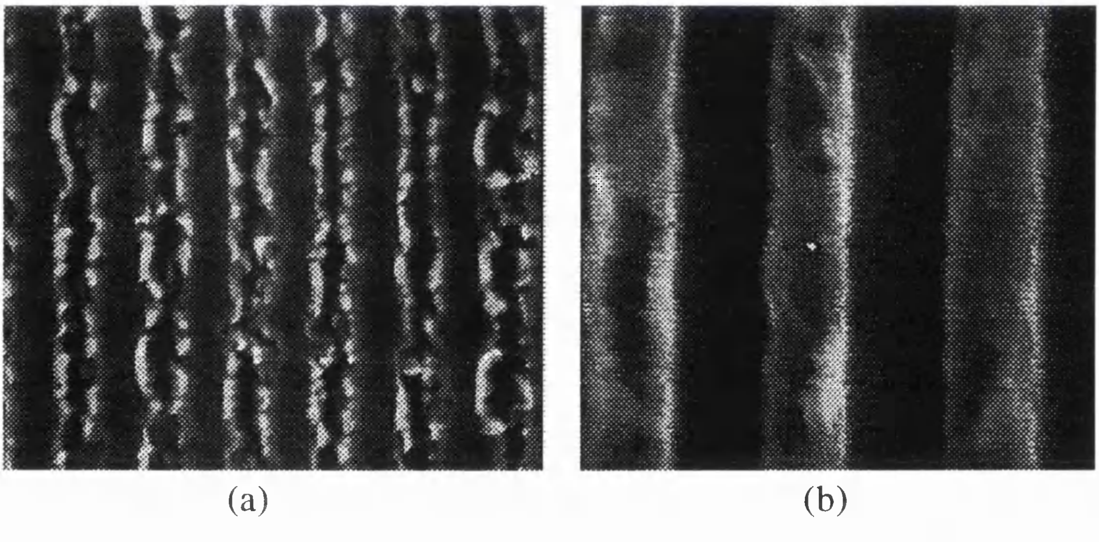

(a) (b)

Figure 5.17. SEM photos showing the etched gratings formed using (a) the holographic method and (b) using the beam writing process.

Furthermore, there is also very little control in selecting the areas where the grating was to be formed in the holographic process as opposed to the beam writing method were the areas to be patterned can be accuratly selected. In fact the use of direct write e-beam allows the duty cycle to be controlled more accurately and more complex filter characteristics can be realised. Linear loss measurements showed that the loss of the gratings formed using the holographic process were much higher than the corresponding grating formed by the e-beam. Another major disadvantage of the holographic method is that the process is multi-stepped and therefore, more complex than the electron beam writing technique which allows both waveguide and grating to be defined in a single writing step. Therefore, it was concluded that for the manufacturing of low loss grating filters on AlGaAs waveguides the e-beam writing technique is the ideal process.

5.6.5. Nonlinear Grating Experiment.

The aim of this experiment was to characterise the nonlinear response of the waveguide grating filters. The idea was to tune the input wavelength with a spectral width comparable to, or smaller than, the stop-band width of the grating close to the stop-gap and to observe any changes in the transmission and the output spectrum as the light intensity was increased. A KCl:Tl coupled cavity mode-locked colour centre laser was availble to test the nonlinear behaviour of the gratings. The experimental set up is shown in fig. 5.18.

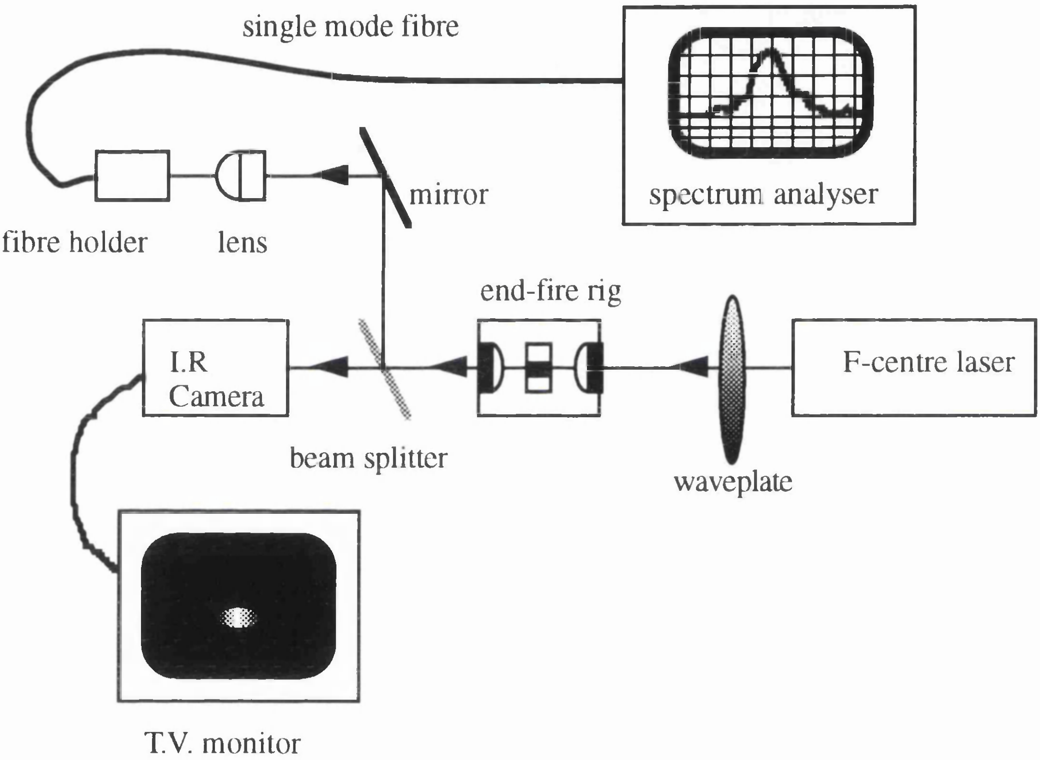

Figure 5.18. Experimental set up for the nonlinear experiment.

Light from the laser was coupled into individual waveguide grating filters, using an endfire rig. The spectrum of both the light launched into the grating filter guides and transmitted by the guides were measured as a function of input power using a spectrum analyser and a power meter. The maximum average power out of the laser was 37 mW and the pulse duration was 265 fs at a repetiton rate of 82 MHz giving a peak pulse power of 1.6 kW.

The linear grating filter tested was 3 mm long with a period of 235 nm, a 70% reflection efficiency at a Bragg wavelength at around 1.4785 μm. The spectral width of the laser ranged from 20 nm to 80 nm (FWHM) and hence, was large when compared to the width of the stop-gap of the grating filter which was approximately 0.9 nm. Figure 5.19 shows the spectral profile of a typical output pulse from the laser.

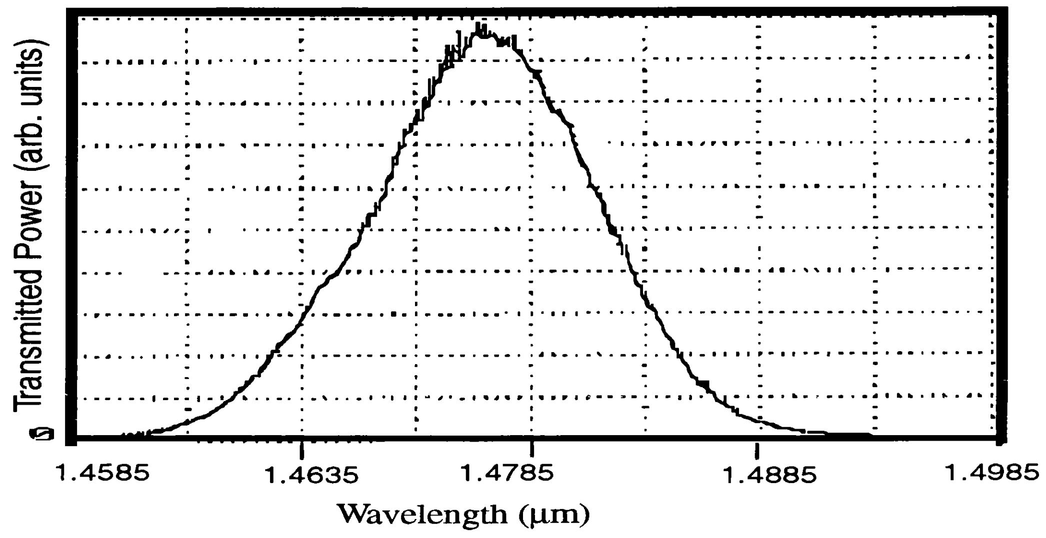

Figure 5.19. Spectral profle of the sech^2 pulses from the colour centre laser.

The spectrum produced by this laser was too wide to lie within the stopband of the grating filter. Instead the wavelength of the laser was tuned in such a way that the grating stopband lay at selected wavelengths within the spectrum of the laser pulse. The following results were obtained by tuning the laser pulse so that the grating stopband lay within the lower wavelength edge of the laser pulse . The spectrum of the output pulse from the filter was obtained at low light intensities as depicted in fig. 5.20 which shows the full spectrum of the output pulse and a close up of the spectrum around the grating stop-band region. The sharp spikes in the pulse spectrum are commonly caused by higher order group velocity dispersion effects introduced by the output mirror of the laser[24].

Figure 5.20 shows a dip in the output power of the pulse spectrum at the Bragg wavelength. This dip was absent in the spectrum of the input light pulse measured at the input of the waveguide and was therefore attributed to the presence of the bragg grating.

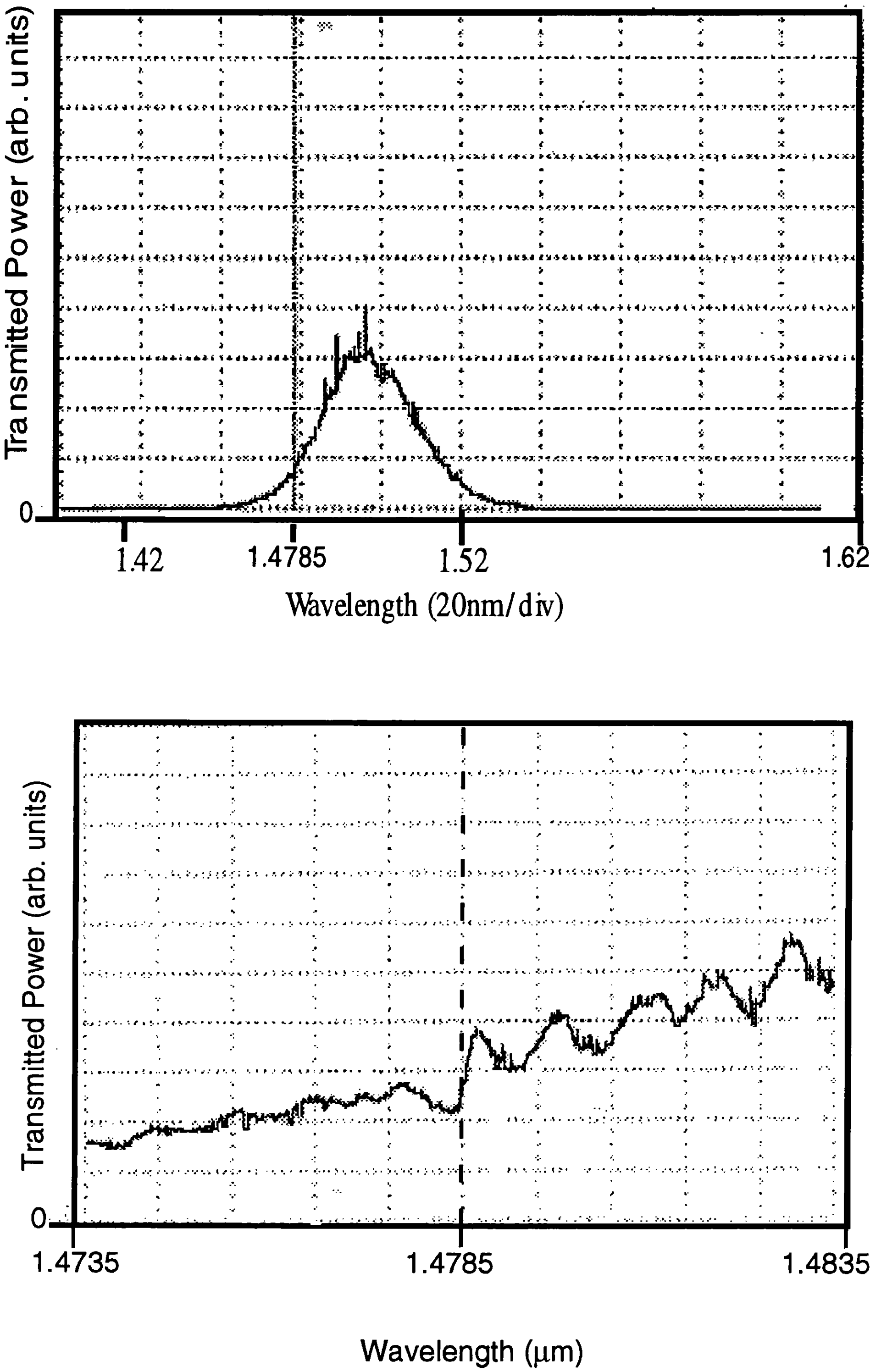

Figure 5.20. Spectral profle of the output pulse from the grating at low input powers.

The input power into the grating was maximised to a peak power of around 1.6 kW. Figure 5.21 shows the output pulse spectral profile at the high input light intensity.

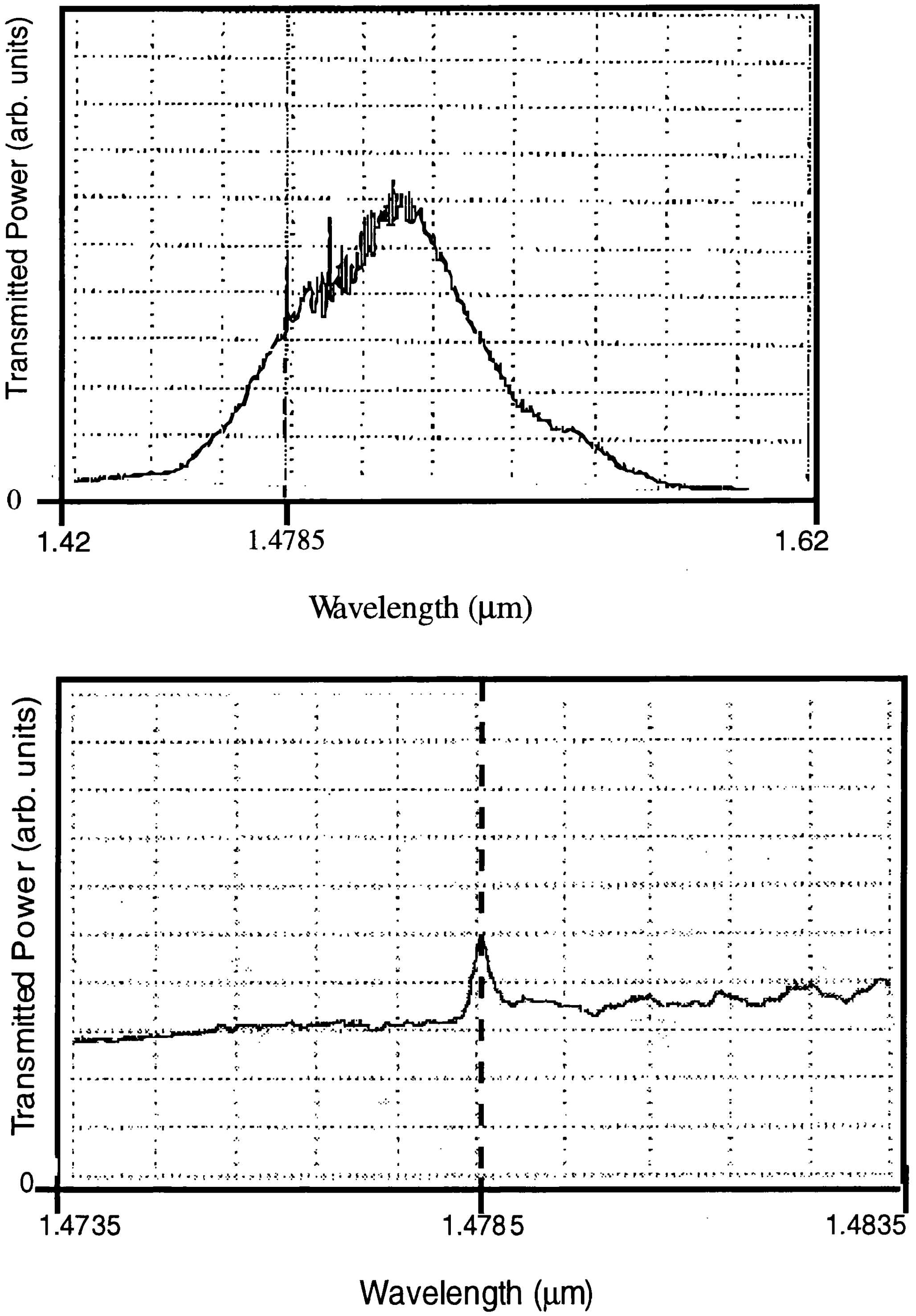

Figure 5.21. Spectral profle of the output pulse from the grating at high input powers.

It was seen that at low light intensities the grating appeared to reflect the spectral component of the laser pulse which lay within the stop-band region of the grating and at high input light intensities the light within the stop-band region appears to be transmitted by the grating. These experiments indicate that there could be a nonlinear effect taking place within the grating at high light intensities.

More convincing nonlinear switching results in these grating filters would have been achieved if the bandwidth of the high powered laser pulses had been comparible in size with the stopband width of the gratings. However, it is difficult to obtain laser pulses with such narrow spectral bandwidths which would have had the same high peak powers required to observe nonlinear switching in the gratings. Alternative matching of the band-width of the gratings and the laser can be achieved using chirped gratings. In the next section the design and fabrication of chirped grating filters will be described.

5.7. Chirped Gratings.

A wider reflection bandwidth can be obtained using gratings where the period varies conitinuously, or quasicontinuously, along the length of the grating section. These non-uniform gratings are commonly known as chirped gratings and have been sucessfully produced in fibres[25,26] and planar waveguides [27].

The Bragg condition is given by 5.13 below, where n_{eff} is the average effective index of the grating structure and λ_B and Λ are the Bragg wavelength and grating period respectivley.

$$\lambda_B = 2n_{eff}\Lambda_z \quad (5.13)$$

The chirp can be introduced in several ways. A common method is to either change the periodicity of the grating, or the width of the grating section as a function of length.

In this research an alternative method of producing chirped gratings was used. This technique involves changing the curvature of the waveguide while keeping the period of the grating itself constant. In this way the periodicity of the grating varies as a function of the radius of curvature (R), of the guide and is given by[25]:

$$\Lambda_z = \frac{\Lambda_o}{\cos\theta} \qquad (5.14)$$

where $\theta = z/R$ and z is the length of the grating section at which R is measured.

Figure 5.25 is a schematic of the curved waveguide grating filter which was designed. The waveguide consisted of a input straight waveguide section of length 4 mm followed by an S-shaped curved section of length 8 mm, with a angle of curvature, θ, and radius of curvature R and finally an output straight guide section, 4 mm in length. The uniform grating was designed to lie across the upward section of the S-shaped bend designated as section X2 in figure 5.25.

A BPM program was used to simulate the propagation of light within these curved guides (without the grating) and the optical confinement of the guides was seen to be high.

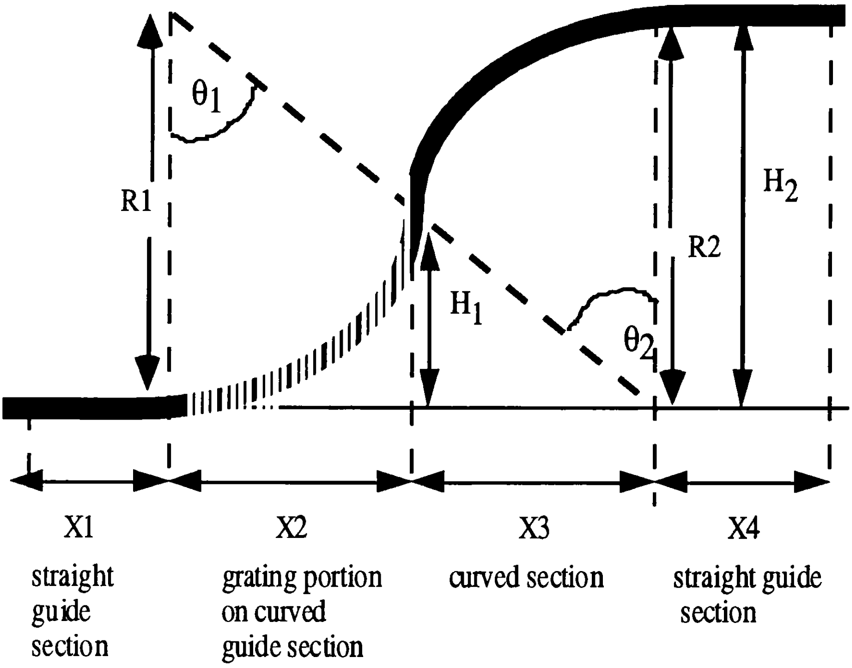

Figure 5.25. Schematic of the curved waveguide design.

$\theta = \theta_1 = \theta_2$ degrees	$\Delta\Lambda$ (nm)	$R = R_1 = R_2$ (mm)	H1 = 0.5 H2 (mm)
1	0.0358	229.18	0.03500
3	0.322	76.390	0.10480
5	0.897	45.830	0.17489
8	2.300	28.648	0.28060
12	5.250	19.090	0.42380
25	24.00	9.1673	0.91870

Figure 5.25. The curved waveguide chirped grating design.

The table in figure 5.25 shows the angles, θ of the designed curved guides along with the radius of curvature the curved sections $R=R_1,R_2$ of each guide and more importantly the approximate change in the grating period, $\Delta\Lambda$, associated with the chirped gratings.

5.7.1 Fabrication of the Chirped Gratings.

The wafer used to fabricate the chirped grating was the same that used to form the uniform gratings. The period of the grating was chosen to be 230 nm with a mark to space ratio of 6:1 to give a stop band at approximatley 1.51 μm. The width of the guides were chosen to be 4 μm, as before.

The one step electron beam process as described fully in section 5.52 was used fabricate the chirped gratings.

Using this process the curved waveguides were successfully fabricated however, the gratings produced were very poor. Figure 5.26 shows an SEM photo of a typical grating produced on the curved guides.

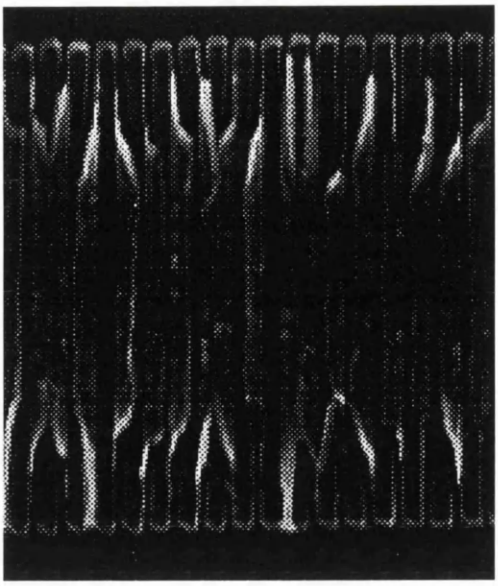

Figure 5.26. SEM showing the poor grating produced on the curved waveguides.

The poor grating quality could have been due to the exposure dose being too low, or could have been the result of a problem occuring at lift off stage of the E-beam process. Unfortunatley due to lack of time these problem could not be explored further and so there was no time to complete the fabrication process.

5.8. Suggested Further Work.

Work is continuing on the exploration of the production of gap and Bragg grating solitons within the chirped grating filters described in section 5.7 .In the following section the intended experimental work in this area is discussed. The experimental set up used in these investigations would be similar to that described in section 5.6.5. Laser pulses with narrow spectral widths would be used so that the pulses could be tuned to lie at either side or completley within the stopband of the grating.

5.8.1. Low power grating experiment.

The input and output pulse spectrum from the grating filter would be measured for pulse shapes tuned close to and far away from the stopband of the grating. The output pulse duration for these pulse shapes would also be measured.

5.8.1.1. Expected Results.

Upon transmission through the grating filter, pulses with wavelengths tuned close to either side of the grating will be broaden considerably more than input pulses at wavelengths far from the Bragg grating resonance. This broadening is due to the strong dispersion introduced by the grating. On the short wavelength side of the grating the group velocity dispersion is negative and on the long wavelength side of the grating it is positive. Pulses near the stopband will also be time delayed with respect to pulses far from the Bragg grating due to the smaller group velocity of the pulse near the stopgap. The total transmitted power for pulses tuned near the band gap should also be less than that for pulses tuned near the stopband due to higher grating reflectivity.

High power grating experiments.

Again the input and output pulse spectrum from the grating filter would be measured for pulse shapes tuned close to and far away from the stopband of the grating as well as the output pulse duration for these pulses.

Expected results

Upon transmission of the grating filter ,pulses tuned closed to the long wavelength side of the stopband will be broadened greatly as the self phase modulation together with the large normal group velocity dispersion at the stopband edge serve to disperse the pulse. Pulses tuned closed to the short wavelength side of the stopband will produce Bragg solitons i.e the pulses will be intially compressed and the peak intensity of the pulse will increase as the nonlinearity balances with the anomalous group velocity dispersion to form a stable soliton. This pulse will also be time delayed with respect to the light pulse tuned far from the stopband. In contrast pulses tuned far from the bragg grating should experience no change in at all.

If the input laser pulses are tuned to lie within the stopband of the grating at low light intensities then at high light intensities it is possible that gap solitons can be produced.

5.8 Conclusions.

First and second order integrated waveguide filters, based on Bragg gratings on AlGAAs waveguides were designed and fabricated using both a holograhic technique and an electron beam writing process. The filters were designed to operate in the 1.55 μm low loss telecommunications window. Linear characterisation of these grating structures was carried out. The electron beam process was found to be the most efficient method of producing these grating structures. The losses of the e-beam written waveguide filters were measured using the Fabry-Perot technique and were found to be the same as for the host waveguide at 2.2 dB/cm. The scattering losses of holographically defined gratings were also measured and found to be higher at 3.5 dB/cm. The negligible change in scattering losses of the beam written gratings were attributed to the high quality of the fabrication process and the ability to control the duty cycle of the grating.

A preliminary nonlinear experiment was carried out on the grating filters using a coupled cavity modelocked colour centre laser. Possible nonlinear switching effects were observed in the grating structures at high peak powers. A major drawback to this experiment was that the band-width of the laser used to test the gratings was significantlly wider than the band-width of the gratings. It was impossible to tune the laser wavelength to lie within the stop-band of the grating.

To overcome this problem, chirped gratings on curved waveguides were designed and fabricated. These chirped gratings are designed to have wider effective stopbands than uniform gratings and so were fabricated in an attempt to match the bandwidths of the laser pulses and the gratings.

The quality of gratings in the first chirped gratings produced using this process were poorly defined. The problem may have been that the exposure dose of the pattern was too low causing problems during the lift off stage. However there was no time left to explore this further. I would suggest that in the future it would be beneficial to explore further the fabrication and testing of the chirped grating discussed in section 5.6. An alternative method is to use a stronger grating, or photonic band gap to produce a wider stop-band.

References.

1. Z. Ahmed, R.S. Tucker, L. Zhai, "Discontinuous modulation response of grating -assisted extended-cavity semiconductor laser", Electron. Lett. **30**, pp 305-306 (1994).
2. Y. Shibata, S. Oku, Y. Kondo, T. Tamamura, "Semiconductor monolithic wavelength selective router using grating switch integrated with directional coupler", Electron. Lett. ,**31**, pp 966-967 (1995).
3. H.G. Winful, J.H. Marburger, E. Garmire ,"Theory of bistability in nonlinear distributed feedback structures" Appl. Phy. Lett. , **35**, pp 379-381 (1979).
4. H.G. Winful and G.D. Cooperman, "Self-pulsing and chaos in distributed feedback bistable optical devices" , Appl. Phy. Lett. , **40**, pp 298-300 (1982).
5. H.G. Winful ," Pulse compression in optical fiber filters", Appl. Phy. Lett. **46**, pp 527-529 (1985).
6. C.M. de Sterke, J.E. Sipe," Switching dynamics of finite period nonlinear media-
a numerical study", Phy. Rev. A , **42,** pp 2858-2869 (1990).
7. S. Trillo, S. Wabnitz, G.I. Stegeman, "Nonlinear co-directional guided wave mode conversion in grating stuctures", J. of Lightwave Tech., **6**, pp 971-976 (1988).
8. C.J. Herbert, W.S. Capinski, M.S. Malcuit,"Optical power limiting with nonlinear periodic structures", Optic Lett., **17**, pp 1037-1039 (1992).
9. C.J.Herbet, M.S.Malcuit, "Optical bistability in nonlinear periodic structures" Opt.Lett., **18**, pp 1783-1785 (1993).
10. J.E. Ehrlich, G. Assanto and G.I. Stegeman, "All-optical tuning of waveguide nonlinear distributed feedback gratings." Appl. Phy. Lett., **56**, pp 602-604 (1990).
11. N.D. Sankey, D.F. Prelewitz and T.G. Brown " All-optical switching in a nonlinear periodic waveguide structure", App.Phy.Lett , **60**, pp1427-1429 (1992).
12. B.U. Chen ,C.C. Ghizoni, C.L. Tang," Phase-matched second harmonic generation in solid thin films using modulation nonlinear susceptibilities", Appl. Phys. Lett. **28**, pp 651-653 (1976).
13. C.T. Seaton, X. Mai, G.I. Stegeman and H.G. Winful, "Nonlinear guided wave applications", Opt.Eng., **24**, pp 593-599 (1985).
14. B.J. Eggleton, C.M. deSterke, R.E. Slusher, J.E. Sipe," Distributed feedback pulse generator based on nonlinear fibre grating", Electron. Lett.,**32**, pp 23412-2342 (1996).

15. C.M. de Sterke and J.E. Sipe, “ Self-localsied light-launching of low velocity solitons in corrugated nonlinear waveguides”, Opt. Lett., **14**, pp 871-873 (1989).
16. S. Wabnitz, “ Forward mode coupling in periodic nonlinear-optical fibres-modal dispersion cancellation and resonance solitons”, Opt. Lett., **14**, p 1071-1073 (1989).
17. N.D. Sankey, D.F. Prelewitz and T.G. Brown, "All-optical swicthing in a nonlinear periodic waveguide sytructure", Appl. Phy. Lett., **60,** pp 1427-1429.
18. A. Yariv and P. Yeh,"Optical Waves in Crystals", Wiley New York, chp.11, (1984).
19. I.Bennion, J.A.R.Williams, L.Zhang, K.Sugden, N.J.Doran, "UV in fibre Bragg gratings", Opt. and Quantum Electron., **28**, pp 93-135 (1996).
20. F.J. Fraile-pelåez and G. Assanto, "Improved coupled mode analysis of nonlinear distributed feedback structures" Opt. and Quan. Elec., **23**, pp 633-637 (1991).
21. R. Steingrüber and M. Hamacher, "Simultaneous exposure of filter gratings and waveguides by direct electron-beam lithography", Microelectronic Eng., **35**, pp.341-344 (1997).
22. T.F. Krauss, B. Vogele, C.R. Stanley, and R. De La Rue,"Waveguide microcavity based on photonic microstructures" IEEE Photon. Tech. Lett., **9**, pp. 176-178 (1997).
23. V.Mizrahi, J.E. Sipe,"Optical propeties of photosensitive fibre phase grating", J. Lightwave Technol. , **11**, pp 1513-1517 (1993).
24. R.S.Grant, "Mode-locked colour centre lasers and their application", University of St Andrews, PhD Thesis (1991).
25. Q. Zhang, D.A. Brown, L.J. Reinhart andT.F Morse, "Linearly and nonlinear chirped bragg gratings fabricated on curved fibers",Opt. Lett., **20**, pp 1122-1124 (1995).
26. K. Sugden, I. Bennion, A. Molony and N.J. Copner, "Chirped gratings produced in photosensitive optical fibers by fiber deformation during exposure", Electron. Lett. **30**, pp 440-441 (1994).
27. C.J. Brooks, G.L. Vossler and K.A. Winick,"Integrated-optic dispersion compensator that uses chirped gratings", Opt. Lett., **20**, pp 368-370 (1995).

CHAPTER 6

Summary of thesis.

All-optical switches have great potential within future optical computing and optical communication networks. The aim of this research was to investigate the ultrafast all-optical switching effects of AlGaAs operated in the half-band gap region. The switching configurations investigated included several different nonlinear coupled waveguide arrays and integrated waveguide filters. The conclusions from this study are summarised below.

6.1 Conclusions on the Design and Modelling of the Devices.

The waveguides were designed to be single moded and to operate at around the low loss 1.55μm spectral region. The switching characterics of the coupler devices were modelled using both a fourth order Runge-Kutta Algorithm and a split step fast fourier BPM code. The BPM model included the effects of linear absorption, dispersion and multi-photon absorption on the operation of the couplers.

Simulations of the transmission characteristics of the nonlinear coupled arrays showed that as the number of guides within the array increased the switching became sharper. In additon, the critical intensity required to observe switching increased. In the uniformly spaced coupled arrays the switching efficiency was seen to decrease as the number of guides within the array increased. Nonuniformly spaced couplers were also modelled and it was shown that the switching characteristics of the array could be altered by changing the spacing between the guides. In addition it was seen that in some cases a switching efficiency of ~100% could be achieved in these non-uniformly spaced arrays.

6.2 Conclusions on the Fabrication of the devices.

The AlGaAs wafers were grown by molecular beam epitaxy. The coupled waveguide arrays were fabricated using a standard combination of photolithography and reactive ion etching and were shown to have low linear losses.

The integrated waveguide filters were fabricated using both a holographic technique and using electron beam lithography. Overall the single step beam writing process was found to be the ideal process for the fabrication of these grating structures. The scattering losses of the grating filters were measured using a Fabrey-Perot technique. The beam written gratings were shown to have considerably lower losses than the holographic gratings and were better defined.

6.3 Conclusions on the Experimental Results.

6.3.1 Experimental results on the waveguide arrays and suggested future work.

The experiments were carried out using a mode-locked colour centre laser. All-optical switching was observed in uniformly and non-uniformly spaced three, four and eight guide couplers. The experimental switching characteristics of the couplers were seen to compare well with the theoretically simulated switching behaviour of the guides. The nonlinear refraction and two photon absorption coefficent at around the half-band gap were also measured. These measurements agreed with previously published experimental results.

Further work in this field could involve the design of nonlinear coupled arrays for soliton switching and beam steering applications. The arrays could also be used to produce logic gates.

6.3.2 Experimental results on the Grating Structures and Suggested Future Work.

The linear characteristics of the AlGaAs grating filters were obtained. A maximum reflection efficiency of ~70% was found in a 3 mm long E-beam written grating with a stopband width of ~ 0.9 nm. A preliminary nonlinear experiment was carried out on the grating filters and a small nonlinear switching effect was shown to take place in the grating structure at high peak powers. A major drawback to this experiment was that the band-width of the laser used to test the gratings was significantly wider than the band-width of the gratings. Therefore, the laser wavelength could not be tuned to lie within the stop-band of the grating. It is therefore, suggeted that the experiment be repeated using chirped gratings with effective wider band-widths to observe more convincing nonlinear behaviour.

Appendix A

Runge-Kutta method

In this research a fourth order Runge-Kutta method was used to numerically analyse the coupling of light between the counter-propagating modes of a grating filter and also the coupling of light between guides in a nonlinear coupled waveguide array. The Runge-Kutta method is both a popular and simple method used for integrating differential equations. In the following example the fourth order method is explained using the following first order differential equation:

$$\frac{dy}{dx} = f(x,y)$$

This function is sketched in the figure below:

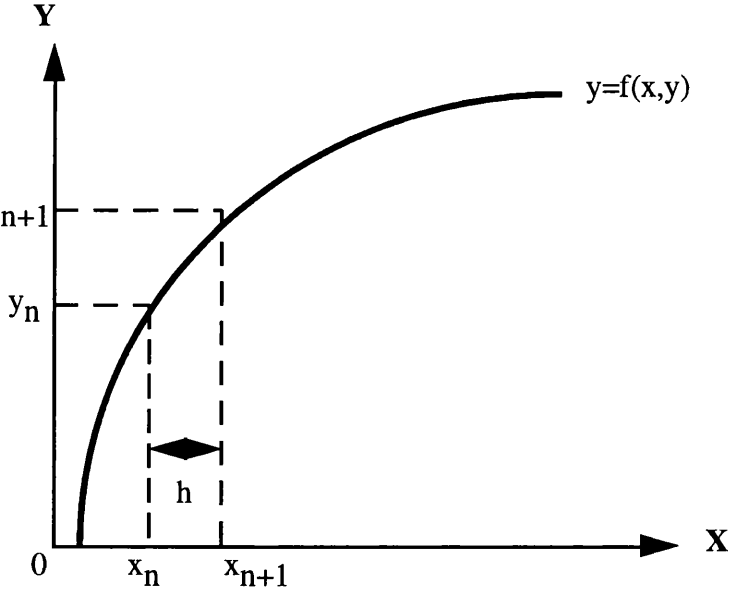

The process is a one step method whereby the function f(x,y) is evaluated for a series of calculated x and y values. Initially a starting value (x_n,y_n) which is a solution of the function must be known. To calculate consecutive points (x_{n+1},y_{n+1}) a step interval h along the x axis seperating the points x_n and x_{n+1} is defined i.e. $x_{n+1}=x_n+h$, as depicted in the figure above of the function. The corresponding values of y i.e. y_{n+1} are then calculated using the following formulae:

$$y_{n+1} = y_n + \frac{h}{6}(k_1 + 2k_2 + 2k_3 + k_4)$$

where

$$k_1 = f(x_n, y_n)$$

$$k_2 = f(x_n + \frac{h}{2}, y_n + \frac{hk_1}{2})$$

$$k_3 = f(x_n + \frac{h}{2}, y_n + \frac{hk_2}{2})$$

$$k_4 = f(x_n + h, y_n + hk_3)$$

R.K. FORTRAN Program Code for the Simulation of the Switching Behaviour of a Three Guide Nonlinear Coupler.

```
PROGRAM threecore_plot
INTEGER n,i,j,isteps,nsteps
CHARACTER ans*1
REAL*8x,h,p1,maxp2,pi,lc,
beta,kap,len,l1,vil,Vin
REAL*8 out1,out2,out3,tot,
tnorm,Tin
REALxdata(100),ydata(100),
y2data(100),y3data(100)
REALNydata(100),Ny2data(100),
Ny3data(100)
COMPLEX*16 v(3),y(3),rk(4,3)
PARAMETER (isteps=50,nsteps=100)

COMMON /TheData/ xdata, nydata,
Ny2data, Ny3data
COMMON /coup/ h,beta,kap,vil,tnorm
```

```
WRITE(*,*)'Enter the number of
coupling lengths'
READ(*,*)l1
WRITE(*,*)'Enter normalised T- and
V- parameters for'
WRITE(*,*)'two and three photon
absorption'
READ(*,*)Tin,Vin
WRITE(*,*)'For a timeaveraged plot
enter t'
WRITE(*,*)'For a cw plot enter c'
READ(*,*)ans
WRITE(*,*)'Program is running......'

beta=1.0
len=1.0
```

```
pi=ACOS(-1.d0)
h=len/DBLE(isteps)
lc=len/l1
kap=pi/(sqrt(2.0)*lc)
tnorm=Tin/(8.0*pi)
vil=Vin/(8.0*pi**2)
maxp2=6.0*SQRT(2.0)*kap
C     Extra factor of 2 for the power range ie maxp2=2Pc
OPEN(9,FILE='doc3')
DO 10 n=1,nsteps
*******************************
C...This section defines the initial power in the guides
p1=DBLE(n)/DBLE(nsteps)*maxp2
xdata(n)=p1
y(1)=DCMPLX(SQRT(p1),0.d0)
y(2)=(0.d0,0.d0)
y(3)=(0.d0,0.d0)
DO 20 i=1,isteps
x=DBLE(i-1)*h
******************************
C....This section defines the R.K algorithm

j=1
u=x
v(1)=y(1)
v(2)=y(2)
v(3)=y(3)
CALL subst(j,v,rk)

j=2
u=x+h/2.d0
v(1)=y(1)+rk(1,1)/2.d0
v(2)=y(2)+rk(1,2)/2.d0
v(3)=y(3)+rk(1,3)/2.d0
CALL subst(j,v,rk)

j=3
u=x+h/2.d0
v(1)=y(1)+rk(2,1)/2.d0
v(2)=y(2)+rk(2,2)/2.d0
v(3)=y(3)+rk(2,3)/2.d0
CALL subst(j,v,rk)

j=4
u=x+h
v(1)=y(1)+rk(3,1)
v(2)=y(2)+rk(3,2)
v(3)=y(3)+rk(3,3)
CALL subst(j,v,rk)

y(1)=y(1)+(rk(1,1)+2.d0*rk(2,1)+2.d0*rk(3,1)+rk(4,1))/6.d0
y(2)=y(2)+(rk(1,2)+2.d0*rk(2,2)+2.d0*rk(3,2)+rk(4,2))/6.d0
y(3)=y(3)+(rk(1,3)+2.d0*rk(2,3)+2.d0*rk(3,3)+rk(4,3))/6.d0

20    CONTINUE
*******************************
C....output files defined in this section

out1=ABS(y(1))**2
out2=ABS(y(2))**2
out3=ABS(y(3))**2
tot=out1+out2+out3

ydata(n)=out1/p1
y2data(n)=out2/p1
y3data(n)=out3/p1
WRITE(9,99)p1,out1/p1,out2/p1,out3/p1,tot/p1
```

```
99
FORMAT(T1,F8.4,',',T15,F6.4,',',T
30,F6.4,',',T45,F6.4,',',T60,F6.4)
10  CONTINUE
C   CLOSE(9)
******************************
c....Type of input pulse defined in this
section

IF (ans.EQ.'t') THEN
Call timeave(ydata,Nydata)
Call timeave(y2data,Ny2data)
Call timeave(y3data,Ny3data)
ELSE
Do 111 n=1,nsteps
Nydata(n)=ydata(n)
Ny2data(n)=y2data(n)
Ny3data(n)=y3data(n)
111     CONTINUE
ENDIF
END

SUBROUTINE timeave(yd,Nyd)
REAL*8 t,delt,sum
REAL yd(100),Nyd(100)
INTEGER n,j,nsteps
nsteps=100
Nyd(1)=yd(1)
Nyd(2)=yd(2)
Do 110 n=3,nsteps
t=0.d0
delt=DFLOAT(3.d0/n)
sum=(1.d0/DCOSH(t))**2*yd(n)
Do 120 j=n,1,-1
t=t+delt
sum=sum+2.0*(1.d0/DCOSH(t))**2*
yd(j)
120     CONTINUE
```

```
Nyd(n)=DFLOAT(sum/n*1.5)
110  CONTINUE
RETURN
END

*****************************
C...equations defining the fields
propagating within the guide defined in
this section.

SUBROUTINE subst(j,v,rk)
INTEGER j
REAL*8 h,beta,kap,vil,tnorm
COMPLEX*16 v(3),rk(4,3)

COMMON /coup/ h,beta,kap,vil,tnorm

rk(j,1)=h*(0.d0,1.d0)*(beta*v(1)+kap
*v(2)+(1.d0+(0.d0,1.d0)*tnorm)*ABS
(v(1))**2*v(1)+(0.d0,1.d0)*vil*ABS(
v(1))**4*v(1))

rk(j,2)=h*(0.d0,1.d0)*(beta*v(2)+kap
*(v(1)+v(3))+(1.d0+(0.d0,1.d0)*tnor
m)*ABS(v(2))**2*v(2)+(0.d0,1.d0)*v
il*ABS(v(2))**4*v(2))

rk(j,3)=h*(0.d0,1.d0)*(beta*v(3)+kap
*v(2)+(1.d0+(0.d0,1.d0)*tnorm)*ABS
(v(3))**2*v(3)+(0.d0,1.d0)*vil*ABS(
v(3))* *4*v(3))

RETURN
END
******************************
```

Appendix B

BPM Program Code For Simulating the Switching Behaviour of a Nonlinear Three Guide Coupler

```
c       Temporal BPM for directional
        coupler
c       This program calcultate the
        switching fraction of a 3 core
        NLDC
c       for soliton or regular pulses.
c       nt: number of points in
        transverse dimension x
c       tmax: maximum value in x
c       nz: number of steps in z
c       zmax: user define parameter
        for propagation distance
c       pi: pi
c       lambda: wavelength
c       To: input pulse width
        Tp/1.763
c       Tp: input pulse width FWHM
c       beam: complex array for the
        electric field
c       beta2: dispersion
c       zo: soliton period
c       aeff : aeffective area
c       Ld: dispersion length
c       Lnl: nonlinear length

complex*16beambar(4096),
beamcross1(4096),beamcross2(4096)
real*8databar(8192),datacross1(8192
),datacross2(8192)
real*8tmax,zmax,dz,delz,beta2,ko,la
mbda,aeff,energyin
real*8pi,zo,powermax,n2,Ld,Lnl,ga
mma,To,Tp,chirp,inten,z
real*8energybar,energycross1,energy
out,kappa12,power,c2pa,c3pa
real*8alpha,calpha,t2pa,t3pa,eta,r,rae
ff,z1,kappa23
real*8ratiobar,ratiocross1,powerin,po
werout,powerbar
real*8powercross2,ratiocross2,
energycross2
character*12file1$,file2$,filecoup$,
filepower$,fileinput$
character*12 fileoutput$
character*4filename$,filespec$,
pulsetype$,dat$
integernt,nz,i,j,sing,tens,inter,nsolito
n,jspec,nbeta2,npower
integer nauto,nsave,nwave,iinit

c       The equivalence is use since
c       the FFT subroutine uses array
c       of real instead of complex.

        equivalence(beambar,databar)
        equivalence(beamcross1,datac
        ross1)
        equivalence(beamcross2,datac
        ross2)
        j=0
        jspec=0

c       SUBROUTINE TO INPUT
        PARAMETER FOR THE
        RUN
call inputparameter
(filename$,filespec$,lambda,Tp,n2,nt
,nz,*inter,interspec,aeff,beta2,nsolito
n,powermax,zmax,nbeta2,chirp,*pul
setype$,kappa12,npower,filecoup$,fi
lepower$,nauto,t2pa,t3pa,*alpha,eta,
nsave,r,raeff,fileinput$,fileoutput$,n
wave,z1,kappa23,*ntmax)

C       DEFINE To FOR THE
        PULSE TYPE
        pi=4.0d0*datan(1.0d0)
        if(pulsetype$.eq.'SECH'.
        or.pulsetype$.eq.'INPT')
        then
                To=Tp/1.763d0
        end if
        if (pulsetype$.eq.'GAUS')
        then
                To=Tp/1.665d0
        end if

c       DEFINE CONSTANT
        ko=2.0d0*pi/lambda
        tmax=dfloat(ntmax)*To
```

```
        gamma=n2*ko/aeff
        Ld=To*To/dabs(beta2)
        zo=pi/2.0d0*Ld
        c2pa=t2pa/aeff/2.0d0
        c3pa=t3pa/aeff/aeff/2.0d0
        calpha=alpha/2.0d0

c       open file for output

open(unit=8,file=filecoup$,status='n
ew')
open(unit=11,file=filepower$,status=
'new')

c       DEFINE POWER AS
POWER MAX OR AS THE
SOLITON POWER
if (powermax.gt.0.0d0) then
        powermax=powermax
        else
        powermax=dabs(dfloat(nsolit
on*nsoliton)/gamma/Ld)
        end if

c       DEFINE THE DZ AS A
FUNCTION OF TOTAL LENGTH
OR AS A FUNCTION
C       OF THE SOLITON PERIOD
        if (zmax.gt.0.0d0) then
                dz=zmax/nz
        else
                dz=zo/nz
        end if
        nz=nz+1

C       MAIN PROGRAM
c       see note in the subroutine
inputparameter
        if (pulsetype$.eq.'INPT')
npower=1
if (npower.eq.1) then
write (*,*)  ' file *0 is the initial field'
iinit=0
else
iinit=1
end if
do 57 m=1,npower
power=dfloat(m)/dfloat(npower)*
powermax
Lnl=1.0d0/gamma/power

c       Defines the input beam to the
bar state
call
definebeam(To,beambar,*tmax,nt,po
wer,chirp,pulsetype$,energyin,fileinp
ut$)
```

```
c       initialises the cross guides to
zero input field

        call initcross(beamcross1,nt)
        call initcross(beamcross2,nt)
z=0.0d0
write(*,*) m
c       Start of propagation in z
do 10 i=iinit,nz
if (mod(i,100).eq.0)
write(*,*) 'i= ',i

c       first and last half step

if (i.eq.1.or.i.eq.nz) then
        delz=dz/2.0d0
        else
                delz=dz
                end if
z=z+delz

C       CALCULATE THE EFFECT
OF DISPERSION IF NBEATA2 NE
0
if (nbeta2.ne.0) then
call four1(databar,nt,1)
call four1(datacross1,nt,1)
call four1(datacross2,nt,1)

call dispersion(beambar,
nt,tmax,beta2,delz)
call dispersion(beamcross1
,nt,tmax,beta2,delz)
call dispersion(beamcross2,
nt,tmax,beta2,delz)


C       SAVE THE SPECTRUM IF
        NSAVE EQ 1
C       BAR STATE HAVE PREFIX
        BR, CROSS STATE CX

if(mod(i,interspec).eq.0.and.nsave.e
q.1) then
        if (jspec.lt.10) then
        file2$='br'//filespec$//char(jsp
        ec+48)
callsavespectrum(beambar,tmax,nt,fil
e2$,To*,NWAVE,LAMBda)

file2$='c1'//filespec$//char(jspec+48)
callsavespectrum(beamcross1,tmax,nt
,file2$,To*,NWAVE,LAMBda)
file2$='c2'//filespec$//char(jspec+48)
call savespectrum(beamcross2,
tmax,nt,file2$,To*,NWAVE,LAMBd
a)
end if
```

```
if (jspec.ge.10) then
sing=mod(jspec,10)
tens=int(float(jspec)/10.0)
file2$='br'//filespec$//char(tens+48)
*//char(sing+48)
call savespectrum(beambar,
tmax,nt,file2$,To
*,NWAVE,LAMBda)
file2$='c1'//filespec$//char(tens+48)
*//char(sing+48)
call savespectrum
(beamcross1,tmax,nt,file2$,To
*,NWAVE,LAMBda)
file2$='c2'//filespec$//char(tens+48)
*//char(sing+48)
call savespectrum(beamcross2,
tmax,nt,file2$,To*,NWAVE,LAMBd
a)
end if
jspec=jspec+1
end if
call four1(databar,nt,-1)
call four1(datacross1,nt,-1)
call four1(datacross2,nt,-1)

call dividebynt(databar,nt)
call dividebynt(datacross1,nt)
call dividebynt(datacross2,nt)

end if
call nlin(beambar,nt,gamma,delz,
c2pa,c3pa,calpha)
call nlin(beamcross1,nt,gamma,delz,
c2pa,c3pa,calpha)
call nlin(beamcross2,nt,gamma,delz,
c2pa,c3pa,calpha)

if (z.ge.z1) then
call coupling(beambar,beamcross1
,nt,kappa12,delz)
call coupling(beamcross1,
beamcross2,nt,kappa23,delz)
            end if

call reflection(beambar,tmax,nt)
call reflection(beamcross1,tmax,nt)
call reflection(beamcross2,tmax,nt)

C       SAVE THE FIELD IF
        NSAVE EQ 1 BUT NEED
        TO BE CALLED TO
        CALCULATE
C       THE POWER IN EACH
        WAVEGUIDE. THIS GIVES
        THE SWITCHING
        FRACTION.
C       WILL CALCULATE AND
        SAVE
        AUTOCORRELATION
        INSTEAD OF THE PULSES
C       IF NAUTO EQ 1
C       BAR STATE HAVE PREFIX
        BR, CROSS1 STATE C1 etc.
              if (mod(i,inter).eq.0)
then
              if (j.lt.10) then

file1$='br'//filename$//char(j+48)
call savefield(beambar,tmax,nt,file1$,
*power,energybar,nauto,nsave)

file1$='c1'//filename$//char(j+48)
call savefield(beamcross1,tmax,nt,
file1$,*power,energycross1,nauto,ns
ave)

file1$='c2'//filename$//char(j+48)
call savefield(beamcross2,tmax,nt,
file1$,*power,energycross2,nauto,ns
ave)
              end if
              if (j.ge.10) then
              sing=mod(j,10)
              tens=int(float(j)/10.0)
file1$='br'//filename$//char(tens+48)
*//char(sing+48)
call savefield(beambar,tmax,nt,
file1$,power,
*energybar,nauto,nsave)
file1$='c1'//filename$//char(tens+48)
*//char(sing+48)
call savefield(beamcross1,tmax,
nt,file1$,*power,energycross1,nauto
,nsave)
file1$='c2'//filename$//char(tens+48)
*//char(sing+48)
call savefield(beamcross2,tmax,nt,
file1$,*power,energycross2,nauto,ns
ave)
end if
j=j+1
end if
c       end of z loop
10      continue

C       PRINT ON THE SCREEN
THE PARAMETER OF THE RUN
        write(*,*)
        write(*,*)
        write(*,1000) zo
        write(*,1010) Ld
        write(*,1020) Lnl
        inten=power/aeff*1.0d-
        9/1.0d4/eta/r*raeff
        write(*,1030) inten
        write(*,1040) power
```

```
          write(*,1050) z
          write(*,1061) energybar
      write(*,1062) energycross1
      write(*,1063) energycross2
          write(*,1060) energyin

energyout=energybar+energycross1+
energycross2
write(*,1070) energyout
energyratio=energyout/energyin
write(*,1080) energyratio
ratiobar=energybar/energyout
ratiocross1=energycross1/energyout
ratiocross2=energycross2/energyout
     write(*,1081) ratiobar
     write(*,1082) ratiocross1
     write(*,1083) ratiocross2
          write(*,*)
          write(*,*)
1000   format(' soliton period =
',f10.6)
 1010  format(' dispersion length =
',f10.6)
 1020  format(' nonlinear length =
',f10.6)
 1030  format(' intensity (GW/cm2)
= ',f9.6)
 1040  format(' power (W) = ',f8.4)
 1050  format(' propagation distance
= ',f8.6)
 1060  format(' input energy =
',E10.4)
 1061  format(' output energy bar =
',E10.4)
 1062  format(' output energy cross1
= ',E10.4)
 1063  format(' output energy cross2
= ',E10.4)
 1070  format(' total output energy =
',E10.4)
 1080  format(' energyratio = ',f8.6)
 1081  format(' output switching
fraction bar = ',f10.6)
 1082  format(' output switching
fraction cross1 = ',f10.6)
 1083  format(' output switching
fraction cross2 = ',f10.6)
 1090 format(4f10.6)
 1100  format(5(E10.4,2x))

C       SAVE AND CALCULATE
THE INTENSITY, THE SF, AND
THE POWERS
C       Calculates real power values.


powerin=energyin*76.0d6/eta/r*1.0d
3
```

```
powerbar=energybar*76.0d6*r*1.0d
3
powercross1=energycross1*76.0d6*
r*1.0d3
powercross2=energycross2*76.0d6*
r*1.0d3
powerout=energyout*76.0d6*r*1.0d
3
write(8,1090) inten,ratiobar,
ratiocross1,ratiocross2
write(11,1100) powerin,powerbar,
powercross1,powercross2,powerout

C       End of Power loop.

57  continue

C       SAVE LAST FIELD IN THE
BAR STATE OF THE LAST
POWER
call savefinalfield(beambar,tmax,
nt,fileoutput$)

close(unit=8)
close(unit=11)
stop
end

C       END MAIN PROGRAM

C       BEGINNING OF THE
SUBROUTINE DEFINITION

c       Perform autocorrelation of the
pulses
SUBROUTINE
AUTOCOR(NT,TMAX,BEAM,FILE
$)
REAL*8
DELT,TMAX,AUTO(9192),F(9192)
,AUTONORM
        COMPLEX*16 BEAM(4096)
        INTEGER NT,NT2,J,K
        CHARACTER*12 FILE$

        DELT=TMAX/DFLOAT(NT)
        AUTO(1)=0.0D0

        K=0
        DO 100 J=1,NT

        F(J)=CDABS(BEAM(J))*CD
        ABS(BEAM(J-K))
                f(j)=f(j)*f(j)

        AUTO(1)=AUTO(1)+F(J)
 100    CONTINUE
        AUTO(1)=AUTO(1)*DELT
```

```
        AUTONORM=AUTO(1)
        AUTO(1)=1.0D0

        DO 110 K=1,NT-1
              AUTO(K+1)=0.0D0
              DO 120 J=1,NT
              IF ((J-K).GE.1)
        THEN
F(J)=CDABS(BEAM(J))*CDABS(B
EAM(J-K))
f(j)=f(j)*f(j)
              ELSE
F(J)=0.0D0
              END IF
AUTO(K+1)=AUTO(K+1)+F(J)
 120          CONTINUE
AUTO(K+1)=AUTO(K+1)*DELT/A
UTONORM
110     CONTINUE
OPEN(UNIT=2,FILE=FILE$,STAT
US='NEW')
DO 130 I=NT,1,-1
WRITE(2,*) -(I-
1)*DELT*1.0d12,AUTO(I)
130     CONTINUE
DO 140 I=1,NT
WRITE(2,*) (I-
1)*DELT*1.0d12,AUTO(I)
 140    CONTINUE

CLOSE(UNIT=2)
RETURN
END

c   coupling for the NLDC
SUBROUTINE
COUPLING(BEAM1,BEAM2,
*NT,KAPPA,DELZ)

COMPLEX*16
BEAM1(4096),BEAM2(4096),TEM
P1,TEMP2
REAL*8 KAPPA,DELZ
INTEGER I,NT

DO 648 I=1,NT
TEMP1=BEAM1(I)
TEMP2=BEAM2(I)
BEAM1(I)=BEAM1(I)+(0.0D0,1.0D
0)*KAPPA*TEMP2*DELZ
BEAM2(I)=BEAM2(I)+(0.0D0,1.0D
0)*KAPPA*TEMP1*DELZ

648     CONTINUE
   RETURN
   END
```

```
C       Define the initial pulse
        (BEAM) asSQRT(POWER)
        *SECH(T/TO) in units of
        SQRT(WATTS)

        SUBROUTINE
DEFINEBEAM(TO,BEAMBAR,
*TMAX,NT,POWER,CHIRP,PULS
ETYPE$,ENERGY,FILEINPUT$)

COMPLEX*16 BEAMBAR(4096),
TEMPCHIRP,TEMPGAUS
REAL*8 TO,TMAX,T,DELT,
POWER,TEMP,TEMP1,TEMP2,EN
ERGY,CHIRP
INTEGER NT,I
CHARACTER*4 PULSETYPE$
CHARACTER*12 FILEINPUT$
DELT=TMAX/DFLOAT(NT)
ENERGY=0.0D0
IF (PULSETYPE$.EQ.'SECH')
THEN
c       define a sech pulse
        DO 34 I=1,NT
T=DFLOAT(I-1-NT/2)*DELT+
DELT/2.0D0
TEMP=(1.0D0/DCOSH(T/TO))
TEMPCHIRP=DCMPLX(0.0d0,-
CHIRP*T*T/2.0D0/TO/TO)
BEAMBAR(I)=DSQRT(POWER)*D
CMPLX(TEMP,0.0d0)*CDEXP(TE
MPCHIRP)
ENERGY=ENERGY+(CDABS(BEA
MBAR(I)))**2
34      continue
        ENERGY=ENERGY*DELT
        END IF

IF (PULSETYPE$.EQ.'GAUS')
THEN
C       define a gaussian pulse
        DO 334 I=1,NT
T=DFLOAT(I-1-NT/2)*DELT
+DELT/2.0D0
TEMP1=-T*T/TO/TO/2.0D0
TEMP2=-CHIRP*T*T/TO/TO/2.0D0
TEMPGAUS=DCMPLX(TEMP1,TE
MP2)
BEAMBAR(I)=DSQRT(POWER)*C
DEXP(TEMPGAUS)
ENERGY=ENERGY+(CDABS(BEA
MBAR(I)))**2
334     CONTINUE
        ENERGY=ENERGY*DELT
        END IF
IF (PULSETYPE$.EQ.'INPT')
THEN
```

```
C       INPUT DATA FILE FOR
        INITIAL PULSE
OPEN(UNIT=7,FILE=FILEINPUT$
,STATUS='OLD')
        DO 344 I=1,NT
READ(7,*) T,ER,EI
BEAMBAR(I)=DCMPLX(ER,EI)
ENERGY=ENERGY+(CDABS(BEA
MBAR(I)))**2
344     CONTINUE
        CLOSE(UNIT=7)
        ENERGY=ENERGY*DELT
        END IF

        RETURN
        END

C       INITIALIZE THE INPUT
PULSE IN THE CROSS STATE
        SUBROUTINE
INITCROSS(BEAMCROSS,NT)
COMPLEX*16 BEAMCROSS(4096)
INTEGER NT
DO 335 I=1,NT
BEAMCROSS(I)=0.0D0
335     CONTINUE
RETURN
END

c       Calculate the effect of
        dispersion on the pulse with
        the eq.
c       idA/dT=Beta2/2*d2A/dT2,
        which after integration
        becomes
c       A(z+dz)=A(z)exp(-
        i*beta2/2*d2/dT2*dz) and
        after taking the Fourier
        transform changes d2/dT2
        into -W2
c       where W are the temporal
        frequency in the temporal
        window spaced
c       by 2pi/TMAX

SUBROUTINE DISPERSIO(BEAM,
NT,TMAX,BETA2,DELZ)
COMPLEX*16 BEAM(4096),TEMP
REAL*8 TMAX,BETA2,DELZ,
PI,WTEMPORAL,Q2,NTFACTOR
INTEGER NT,I,NTT,NT2
PI=4.0D0*DATAN(1.0D0)
NTFACTOR=DFLOAT(NT-
1)/DFLOAT(NT)
WTEMPORAL=2.0D0*PI/
TMAX*NTFACTOR
NT2=NT/2
DO 133 I=1,NT
        IF (I .LE. NT2) NTT=0
        IF (I .GT. NT2) NTT=NT
Q2=DFLOAT(I-NTT-1)*
WTEMPORAL
TEMP=DCMPLX(0.0D0,+DELZ*Q
2*Q2/2.0D0*BETA2)
BEAM(I)=BEAM(I)*CDEXP
(TEMP)
133     CONTINUE
        RETURN
        END

c       Divide DATA by NT by
definition of the Fourier transform
c       see numerical recipe

SUBROUTINE
DIVIDEBYNT(DATA,NT)
        REAL*8 DATA(8192)
        INTEGER NT,I
        DO 177 I=1,2*NT
DATA(I)=DATA(I)/DFLOAT(NT)
177     CONTINUE
        RETURN
        END

c       FFT subroutine from
        numerical recipe
c       DATA: is the input/output
        REAL array
c       nn: is the number of points
        (must be a power of 2)
c       isign: =1 for FFT, =-1 for
        inverse FFT

SUBROUTINE FOUR1(DATA,NN,
ISIGN)
REAL*8 WR,WI,WPR,WPI,
WTEMP,THETA
REAL*8 DATA(*)N=2*NN
    J=1
    DO 11 I=1,N,2
      IF(J.GT.I)THEN
       TEMPR=DATA(J)
       TEMPI=DATA(J+1)
       DATA(J)=DATA(I)
       DATA(J+1)=DATA(I+1)
       DATA(I)=TEMPR
       DATA(I+1)=TEMPI
      ENDIF
      M=N/2
1     IF ((M.GE.2).AND.(J.GT.M))
THEN
       J=J-M
       M=M/2
      GO TO 1
      ENDIF
      J=J+M
```

```
11  CONTINUE
   MMAX=2
2   IF (N.GT.MMAX) THEN
     ISTEP=2*MMAX

THETA=6.28318530717959D0/(ISI
GN*MMAX)
WPR=-2.D0*DSIN(0.5D0*
THETA)**2
WPI=DSIN(THETA)
WR=1.D0
WI=0.D0
     DO 13 M=1,MMAX,2
       DO 12 I=M,N,ISTEP
         J=I+MMAX
TEMPR=SNGL(WR)*DATA(J)-
SNGL(WI)*DATA(J+1)

TEMPI=SNGL(WR)*DATA(J+1)+S
NGL(WI)*DATA(J)
        DATA(J)=DATA(I)-TEMPR
        DATA(J+1)=DATA(I+1)-
TEMPI
        DATA(I)=DATA(I)+TEMPR

DATA(I+1)=DATA(I+1)+TEMPI
12      CONTINUE
      WTEMP=WR
      WR=WR*WPR-WI*WPI+WR

WI=WI*WPR+WTEMP*WPI+WI
13    CONTINUE
     MMAX=ISTEP
   GO TO 2
   ENDIF
   RETURN
   END


c       Input parameter from the file
c       TBPM3.DAT

subroutine inputparameter(filename$
,filespec$,lambda,Tp,n2,nt,
*nz,inter,interspec,aeff,beta2,nsolito
n,powermax,zmax,nbeta2,
*chirp,pulsetype$,kappa12,npower,fi
lecoup$,filepower$,nauto,
*t2pa,t3pa,alpha,eta,nsave,r,raeff,file
input$,fileoutput$,*nwave,z1,kappa2
3,ntmax)

real* 8zmax,beta2,lambda,aeff,
powermax,n2,Tp,chirp,t2pa
real* 8t3pa,alpha,eta,r,raeff,
kappa12,kappa23,z1
character*4 filename$,filespec$,
pulsetype$
```

```
character*12 filecoup$,filepower$,
fileinput$,fileoutput$
integer nt,nz,inter,interspec,
nsoliton,nbeta2,npower,nauto,nsave
integer nwave,ntmax

c       filename$: Filename 4
c       characters long in which the
c       data forthe temporal profile
c       will be save (****0,****1...)
c       filespec$: Filename4characters
c       long in which the data for
c       the spectrum will be save
c       (****0,****1...)filecoup$:
c       filename 12 characters
c       containing the input intensity ,
c       the osfbar, osfcross,
c       powerbar, powercross
c       filepower$: filename of
c       powerin,poweroutbar,
c       lambda: wavelength in meter
c       Tp: pulse width FWHM in
c       seconds
c       n2: nonlinear index of
c       refraction in m2/W
c       nt: number of transverse
c       points in time (must be a
c       power of 2)
c       ntmax:multiply To to give
c       time window width
c       aeff: effective area in m2
c       raeff: ratio of the effective area
c       between aeff and the
c       one use in the experiement
c       beta2: second order dispersion
c       in s2/m
c       nsoliton: soliton order ,
c       N2=Ld/Lnl
c       powermax: maximum power
c       of the input pulse in W
c       (negative number if want to
c       have a n order soliton)
c       npower: number of points
c       between 0W and power W
c       zmax: propagation length
c       (negative if propagation
c       distance is one Ld)
c       nbeta2: =0 if do not want
c       dispersion
c       inter: number of steps
c       between file of temp profile
c       interspec : number of steps
c       between file of the spectrum
c       chirp: chirp factor as defined
c       p58-59 of Agrawal
c       deltaw=sqrt(1+chirp**2)/To
c       pulsetype$: type of pulse,
c       'GAUS' for gaussian, or
```

```
c       'SECH'for sech pulse,
c       'INPT' for input file
c        NB. Would be a good idea
c       to put npower to 1, since it
c       will calculate
c       the same thing npower time,
c       because when INPT is used
c       the power is define by the
c       previouly define pulse.Also,
c       because of the definition of To
c       on line 51, the previously
c       define pulse should be
c       'SECH'
c       fileinput$: filename for input
c       pulse if pulsetype$='INPT'
c       fileoutput$: filename of output
c       file with T,ER,EI
c       kappa: coupling coefficient ,
c       K=pi/2/Lc
c       nauto: =1 if autocorrelation
c       wanted instead of pulses
c       t2pa: two photon absorption
c       coefficient m/W
c       t3pa: three photon absorption
c       coefficient m3/W2
c       alpha: linear loss in m-1
c       eta: coupling efficiency
c       nsave: =1 if want to save
c       spectrum and pulse
c       r: reflectivity of facettes
c       nwave  : =1 if wavelength is
c       wanted in the spectrum file

open(unit=1,file='tbpm3core.dat',stat
us='old')

        read(1,*) filename$
        read(1,*) filespec$
        read(1,*) filecoup$
        read(1,*) filepower$
        read(1,*) lambda
        read(1,*) Tp
        read(1,*) pulsetype$
        read(1,*) fileinput$
        read(1,*) fileoutput$
        read(1,*) n2
        read(1,*) t2pa
        read(1,*) t3pa
        read(1,*) alpha
        read(1,*) nt
        read(1,*) ntmax
        read(1,*) nz
        read(1,*) inter
        read(1,*) interspec
        read(1,*) aeff
        read(1,*) raeff
        read(1,*) beta2
        read(1,*) nsoliton
        read(1,*) powermax
        read(1,*) npower
        read(1,*) zmax
        read(1,*) z1
        read(1,*) nbeta2
        read(1,*) chirp
        read(1,*) kappa12
        read(1,*) kappa23
        read(1,*) nauto
        read(1,*) eta
        read(1,*) r
        read(1,*) nsave
        read(1,*) nwave
        close(unit=1)
        return
        end

c       Calculate the effect of the
nonlinearity on the pulse with the
c       equation idA/dT=-
GAMMA*|A|2*A, which after
integration becomes
c       A(z+dz)=A(z)exp(-
i*GAMMA*|A|2*dz)

SUBROUTINE
NLIN(BEAM,NT,GAMMA,DELZ,C
2PA,C3PA,ALPHA)
COMPLEX*16 BEAM(4096),TEMP
REAL*8DELZ,E,GAMMA,C2PA,C
3PA,ALPHA
INTEGER NT,I

DO 144 I=1,NT
        E=CDABS(BEAM(I))
        TEMP=DCMPLX(0.0D0,+D
        ELZ*GAMMA*E*E)

        TEMP=TEMP+DCMPLX(-
        C2PA*DELZ*E*E,0.0D0)

        TEMP=TEMP+DCMPLX(-
        C3PA*DELZ*E*E*E*E,0.0D
        0)

        TEMP=TEMP+DCMPLX(-
        ALPHA*DELZ)

        BEAM(I)=BEAM(I)*CDEXP
        (TEMP)
 144    CONTINUE
        RETURN
        END

c       To avoid reflection at the
c       boundaries we put an
c       absorber near
```

```
c       the boundaries, after Dave c
        Heatley's thesis

SUBROUTINE
REFLECTION(BEAM,TMAX,NT)
        COMPLEX*16 BEAM(4096)
        REAL*8 TMAX,T,DELT
        INTEGER NT,I

        DELT=TMAX/DFLOAT(NT)
        DO 199 I=1,NT
T=DFLOAT(I-1-NT/2)*DELT+
DELT/2.0D0
BEAM(I)=BEAM(I)*DEXP(-
(0.95D0*T/(TMAX/2.0D0))**10)
199     CONTINUE
        RETURN
        END

c       Save field

SUBROUTINE
SAVEFIELD(BEAM,TMAX,NT,FIL
E1$,POWER,ENERGY,NAUTO,N
SAVE)
        COMPLEX*16 BEAM(4096)
        REAL*8
TMAX,DELT,T,E,ER,EI,C,ESP0,I
NTEN,POWER,ENERGY
INTEGER NT,I,NAUTO,NSAVE
CHARACTER*12 FILE1$
        C=3.0D10
        ESP0=8.85D-14
ENERGY=0.0D0
        IF
(NAUTO.NE.1.AND.NSAVE.EQ.1)
THEN
OPEN(UNIT=3,FILE=FILE1$,STA
TUS='NEW')
        END IF

        DELT=TMAX/DFLOAT(NT)
        DO 166 I=1,NT
        ER=DREAL(BEAM(I))
        EI=DIMAG(BEAM(I))
        E=(CDABS(BEAM(I)))**2/P
        OWER

        ENERGY=ENERGY+E
T=DFLOAT(I-1-NT/2)*DELT+
DELT/2.0D0
T=T*1.0d12
                IF
(NAUTO.NE.1.AND.NSAVE.EQ.1)
WRITE(3,*) T,E
C       INTEN=C*ESP0*E*E/2.0d0
 166    CONTINUE
```

```
        ENERGY=ENERGY*POWE
        R*DELT
                IF
(NAUTO.NE.1.AND.NSAVE.EQ.1)
CLOSE (UNIT=3)
                IF
(NAUTO.EQ.1.AND.NSAVE.EQ.1)
THEN
CALL AUTOCOR(NT,TMAX,
BEAM,FILE1$)
        END IF
RETURN
END

c       save final field
SUBROUTINE
SAVEFINALFIELD(BEAM,TMAX,
NT,FILE1$)
COMPLEX*16 BEAM(4096)
REAL*8 TMAX,DELT,T,E,ER,EI
        INTEGER NT,I
        CHARACTER*12 FILE1$
OPEN(UNIT=3,FILE=FILE1$,STA
TUS='NEW')
DELT=TMAX/DFLOAT(NT)
DO 176 I=1,NT
ER=DREAL(BEAM(I))
EI=DIMAG(BEAM(I))
T=DFLOAT(I-1-NT/2)*DELT+
DELT/2.0D0
WRITE(3,*) T,ER,EI
 176    CONTINUE
        CLOSE(UNIT=3)
        RETURN
        END

SUBROUTINE
SAVESPECTRUM(BEAM,TMAX,
NT,FILE$,TO,NWAVE,LAMB)
COMPLEX*16 BEAM(4096)
REAL*8 TMAX,PI,WTEMPORAL,
Q2,NTFACTOR,SPECTRUM,TO,
specmax
REAL*8 LAMB,NU0
INTEGER NT,I,NT2,NT21,
NWAVE
CHARACTER*12 FILE$
PI=4.0D0*DATAN(1.0D0)
NTFACTOR=DFLOAT(NT-1)/
DFLOAT(NT)
WTEMPORAL=1.0D0/TMAX*NTF
ACTOR*TO
NT2=NT/2
NT21=NT2+1
NU0=2.997925d8/LAMB
        specmax=0.0d0
```

```
        OPEN
(UNIT=4,FILE=FILE$,STATUS='
NEW')

DO 1155 I=NT21,NT
SPECTRUM=((CDABS(BEAM(I)))*
*2)/NT/NT
if (spectrum.gt.specmax)
specmax=spectrum
 1155  CONTINUE
DO 1156 I=1,NT21
SPECTRUM=((CDABS(BEAM(I)))*
*2)/NT/NT
                if
(spectrum.gt.specmax)
specmax=spectrum
 1156  CONTINUE

DO 155 I=NT21,NT
if (nwave.eq.0) then
Q2=DFLOAT(I-NT-
1)*WTEMPORAL
SPECTRUM=((CDABS(BEAM(I)))*
*2)/NT/NT/specmax
WRITE(4,*) Q2,SPECTRUM
                else
Q2=DFLOAT(I-NT-
1)*1.0d0/TMAX*NTFACTOR
Q2=Q2+NU0
Q2=2.997925D8/Q2
SPECTRUM=((CDABS(BEAM(I)))*
*2)/NT/NT/specmax
WRITE(4,*) Q2*1.0d9,SPECTRUM
END IF
155    CONTINUE
DO 156 I=1,NT21
IF (NWAVE.EQ.0) THEN
Q2=DFLOAT(I-1)*WTEMPORAL
SPECTRUM=((CDABS(BEAM(I)))*
*2)/NT/NT/specmax
WRITE(4,*) Q2,SPECTRUM
ELSE
Q2=DFLOAT(I-1)*1.0d0/TMAX*
NTFACTOR
Q2=Q2+NU0
Q2=2.997925D8/Q2
SPECTRUM=((CDABS(BEAM(I)))*
*2)/NT/NT/specmax
WRITE(4,*) Q2*1.0d9,SPECTRUM
END IF
156    CONTINUE
       CLOSE(UNIT=4)
       RETURN
       END
```